Spectral control of lasers and optical parametric oscillators with volume Bragg gratings

BJÖRN JACOBSSON

KTH Engineering Sciences

Doctoral Thesis
Department of Applied Physics
KTH – Royal Institute of Technology
Stockholm, Sweden 2008

Spectral control of lasers and optical parametric oscillators with volume Bragg gratings

Laser Physics
Department of Applied Physics
KTH – Royal Institute of Technology
106 91 Stockholm
Sweden

ISBN 978-91-7178-914-3
TRITA-FYS 2008:13
ISSN 0280-316X
ISRN KTH/FYS/--08:13--SE

Akademisk avhandling som med tillstånd av Kungliga Tekniska Högskolan framläggs till offentlig granskning för avläggande av teknologie doktorsexamen fredagen den 25 april 2008 kl. 10.00 i sal FB53, Albanova, Roslagstullsbacken 21, KTH, Stockholm. Avhandlingen kommer att försvaras på engelska.

Cover picture: Scattering of pump and laser light in a volume Bragg grating used as the input coupler of the Yb:KYW laser of paper V.

Printed by Universitetsservice US AB, Stockholm 2008

Björn Jacobsson
Spectral control of lasers and optical parametric oscillators with volume Bragg gratings
Laser Physics, Department of Applied Physics, KTH – Royal Institute of Technology, 106 91 Stockholm, Sweden
ISBN 978-91-7178-914-3, TRITA-FYS 2008:13, ISSN 0280-316X, ISRN KTH/FYS/--08:13--SE

Abstract

The object of this thesis is to explore the usage of reflective volume Bragg gratings in photo-thermo-refractive glass for spectral control of solid-state lasers and optical parametric oscillators, to build tunable and narrowband coherent light-sources.

In order to provide a design tool for use of reflective volume Bragg gratings in laser cavities, a theory was developed that describes the performance of the gratings if the incident beam has finite width with an angular spectrum that is comparable to the grating's angular acceptance bandwidth.

Spectral control was demonstrated in a number of cw solid-state lasers, in terms of narrow bandwidth and tunable wavelength, by use of a volume Bragg grating. The design could be made very simple by replacing one of the cavity mirrors with the grating. Thanks to the grating's strong spectral selectivity, the lasers could be locked anywhere in the gain spectrum, while the laser bandwidth was substantially narrowed. In particular, the following lasers were demonstrated: Single-longitudinal-mode lasing in ErYb:glass at 1553 nm with 90 kHz linewidth and in Nd:$GdVO_4$ at 1066 nm with a linewidth below 40 MHz. Very low quantum defect in Yb:KYW lasers, diode-pumped at 982 nm and lasing at 998 nm with 10 GHz bandwidth, as well as Ti:sapphire-pumped at 980 nm and lasing at 990 nm. An Yb:KYW laser that was widely tunable from 996 nm to 1048 nm with 10 GHz bandwidth.

In nanosecond pulsed optical parametric oscillators (OPOs) based on periodically poled $KTiOPO_4$, narrowband operation and a tunable wavelength were demonstrated with a volume Bragg grating as a cavity mirror. At a signal wavelength of 975 nm, the bandwidth was 50 GHz, a reduction by 20 times compared to using a conventional mirror. A tuning range of 21 THz was also demonstrated. In another OPO at a signal wavelength of 760 nm, a ring-cavity design was demonstrated to provide convenient tuning. A tuning range of 2.6 THz and a bandwidth of 130 GHz was shown. Also, narrowband operation and tuning in an OPO around 1 μm was demonstrated by use of a transversely chirped Bragg grating.

Keywords: volume Bragg gratings, single-longitudinal-mode laser, laser tuning, erbium, neodymium, ytterbium, nonlinear optics, optical parametric oscillator, KTP, tunable optical parametric oscillator, narrowband optical parametric oscillator.

Sammanfattning

I den här avhandlingen visas hur lasrar och optiska parametriska oscillatorer (OPO:er) kan styras spektralt med hjälp av volymbraggitter.

Volymbraggitter utgörs av ett periodiskt varierande brytningsindex som skrivits i ett fototermorefraktivt glas. Gittret reflekterar därmed en specifik våglängd som bestäms av perioden hos modulationen, och kan tillverkas med smal bandbredd och hög reflektans beroende på modulationens längd och styrka.

En teoretisk modell har utvecklats för reflektiva volymbraggitters egenskaper om den infallande strålen har en större vinkelspridning än gittrets vinkeltolerans. Detta kan bl.a. inträffa i en laserkavitet där gittret används vid snett infall, och en teoretisk beskrivning är därför ett viktigt redskap för att kunna designa sådana lasrar.

Spektral kontroll av ett antal fasta tillståndslasrar med hjälp av volymbraggitter har i försök påvisats, och lasern har därvid både kunnat avstämmas spektralt samtidigt som en avsmalnad spektral bandbredd erhållits. Lasern kan göras väldigt enkel genom att byta ut en av kavitetsspeglarna mot gittret. Tack vare gittrets goda spektrala urvalsmekanism kan lasern låsas var som helst i förstärkningsspektrumet. De tekniker och lasrar som demonstrerats experimentellt är följande:

Lasring i en enda longitudinell mod erhölls både för en diodpumpad ErYb:glas-laser vid 1553 nm med ca 10 mW:s effekt och 90 kHz linjebredd samt för en diodpumpad Nd:$GdVO_4$-laser vid 1066 nm med 0.85 W:s effekt. Lasrarnas våglängd kunde avstämmas över större delen av gittrets bandbredd på ca. 30 GHz. Genom att bygga Nd:$GdVO_4$-lasern med en monolitisk kavitet kunde även en spektralt synnerligen stabil laser erhållas med under 40 MHz bandbredd. Tillämpningar för dessa lasrar finns både inom spektroskopi samt som källor för intrakavitetsfördubbling till synliga våglängder.

Genom att använda gittret som inkopplingsspegel går det även att framställa lasrar med en väldigt låg kvantdefekt, som därför får minskad värmeutveckling i lasermediet. Detta medger i sin tur att lasrar med höga medeleffekter kan konstrueras, som kan användas bl.a. för olika former av materialbearbetning. I detta arbete har lasrar med låg kvantdefekt byggts med Yb:KYW som laserkristall; både en laser vid 998 nm på 3.6 W som diodpumpades vid 982 nm och med en bandbredd på 10 GHz, samt en laser vid 990 nm på 70 mW som pumpades av en Ti:safir-laser vid 980 nm.

Om volymbraggittret används vid snett infall kan den reflekterade våglängden avstämmas genom att gittret roteras. Denna princip användes i en diodpumpad Yb:KYW-laser till att erhålla en brett avstämbar laservåglängd mellan 996 nm och 1048 nm med en maximal effekt på 3 W och med 10 GHz bandbredd. Genom att placera gittret i en retroreflektor kunde avstämningen göras utan att kaviteten behövde linjeras om. En laser som denna kan exempelvis användas för olika typer av materialkarakterisering och spektroskopi.

Med optiska parametriska oscillatorer (OPO:er) kan laserljus omvandlas till nya

våglängder. Därmed kan OPO:er användas som koherenta ljuskällor där inga effektiva lasrar existerar. OPO-processen kan göras effektiv om en pulsad pump används, och den genererade våglängden kan enkelt styras med hjälp av periodiskt polade (PP) icke-linjära kristaller, såsom PP-$KTiOPO_4$, som användes i detta arbete. En nackdel med OPO:er är att i allmänhet är den genererade signalen tämligen spektralt bredbandig. Signalens bandbredd kan dock avsmalnas betydligt om ett spektralt filter såsom ett volymbraggitter används. Genom att byta ut en av speglarna i OPO-kaviteten mot gittret kan utformningen av OPO:n göras väldigt enkel.

I en OPO med en signalvåglängd på 975 nm kunde en avsmalning av bandbredden till 50 GHz påvisas med hjälp av ett braggitter. Detta motsvarar 20 gångers minskning jämfört med om en konventionell spegel används. Som mest erhölls en pulsenergi på 0.34 mJ i signalen. Genom att rotera gittret kunde våglängden avstämmas 21 THz. För att förenkla avstämningen konstruerades även en OPO med gittret i en retroreflektor, samtidigt som kaviteten var av ringtyp. I denna OPO vid en våglängd på 760 nm och med en pulsenergi i signalen på upp till 0.42 mJ erhölls en bandbredd på 130 GHz och ett avstämningsområde på 2.6 THz. Slutligen har en OPO vid 1 μm konstruerats med ett gitter med en transversellt varierande period, s.k. chirp. Därigenom kan våglängden avstämmas väldigt enkelt genom att bara flytta gittret transversellt.

En tillämpning av dessa OPO:er är såsom ljuskällor i olika typer av laserbaserade sensorer, i vilka en specifik och stabil våglängd erfordras. Dessutom kan de smalbandiga OPO:erna användas som första steg i ickelinjära processer i flera steg. Smal bandbredd är då viktig för effektiviteten i den påföljande ickelinjära omvandlingen i nästa steg.

Contents

List of publications

This thesis is based on the following journal papers.

I J. E. Hellström, B. Jacobsson, V. Pasiskevicius and F. Laurell, *Finite beams in reflective volume Bragg gratings: theory and experiments*, IEEE J. Quantum Electron. **44**, 81 (2008).

II B. Jacobsson, V. Pasiskevicius and F. Laurell, *Tunable single-longitudinal-mode ErYb:glass laser locked by a bulk glass Bragg grating*, Opt. Lett. **31**, 1663 (2006).

III B. Jacobsson, V. Pasiskevicius and F. Laurell, *Single-longitudinal-mode Nd-laser with a Bragg grating Fabry-Perot cavity*, Opt. Express **14**, 9284 (2006). [*Erratum*, Opt. Express, **15**, 9387 (2007).]

IV I. Häggström, B. Jacobsson and F. Laurell, *Monolithic Bragg-locked Nd:$GdVO_4$ laser*, Opt. Express **15**, 11589 (2007).

V J. E. Hellström, B. Jacobsson, V. Pasiskevicius and F. Laurell, *Quasi-two-level Yb:KYW laser with a volume Bragg grating*, Opt. Express **15**, 13930 (2007).

VI B. Jacobsson, *Experimental and theoretical investigation of a volume-Bragg-grating-locked Yb:KYW laser at selected wavelengths*, submitted (2008).

VII B. Jacobsson, J. E. Hellström, V. Pasiskevicius and F. Laurell, *Widely tunable Yb:KYW laser with a volume Bragg grating*, Opt. Express **15**, 1003 (2007).

VIII B. Jacobsson, J. E. Hellström, V. Pasiskevicius and F. Laurell, *Tunable Yb:KYW laser using volume Bragg grating in s-polarization*, Appl. Phys. B **91**, 85 (2008).

IX B. Jacobsson, M. Tiihonen, V. Pasiskevicius and F. Laurell, *Narrowband bulk Bragg grating optical parametric oscillator*, Opt. Lett. **30**, 2281 (2005).

X B. Jacobsson, C. Canalias, V. Pasiskevicius and F. Laurell, *Narrowband and tunable ring optical parametric oscillator with a volume Bragg grating*, Opt. Lett. **32**, 3278 (2007).

Related publications not included in the thesis

The following journal papers and conference contributions by the author are related to the subject, but not included in the thesis.

A B. Jacobsson, M. Tiihonen, V. Pasiskevicius and F. Laurell, *Narrow-band optical parametric oscillator using a bulk Bragg grating*, Conference on Lasers and Electro-Optics/Europe (Munich, Germany, 2005), CD2-5-MON.

B B. Jacobsson, V. Pasiskevicius and F. Laurell, *Tunable single mode ErYb:glass laser locked by a bulk glass Bragg grating*, Advanced Solid-State Photonics (Lake Tahoe, USA, 2006), TuB8.

C S. Bertani, B. Jacobsson, F. Laurell, V. Pasiskevicius and M. Stjernström, *Stretching-tunable external-cavity laser locked by an elastic silicone grating*, Opt. Express **14**, 11982 (2006).

D J. E. Hellström, B. Jacobsson, V. Pasiskevicius and F. Laurell, *Tunable Yb:KYW laser with a volume Bragg grating*, Advanced Solid-State Photonics (Vancouver, Canada, 2007), MC4.

E B. Jacobsson, J. E. Hellström, V. Pasiskevicius and F. Laurell, *Transversal mode transformation in reflective volume Bragg gratings, theory and experiments*, Advanced Solid-State Photonics (Vancouver, Canada, 2007), TuB8.

F B. Jacobsson, J. E. Hellström, V. Pasiskevicius and F. Laurell, *Widely tunable Yb:KYW laser locked by a volume Bragg grating*, Conference on Lasers and Electro-Optics (Baltimore, USA, 2007), CThE1.

G I. Häggström, B. Jacobsson and F. Laurell, *Monolithic Bragg-locked Nd-laser*, Conference on Lasers and Electro-Optics (Baltimore, USA, 2007), CThE2.

H B. Jacobsson, V. Pasiskevicius and F. Laurell, *Tunable ring optical parametric oscillator with a volume Bragg grating*, Conference on Lasers and Electro-Optics (Baltimore, USA, 2007), CThC7.

I B. Jacobsson, J. E. Hellström, V. Pasiskevicius and F. Laurell, *Quasi-two-level Yb:KYW laser using a volume Bragg grating*, Advanced Solid-State Photonics (Nara, Japan, 2008), MD3.

J B. Jacobsson, V. Pasiskevicius., F. Laurell, V. Smirnov and L. Glebov, *Tunable optical parametric oscillator controlled by a transversely chirped Bragg grating*, Conference on Lasers and Electro-Optics (San-Jose, USA, 2008), CTuY3.

Author contribution

My contribution in the original papers was the following.

I I performed the experiments and developed the theory together with J. Hellström. I wrote the paper together with J. Hellström, with assistance from V. Pasiskevicius and F. Laurell.

II I performed the experiments with assistance from V. Pasiskevicius. I wrote the paper with assistance from V. Pasiskevicius and F. Laurell.

III I performed the experiments and the numerical simulations. I wrote the paper with assistance from V. Pasiskevicius and F. Laurell.

IV I took part in the experiments, that were primarily conducted by I. Häggström. I wrote the paper with assistance from I. Häggström and F. Laurell.

V I performed the experiments together with J. Hellström. I wrote the paper together with J. Hellström, with assistance from V. Pasiskevicius and F. Laurell.

VI I performed the experiments, developed the theory and wrote the paper.

VII I performed the experiments together with J. Hellström. I wrote the paper together with J. Hellström, with assistance from V. Pasiskevicius and F. Laurell.

VIII I performed the experiments together with J. Hellström. I wrote the paper together with J. Hellström, with assistance from V. Pasiskevicius and F. Laurell.

IX I performed the experiments together with Mikael Tiihonen. I wrote the paper together with Mikael Tiihonen, with assistance from V. Pasiskevicius and F. Laurell.

X I performed the optical experiments, while C. Canalias poled the PPKTP. I wrote the paper, with assistance from V. Pasiskevicius and F. Laurell.

Preface

The research forming this thesis was performed at the Laser Physics group, Department of Applied Physics, KTH from 2004 to 2008.

The work of the thesis is based on the arrival of a new optical component, volume Bragg gratings written in photo-thermo-refractive glass. The idea of such gratings is certainly not new, but at the time I started working on this thesis, the material development had reached a state where durable gratings had become commercially available. At first, the gratings had only been used to lock high power diode lasers, but we took the gratings and used them in new areas: nonlinear optics and solid-state lasers.

The first OPO (paper IX) that we locked with a volume Bragg grating was a good example of what I like about optics research, that the step from idea to realization is not so long. If only you have the right components from a previous experiment, building a working setup can be fairly quick and easy. For this experiment, Fredrik had bought a grating at a laser exibition, and had the idea to try it out in an OPO. So we just went to the lab, used some equipment that was around from before, and set up the experiment. And straight away, the OPO was up and running.

Still, life is not always that easy. For the tunable Yb-lasers (paper VII, paper VIII), the development from first idea to a properly running laser took quite some time and effort. The main reason was that we had to understand the laser system and the complications that come along when you use a volume Bragg grating at oblique incidence with spatially narrow laser beams. In the end, we had to develop a theoretical description of the system ourselves (paper I), that was then used as a tool for designing the laser.

During my years as a PhD student, my salary has been kindly provided by KTH in the form of an “excellenstjänst”. Additional funding has been obtained from the EU project DT-CRYS, Carl Tryggers stiftelse, Göran Gustafssons stiftelse, Knut och Alice Wallenbergs stiftelse, Stiftelsen Lars Hiertas minne and Helge Ax:son Johnsons stiftelse.

Acknowledgements

First and foremost, I want to thank my supervisor Fredrik Laurell. He took me on as a PhD student when I came empty-handed and has always shown confidence in my ability. Without Fredrik's crazy ideas, never-ending enthusiasm and optimism in that the experiments would work and the papers be accepted, this thesis would not have been written. Fredrik, I hope next time we go skiing, there won't be any broken bones.

I am also very greatful to my other supervisor Valdas Pasiskevicius for always finding the time to help me in the lab and to discuss physics. Research is about asking questions, and with the assistance from Valdas, many answers could be found. Furthermore, with his encouragement, and him acting as the devil's advocate, the publications could always be improved. Also, thanks for showing me the best beer in Vilnius.

I also thank all the friendly people in the Laser Physics group, for making my time as a PhD-student enjoyable and not lonely, sharing the good and bad days, for the lunch company, the coffe-breaks, the football and not least the parties. Especially, I want to thank:
– Jonas Hellström, for all the papers we co-authored, teaching me about Yb-lasers, the endless hours spent together in the lab, all the fun discussions on lasers, his enthusiasm and also his fearless skiing.
– Mikael Tiihonen for teaching me about OPOs and always getting to the point.
– Ida Häggström for building the monolithic laser together and telling all those wild stories.
– Carlota Canalias for poling the best crystals and sharing her Catalan wisdom.
– Anna Fragemann for the discussions on parametrics, the fights over the pump laser and the good time in München.
– Stefan Holmgren for all the interesting discussions on optics.
– Stefano Bertani for his persistance with silicone and for being a good room-mate.
– Pär Jelger for the discussions on (im)possible laser setups and the fun conference trips.
– Gunnar Elgcrona (Karlsson) for teching me about ErYb-lasers.
– Markus Henriksson for sharing the interest in volume-Bragg-grating OPOs.
– Junji Hirohashi, Sandra Johansson, Kai Seger, Gustav Strömqvist, Stefan Bjurshagen, Jimmy Johansson, Lars-Gunnar Andersson and Jens Tellefsen.

I am also greatful to my fellow PhD-student friends outside the laser world for the sharing and understanding of this strange occupation. My friends outside KTH are thanked for bringing my mind off lasers, and for playing football and music with me. I also want to thank the people at former Innolite for leading me onto the right path and showing me how fun it can be in a lab.

Finally, I want to thank my family both for actually trying to understand what I do in the lab, but also for not caring so much. Tack mamma, pappa, Karin, Sara, Martin och Filippa.

List of abbreviations and symbols

The following abbreviations and symbols for physical quantities are used throughout the thesis.

cw	continuous wave (not pulsed)
DFG	difference frequency generation
FWHM	full width at half maximum
IR	infrared
OPA	optical parametric amplification/-er
OPG	optical parametric generation
OPO	optical parametric oscillation/-or
PP	periodically poled
QPM	quasi phase-matching/-ed
SFG	sum frequency generation
SHG	second harmonic generation
UV	ultraviolet

$c = \lambda\nu$	speed of light in vacuum
λ	vacuum wavelength
ν	frequency
$\omega = 2\pi\nu$	angular frequency
$k = 2\pi n/\lambda = \omega n/c$	wavenumber
n	refractive index
Λ	spatial period
E	electric field
$I = \lvert E\rvert^2 \epsilon_0 cn/2$	intensity
P	material polarization
$\mathcal{E}$	energy
$\mathcal{P}$	power
T	temperature
R	(power) reflectivity
ϵ_0	permittivity of vacuum
k_B	Boltzmann's constant
h	Planck's constant
$\hat{\mathbf{x}}, \hat{\mathbf{y}}, \hat{\mathbf{z}}$	unit vectors
$\mathbf{r} = x\hat{\mathbf{x}} + y\hat{\mathbf{y}} + z\hat{\mathbf{z}}$	spatial coordinate

Part I

Background and overview

Chapter 1

Introduction

1.1 Background

The first experimental demonstrations of laser action were done in the early 1960s, and several different laser types were presented. The first laser was Maiman's famous 1960 experiment with a pulsed Ruby (Cr^{3+}:Al_2O_3) laser; a flashlamp-pumped pulsed solid-state laser [1]. Soon after, lasing in many other important solid-state laser ions was demonstrated, such as Nd:$CaWO_4$ [2], Yb:glass [3] and ErYb:glass [4]. Other laser types that were shown early on was the HeNe gas laser in 1961 [5], which was the first cw laser, and the first semiconductor laser in 1962 [6], using GaAs at liquid nitrogen temperature and pumped by a pulsed electrical current. A few years later, in 1964, the first diode-pumped solid-state laser was demonstrated with a GaAs diode pumping U^{3+}:CaF_2 [7]. In the early years, several important technologies for laser control were also demonstrated, including Q-switching [8], mode-locking [9] and spectral control with both etalons [10, 11] and surface gratings [12, 13].

To extend lasers in the spectral domain, nonlinear optics is an important tool. Also in this field, many of the fundamental phenomena were demonstrated in the 1960s, closely following the laser development. The early experiments included non phase-matched second harmonic generation (SHG) in quartz in 1961 [14], followed in 1962 by birefringently phase-matched SHG [15, 16], sum frequency generation (SFG) [17] and difference frequency generation (DFG) [18]. The optical parametric processes came next. In 1965 the first optical parametric amplifiers (OPA) were demonstrated [19, 20] as well as the first optical parametric oscillator (OPO) [21].

As can be seen, most of the fundamental concepts in laser physics and nonlinear optics were developed during the first decade of research. Nevertheless, these early systems were often far from being useful for a main reason, inadequate performance of the involved materials. Thus, a second wave of research has been aimed at material development to obtain better lifetime and efficiency. Important tech-

nologies that have been developed include single-mode laser diodes operating at room temperature at a number of wavelengths, high power laser diodes for pumping of lanthanide ions, new solid-state laser crystals as well as efficient materials for nonlinear optics. By usage of solid-state materials instead of gases or liquids, compact and reliable lasers are nowadays available. The laser systems of today find applications in a number of areas, that make use of the highly refined laser light performance, with properties such as high intensity, strong coherence, narrow bandwidth or short pulse-length.

Today, the world market yearly revenues of lasers is about 7 billion (10^9) US$ [22, 23], coarsely divided into the following segments (2007 revenue given): material processing (2.2 B$), telecommunication (1.7 B$), optical storage (1.6 B$), medical therapy (0.54 B$), scientific research (170 M$), instrumentation (87 M$), printing (65 M$), sensing (46 M$) and entertainment and displays (20 M$).

For material processing, CO_2 lasers, solid-state lasers and fibre lasers are used as a tool in the manufacturing industry for cutting, welding, drilling, marking etc. Mainly, the required performance is high peak intensity and good focussability. For laser printing, the requirements are fairly equivalent. Also, excimer lasers and harmonics of diode-pumped solid-state lasers at short wavelengths are used for lithography and repair in the manufacturing of semiconductor integrated circuits and flat panel displays, where good focussability is required.

In the area of optical storage, semiconductor lasers are being used for data reading and writing of cd's, dvd's and hd-dvd's/blu-ray discs. The laser properties that are used there are primarily the minimal-diffraction focussability and good coherence.

In telecommunication, semiconductor lasers are used as transmitters in fibre communication systems, making use of both good focussability and narrow linewidth.

Medical therapy includes lasers used for cosmetics and opthalmology. Both solid-state lasers and excimer lasers are used, as a means to deliver energy of a certain wavelength and temporal shape at a well-defined position at the patient.

For general scientific purposes, lasers can be used as a precise tool in a variety of applications. For spectroscopy and sensing, narrow bandwidth and tunability are most important, while detection of ultra-fast processes require very short pulses.

The instrumentation market includes diode-pumped solid-state lasers for microscopy as well as fluorescence excitation for applications in life-sciences.

Lasers for measurement and sensing constitute a growing market, where the applications include geodetic distance measurements, as well as environmental and security monitoring.

The entertainment and display segment uses visible semiconductor, solid-state and ion lasers, for information displays, as laser pointers, for lasershows and for laser video displays.

Finally, in addition to the above mentioned areas of applications, there are a number of other applications of laser technology, too many to be mentioned here.

1.2 Subject of the thesis

The object of this thesis is to explore the usage of volume Bragg gratings in solid-state lasers and optical parametric oscillators.

For the results I report in this thesis, a number of material breakthroughs in recent years have paved the way for the experiments. Primarily, volume Bragg gratings in photo-thermo-refractive glass have become commercially available as durable elements with strong spectral selectivity. Also, all laser experiments in this thesis rely on the currently available high power and high brightness semiconductor pump diodes at 808 nm and 980 nm. The development of new laser crystals, such as the vanadates and the double tungstates, has also been important. Furthermore, the optical parametric oscillators that were built would not be possible without the efficient nonlinear crystals: periodically poled KTP that can be conveniently tailored for the intended purpose.

1.3 Applications

Applications for the coherent light sources that were developed in this thesis can be found in the following areas.

The single-longitudinal-mode lasers [paper II, paper III, paper IV] can be used for precision spectroscopy or as sources for intracavity frequency doubling, used to reach visible wavelengths. Thanks to the volume Bragg gratings, these lasers have a simpler design than conventional single-mode lasers. In addition, the laser wavelength can very easily be chosen anywhere in the gain spectrum, to perfectly match the intended application.

The tunable Yb lasers [paper VII, paper VIII] can be used as a high power source for spectroscopy, while the novel tuning method is widely applicable in any tunable laser, as an addition to previously demonstrated techniques.

The demonstration of a method to obtain very low quantum defects [paper V, paper VI] shows a way to increase the power in end-pumped solid-state lasers. High power lasers find applications in material processing, and the laser we demonstrate can be scaled to high powers, while maintaining a simple cavity design.

OPOs are used as coherent light-sources at wavelengths where no efficient conventional lasers exist. With the method given in paper IX and paper X, a way to significantly decrease the OPO signal bandwidth is given, while keeping a simple cavity design. An application for these OPOs is various types of laser-based sensing, where a specific and stabilized wavelength is needed. Also, these OPOs are useful in multistep nonlinear processes, where it is of importance that the bandwidth is kept narrow at the intermediate stages. These systems can be used to give high pulse-energies at arbitrary wavelengths, both in the mid IR and in the UV. Sources in the mid-IR are needed for trace-gas spectroscopy, as well as for laser surgery. Applications in the UV include fluorescence spectroscopy for biological sensing, as well as various industrial manufacturing processes.

1.4 Outline of the thesis

This thesis is based on the original research of papers I-X, which are reproduced in the second part. The first part of the thesis serves to give a background to and an overview of these papers, and is organized as follows. First, in Chapter 2, volume Bragg gratings are described, with emphasis on their usage in lasers and OPOs. Second, the use of volume Bragg gratings for spectral management of lanthanide-doped solid-state lasers is explored in Chapters 3 and 4. Fixed wavelength narrowband lasers and tunable narrowband lasers are investigated, as well as a scheme to obtain a very low laser quantum defect. Third, nonlinear optical parametric oscillators are spectrally narrowed and tuned with volume Bragg gratings, as described in Chapters 5 and 6. Finally, a conclusion of the work is given in Chapter 7.

Chapter 2

Volume Bragg gratings

A Bragg grating consists of a periodic modulation of the material properties along the propagation direction of the electromagnetic radiation. The name stems from the early work in solid-state physics on x-ray diffraction in crystals by W. H. Bragg and W. L. Bragg [24], though here we consider artificially created gratings in a dielectric medium and radiation in the visible or near IR. In this thesis the term *volume Bragg grating* is reserved for a sinusoidal periodic structure written throughout the bulk of a piece of photo-thermo-refractive glass, since this terminology has lately become most widely used in the optics community. Also, all the gratings that were used in this thesis were of the reflective type, why this is the main focus. Still, in principle, there is no reason why the term volume Bragg grating could not apply equally well to gratings with different modulation profiles written in other materials, of which there is a large number. *Volume*, though it may seem superfluous, is used to emphasize that the grating is a bulk optical component, as opposed to *fibre* Bragg gratings. Other names for a volume Bragg grating that can be found in the literature are volume holographic grating, thick hologram grating, bulk (glass) Bragg grating, volumetric (photothermal refractive) Bragg grating and (phase) volume diffractive grating.

Over the last years, volume Bragg gratings have become commercially available from three suppliers in the USA, Optigrate (FL), Ondax (CA) and PD-LD (NJ), from which all the gratings used in this thesis were obtained. The origin of the glass technology used for writing these gratings was a discovery in the 1940s of a photosensitive silicate glass that could be processed by UV radiation and heat treatment, originally intended for image formation [25]. Further development of the glass technology was later done by a group in St. Petersburg in the former Soviet Union/Russia [26–28]. This group found that the photothermal treatment induced a change in the refractive index, that made it possible to write phase gratings in the glass. Initially, the scattering loss in the glass was rather high, a problem that was subsequently solved by a refined processing technology [29].

2.1 Material properties

A main reason for the interest in volume Bragg gratings is their beneficial material properties, with a long lifetime, good stability and relatively easy manufacturing. Here I give a brief overview of the grating manufacturing process based on [29–33]. The goal of the process is to form a periodic modulation of the refractive index in the material, which is done by exposure to UV radiation and thermal development, why the glass is called photo-thermo-refractive.

The typical glass used for the grating formation is a silicate glass with a composition of (mol.%) $70\,SiO_2$, $15\,Na_2O$, $5\,ZnO$, $5\,NaF$, $4\,Al_2O_3$, $1\,KBr$, $0.01\,Ag_2O$, $0.01\,CeO_2$. Presently, glass blanks with an aperture of 50 mm × 50 mm are available [34]. The glass is exposed to an interference pattern formed by a UV laser, where the period of the pattern determines the final grating period. The UV radiation photoionizes Ce^{3+} ions to Ce^{4+}, releasing a free electron. For an efficient process, the UV wavelength should correspond to the Ce^{3+}absorption band, which is centered at 305 nm. Typically, HeCd lasers at 325 nm are used. Subsequently, the produced free electrons are captured by Ag^+, forming Ag^0. At this point, there is only a slight increase of the refractive index, at a level of $\sim 10^{-6}$ for a dosage of about 100 mJ/cm^2 at 325 nm. The exposure process sets the limitations on one of the grating's dimensions, approximately given by to the absorption length at 325 nm of 18 mm.

The next process step is to heat the glass, typically to 520 °C for a few hours. Two things then happen in the material. First, there is a diffusion of the Ag atoms to congregate and form tiny Ag crystals. Second, these Ag particles serve as nucleation centres for formation of NaF crystals. This step leads to the important alteration of the refractive index, that is decreased due to the NaF crystal formation. In addition to the above described process, recent experiments show that also the Br in the glass plays a role for the grating formation [35].

As an example, the decrease of the refractive index is about $0.4 \cdot 10^{-3}$ for a dosage of 1 J/cm^2 at 325 nm and thermal development during 1 hour. The volume fraction of NaF to glass for such a dosage is about 2%, considering the refractive index of 1.32 for NaF [36]. Here, it is important to note the the refractive index modulation strength can be adjusted by changes of the dosage and the thermal development time. The highest reported modulation strength is a refractive index change of $1.2 \cdot 10^{-3}$ [34].

With the process described above, it is possible to tailor the grating properties such as peak wavelength, bandwidth and reflectivity to suit the application needs over a range of parameters. One important limitation is the transparency range of the photo-thermo-refractive glass, reported to be between 550 nm and 2800 nm at a loss level below 0.1 cm^{-1} [29]. The largest source for loss in the gratings is scattering, which most likely has its origin in irregularities in the formation of the NaF crystals. As with all scattering processes, the strength is strongly wavelength dependent, while it is also affected by the manufacturing process [37, 38]. We have measured scattering losses in high reflective ~ 5 mm long gratings of 2% at 1 μm,

6% at 630 nm and 24% at 532 nm. In addition, there is also a little absorption in the glass, as is evident from the tuning of the peak wavelength with increased incident power shown in paper III and paper V. In [38], the absorption in the near IR is shown to depend on the UV exposure process, with an absorption of the order of 10^{-3} cm^{-1}. Other reported material properties are a refractive index around 0.7 μm of $n_0 = 1.49$ [28, 29], a thermal expansion coefficient $\alpha = 8.4\,\mathrm{ppm/K}$ [39], a thermo-optic coefficient $\mathrm{d}n/\mathrm{d}T = 0.05\,\mathrm{ppm/K}$ [40] and a nonlinear refractive index of $n_2 = 3.3 \cdot 10^{-20}\,\mathrm{m^2/W}$ [41] .

Volume Bragg gratings show a good durability, which can be understood from the fact that the grating formation results from a permanent change of the structure of the material. For cw radiation, the gratings have been shown to withstand intensities of 0.25 MW/cm^2 for a 70 μm beam at a power of 45 W [paper V] as well as 10 kW/cm^2 for a 1.5 mm beam at 750 W [42]. In the nanosecond pulsed regime, the damage threshold is $\sim$ 10 J/cm^2[43, 44], only an order of magnitude lower than e.g. BK7 glass that has a damage threshold of 140 J/cm^2 [45]. Furthermore, experiments show that the gratings can be heated up to 400 °C without changing the grating strength [34].

2.2 Grating optical properties

The first theoretical treatment of the optical properties of volume gratings, both in reflection and transmission, was presented by Kogelnik in 1969 [46]. The main assumption of the theory is that the incident light is in the form of plane waves. Subsequently, this plane wave theory has been extended to handle the finer details, (see eg. [47]), though the basic Kogelnik theory is still very useful. Below in Sec. 2.3, I give a short recapitulation of the main assumptions and results.

If the incident beam on the grating has a too narrow beam waist, i.e consist of a wide spectrum of angular components, plane wave theory fails to describe the experiments correctly, and an extended theory is needed. Such a theory was first developed for transmissive volume gratings gratings, either using the method of plane wave decomposition [48–50] or coupled wave analysis in 2 dimensions [51, 52]. An extensive general theory that can be used for numerical simulations, which is valid for both transmission and reflection in all periodic media and all polarization states has also been put forward [53]. Nevertheless, due to its generality it is not easy to draw conclusions for specific cases based on it. The experimental behaviour of narrow beams incident on transmission gratings has also been reported in [54].

Still, this thesis deals with reflective gratings, and at the time when a theory for finite beams and reflective gratings was needed to design our experiments, none was available. This was a main reason for developing the theory which is presented in paper I, which is also supported by experimental examples. An overview of this finite beam theory is given below in Sec. 2.4, as well as a discussion on where the limit to plane-wave theory lies. In parallel to our investigation, a similar theory was

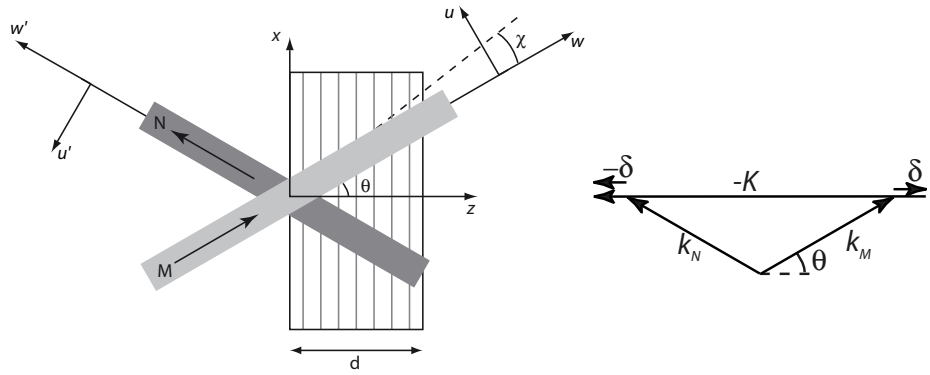

(a) (b)

Figure 2.1: Illustration of the setup and definitions of coordinates in (a) real space and (b) momentum space.

developed as presented in [55], also with a comparison to experiments, although the focus of that work was on a slightly different physical situation.

Setup

As shown in Fig. 2.1 (a), we assume a grating of thickness d with a periodic modulation f of the refractive index in the z-direction, $n(z) = n_0 + n_1 f(z)$, where n_1 is the strength of the modulation with period Λ. For a sinusoidal grating, $f(z) = \sin(Kz) = \sum_{l=-\infty}^{\infty} c_l e^{ilKz}$. For the Fourier series expansion, the grating vector $\mathbf{K} = (0, 0, 2\pi/\Lambda)$ is used as a basis, and the only non-zero coefficients are $c_{\pm 1} = \pm\frac{1}{2i}$, meaning that we will only have first order diffraction. To account for other types of gratings, other periodic functions and their Fourier expansion could be used instead, yielding diffraction into higher orders too. Furthermore, we assume an infinite extent of the grating in x and y and that the medium surrounding the grating has the same average index n_0. The refraction that occurs for a real grating surrounded by air can easily be dealt with separately.

Incident on the grating, we consider a beam with a field $M_{\text{in}}(\mathbf{r})$ and a propagation vector $\mathbf{k}_M$ that makes an angle θ with respect to the z-axis, as shown in Fig. 2.1.

Next we consider the Bragg condition which suggests that there will be a diffracted beam $N(\mathbf{r})$ in the direction $\mathbf{k}_N$, given by

$$\mathbf{k}_N = \mathbf{k}_M - \mathbf{K} + 2\boldsymbol{\delta}, \tag{2.1}$$

as shown in Fig. 2.1(b). Here we allow for a small wavevector mismatch given by $\boldsymbol{\delta} = \delta\hat{\mathbf{z}}$, that will be used to model non-perfect phase matching to obtain the

bandwidth of the grating. The diffracted beam has the same wavelength as the incident one, why $k_N = k_M = 2\pi n_0/\lambda \equiv \beta$. Also, momentum is preserved in the x direction, whereby $\mathbf{k}_M = \beta(\sin\theta\hat{\mathbf{x}} + \cos\theta\hat{\mathbf{z}})$ and $\mathbf{k}_N = \beta(\sin\theta\hat{\mathbf{x}} - \cos\theta\hat{\mathbf{z}})$. For perfect Bragg matching, (2.1) is reduced to the well known expression $2k_B\cos\theta_0 = K$, or in term of length,

$$\lambda_B = 2n_0\Lambda\cos\theta_0. \tag{2.2}$$

As shown in Fig. 2.1, we also define rotated coordinates uvw and $u'v'w'$ along the beam direction of M and N, respectively, as well as far field angles $(\chi, \psi) = (u/w, v/w)$ and $(\chi', \psi') = (u'/w', v'/w')$.

Wave equation

Next we assume light polarized along the y-axis orthogonal to the plane of incidence (s- or TE-polarized), for which the wave equation is $\left(\nabla^2 + k^2(z)\right) E(\mathbf{r}) = 0$. Here we do not treat p-polarization, since the wave equation becomes more complicated. As shown experimentally in paper I, p-polarization is also of less practical interest.

Inserting the periodic index variation into the wave equation, we get

$$\left(\nabla^2 + \beta^2 + 4\beta\kappa f(z)\right) E(\mathbf{r}) = 0, \tag{2.3}$$

where $\kappa = \pi n_1/\lambda$ is the coupling strength.

Since the M and N fields are the ones predicted by the Bragg condition, as well as the only ones observed by us in experiments, we assume a total electric field inside the grating of the form

$$E(\mathbf{r}) = M(\mathbf{r}) + N(\mathbf{r}) = \tilde{M}(\mathbf{r})e^{-i\mathbf{k_M}\cdot\mathbf{r}} + \tilde{N}(\mathbf{r})e^{-i\mathbf{k_N}\cdot\mathbf{r}}. \tag{2.4}$$

If we assume that the only incident light, denoted $M_{\text{in}}(\mathbf{r}) = M_0(\mathbf{r})\exp(-i\mathbf{k}_M\cdot\mathbf{r})$, is from the negative z-direction, we can state the boundary conditions as:

$$\tilde{M}(x, y, 0) = M_0(x, y, 0), \tag{2.5}$$

$$\tilde{N}(x, y, d) = 0. \tag{2.6}$$

2.3 Plane wave theory

If we assume that the incident wave on the grating is a plane wave in the $\mathbf{k}_M$-direction, $M_{\text{in}}(\mathbf{r}) = M_0\exp(-i\mathbf{k}_M\cdot\mathbf{r})$, we can simplify the fields in the grating to only have a z-dependence. With these assumptions, the electric field of (2.4) is inserted into the wave equation (2.3). At this point, we assume a slowly varying field envelope and neglect second order derivatives in z. By insertion of the Fourier expansion of $f(z)$, it can be seen that there is a coupling between the the forward and backward fields at Bragg matching. The differential equation can be further simplified by assuming that all fast oscillating exponential terms average to zero.

Finally, terms of the same exponents are collected and the change of variables $\tilde{M} = \bar{M}e^{-i\delta z}$ and $\tilde{N} = \bar{N}e^{i\delta z}$ is done. The resulting differential equations are

$$\frac{\mathrm{d}\bar{M}}{\mathrm{d}z} = i\delta\bar{M} + \kappa'\bar{N}, \tag{2.7}$$

$$\frac{\mathrm{d}\bar{N}}{\mathrm{d}z} = \kappa'\bar{M} - i\delta\bar{N}, \tag{2.8}$$

which are called the coupled wave equations. Here $\kappa' = \kappa/\cos\theta$. The boundary conditions are given from (2.5), (2.6) as

$$\tilde{M}(0) = \bar{M}(0) = M_0 \tag{2.9}$$

$$\bar{N}(d) = 0. \tag{2.10}$$

A solution can be found in the standard way by computing the eigenvalues, $\pm\gamma = \pm\sqrt{\kappa'^2 - \delta^2}$, and eigenvectors, $(\pm\gamma + i\delta, \kappa')$, of the coefficient matrix. To simplify further expressions, at this point we define two functions, t and r, which represent the interesting parts of the solution in transmission and reflection, respectively:

$$t(\delta, z) = \frac{-\gamma\cosh\gamma(d-z) + i\delta\sinh\gamma(d-z)}{-\gamma\cosh\gamma d + i\delta\sinh\gamma d}, \tag{2.11}$$

$$r(\delta, z) = \frac{\kappa'\sinh\gamma(d-z)}{-\gamma\cosh\gamma d + i\delta\sinh\gamma d}. \tag{2.12}$$

By the use of these, the solutions inside the grating can be expressed as:

$$M(\mathbf{r}) = M_0 t(\delta, z) e^{-i(\mathbf{k}_M + \boldsymbol{\delta})\cdot\mathbf{r}}, \tag{2.13}$$

$$N(\mathbf{r}) = M_0 r(\delta, z) e^{-i(\mathbf{k}_N - \boldsymbol{\delta})\cdot\mathbf{r}}. \tag{2.14}$$

From this, the total power reflectivity is found as

$$R_{\mathrm{pw}}(\delta) \equiv \left|\frac{N(x,y,0)}{M_{\mathrm{in}}(x,y,0)}\right|^2 = |r(\delta,0)|^2 = \frac{\kappa'^2\sinh^2\left(\sqrt{\kappa'^2-\delta^2}\,d\right)}{\kappa'^2\cosh^2\left(\sqrt{\kappa'^2-\delta^2}\,d\right) - \delta^2}, \tag{2.15}$$

where we recall that δ is the detuning from perfect Bragg matching given by $\delta = K/2 - \beta\cos\theta = \pi/\Lambda - 2\pi n_0\cos\theta/\lambda$. The phase of the reflection is given by

$$\begin{aligned}\varphi_{\mathrm{pw}}(\delta) &\equiv \arg\left(\frac{N(x,y,0)}{M_{\mathrm{in}}(x,y,0)}\right) = \arg\left(r(\delta,0)\right) \\ &= \arctan\left(\frac{\delta}{\sqrt{\kappa'^2-\delta^2}}\tanh\left(\sqrt{\kappa'^2-\delta^2}\,d\right)\right) + m\pi,\end{aligned} \tag{2.16}$$

where m is an integer. To give the phase continuity, m should be altered at the reflectivity zero points. An example of grating reflective properties is given in Fig. 2.2 for the grating that was used in the experiments of paper III and paper IV.

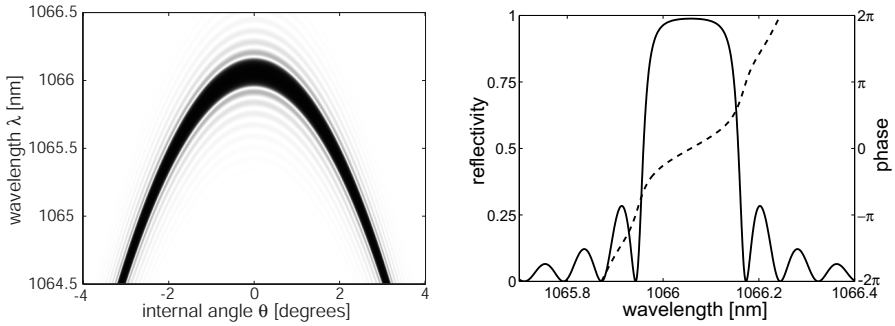

(a) (b)

Figure 2.2: Example of grating properties: (a) map of grating reflectivity; (b) grating reflectivity (solid) and phase (dashed) at normal incidence. Theoretical simulations based on measurements [paper III, paper IV].

The three most important characteristics of a filter are its centre wavelength, peak response and bandwidth. The centre wavelength is given by the Bragg condition (2.2). From (2.15) it can be seen that the peak reflectivity is

$$R_{\max} = \tanh^2 \kappa' d, \tag{2.17}$$

motivating calling κ the strength of the coupling. To get a simple expression for the bandwidth, we use the zero-to-zero bandwidth, defined as the distance between the two zeros closest to the peak, which are located at $\delta_0 = \pm\sqrt{\kappa'^2 + \pi^2/d^2}$. From this we get the zero-to-zero spectral bandwidth at constant incidence angle

$$\Delta\lambda = \lambda_B \sqrt{\frac{n_1^2}{n_0^2 \cos^4\theta_0} + \frac{4\Lambda^2}{d^2}}. \tag{2.18}$$

The FWHM bandwidth $\Delta\lambda_{1/2}$ is smaller than the zero-to-zero bandwidth $\Delta\lambda$ by a factor that depends on the grating reflectivity. $\Delta\lambda_{1/2} = 0.44\Delta\lambda$ for weak gratings and $\Delta\lambda_{1/2} = \Delta\lambda$ for strong gratings.

For the angular bandwidth $\Delta\theta$ at constant wavelength, two separate cases can be identified, normal and oblique incidence, which are separated at approximately $\theta \sim \Delta\theta$. The reason for this division in two cases can be understood by considering Fig. 2.2(a), where it is very clear that the angular bandwidth at $\theta = 0$ is much larger than at other angles. For normal incidence, we get

$$\Delta\theta_n = 2\sqrt{\frac{\Delta\lambda}{\lambda_B}} \tag{2.19}$$

while for oblique incidence

$$\Delta\theta_o = \frac{1}{\tan\theta_0}\frac{\Delta\lambda}{\lambda_B}. \tag{2.20}$$

At this point it should be noted that the Bragg grating can be completely described either by its optical properties in terms of peak wavelength λ_B, peak reflectivity $R_{\max}$ and bandwidth $\Delta\lambda$ or by its material properties given by the grating period Λ, refractive index modulation n_1 and thickness d. For the example grating, the optical parameters are $\lambda_B = 1066.06\,\text{nm}$, $R_{\max} = 98.8\%$ and $\Delta\lambda = 0.23\,\text{nm}$, while the material ones are $\Lambda = 358$ nm, $n_1 = 2.2 \cdot 10^{-4}$ and $d = 4.5\,\text{mm}$, which corresponds to a number of 12,000 periods throughout the grating. From the bandwidth expressions above, one can see that to achieve a very narrow bandwidth, the grating should be very long with as small modulation as possible to still reach a high enough reflectivity. To the author's knowledge, the most narrowband volume Bragg grating reported had a FWHM bandwidth of 0.013 nm or 7 GHz for 25% reflectivity [56], while the reflectivity can at least reach 99.7% (in addition to 0.1% transmission and 0.2% scattering loss), as measured for the grating used in paper V.

2.4 Finite beam theory

If the incident beam on the grating is not a plane-wave, the optical properties of the grating is no longer as described in the previous section, but rather as for a finite beam, the subject of this section. Here, I give a summary of the theory for finite beams incident on a volume Bragg grating based on the findings in paper I.

Plane wave theory limit

In order to establish a limit for when the plane wave approximation is no longer valid, the angular bandwidth of the grating must be considered. Due to the large difference in angular bandwidth for normal and oblique incidence, the limits between the plane wave and finite beam regimes are quite different for the two. An approximate condition, or rule-of-thumb, for when the plane wave theory is valid can be obtained by comparing the grating's angular bandwidth with the incident beam's angular divergence. In paper I, we show that a resonable limit is found for normal incidence as

$$\frac{\pi^2}{4} n_0^2 \frac{w_{e^{-2}}^2}{\lambda_B^2} \frac{\Delta\lambda}{\lambda_B} > 1, \tag{2.21}$$

and for oblique indcidence as

$$\frac{\pi}{4} n_0 \frac{w_{e^{-2}}}{\lambda_B} \frac{\Delta\lambda}{\lambda_B} > \sin\theta_0. \tag{2.22}$$

The beam parameters enter the expressions through $w_{e^{-2}}$, which is the e^{-2} intensity beam waist radius, as measured in air, while the incidence angle θ_0 still is defined internally. As can be seen, the limitation is much more strict for oblique incidence, which is where it has the largest practical consequences.

Finite beam solutions

Here, two alternative solutions are presented, based on either 3-dimensional coupled wave equations or plane-wave decomposition. The initial assumption is that the incident light is a finite beam with a varying distribution in the transverse direction, $M_{\text{in}}(\mathbf{r}) = M_0(\mathbf{r}) \exp(-i\mathbf{k}_M \cdot \mathbf{r})$.

3-dimensional coupled wave equations

For this solution, we can essentially follow the same procedure as for the plane-waves solution, except that there are now also an x- and a y-dependence to take into account. We insert the electric field of (2.4) into the wave equation (2.3) and retain the second order derivatives in x and y to allow for a sharply focussed beam. Still, we neglect the second order derivatives in z. Effectively, this means that we restrict the incidence angle to small enough angles, so that the variation in z is slower than in x. The coupled-wave equations are next obtained by noting the coupling between $\tilde{M}$ and $\tilde{N}$ at Bragg matching, neglecting fast oscillating terms, collecting terms with the same exponent and transforming to $\bar{M}$ and $\bar{N}$. In addition, the differentiations in the x- and y-directions are handled by the Fourier transformation. Here we use the inverse transformation in order to avoid minus signs in the later far-field results. We denote $\mathfrak{F}_{xy}^{-1}[\bar{M}(x,y)](\rho,\sigma) = \iint \bar{M}(x,y) \exp(i(x\rho+y\sigma))\mathrm{d}x\mathrm{d}y = \check{M}(\rho,\sigma)$, etc. To simplify the expressions, we define a generalized phase mismatch $\delta' = \rho \tan\theta + (\rho^2+\sigma^2)/(2\beta\cos\theta) + \delta$ and arrive at the coupled wave equations

$$\frac{\mathrm{d}\check{M}}{\mathrm{d}z} = i\delta'\check{M} + \kappa'\check{N}, \tag{2.23}$$

$$\frac{\mathrm{d}\check{N}}{\mathrm{d}z} = \kappa'\check{M} - i\delta'\check{N}. \tag{2.24}$$

Formally, these are identical to (2.7), (2.8), so the solutions are formally identical as well,

$$\check{M}(\rho,\sigma) = \check{M}_0\, t(\delta'(\rho,\sigma), z), \tag{2.25}$$

$$\check{N}(\rho,\sigma) = \check{M}_0\, r(\delta'(\rho,\sigma), z), \tag{2.26}$$

bearing in mind the transformed boundary condition $\check{M}_0(\rho,\sigma) = \mathfrak{F}_{xy}^{-1}[M_0(x,y,0)]$. Finally, we recover the spatial dependence of the fields by a forward Fourier transformation

$$M(\mathbf{r}) = \mathfrak{F}_{\rho\sigma}\left[\check{M}_0(\rho,\sigma)\, t(\delta'(\rho,\sigma), z)\right] e^{-i(\mathbf{k}_M+\boldsymbol{\delta})\cdot\mathbf{r}}, \tag{2.27}$$

$$N(\mathbf{r}) = \mathfrak{F}_{\rho\sigma}\left[\check{M}_0(\rho,\sigma)\, r(\delta'(\rho,\sigma), z)\right] e^{-i(\mathbf{k}_N-\boldsymbol{\delta})\cdot\mathbf{r}}. \tag{2.28}$$

From these expressions, it is clear that for a finite beam, the near-field solution is a convolution of the incident beam in the far-field with the plane wave filter functions, except that in the finite beam case, a generalized phase mismatch δ' should be used.

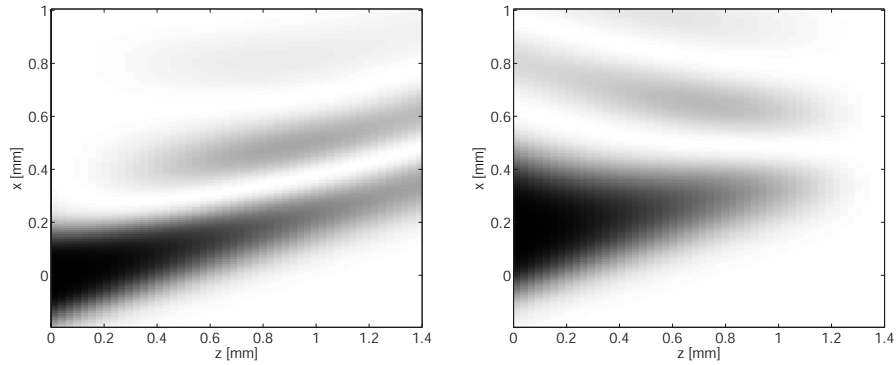

(a) (b)

Figure 2.3: Example of the intensity distribution inside a Bragg grating under oblique incidence; (a) transmitted intensity M and (b) reflected intensity N. The simulation is based on the grating in paper VII, and the incident beam from the left is Bragg matched at 16° internal angle with a waist of 165 μm at $z = 0$.

An example of the fields in a grating at oblique incidence, using (2.27) and (2.28) is shown in Fig. 2.3.

To determine the power reflectivity of a finite beam, we consider an input beam M_{in}, which is normalized such that $\iint \left|\check{M}_0\right|^2 \mathrm{d}\rho\mathrm{d}\sigma = 1$. Then, by Parsevals formula, we get

$$R = \iint_{-\infty}^{\infty} |N(x, y, 0)|^2 \,\mathrm{d}x\mathrm{d}y = \iint_{-\infty}^{\infty} \left|\check{M}_0(\rho, \sigma)\right|^2 R_{\text{pw}}(\delta'(\rho, \sigma))\mathrm{d}\rho\mathrm{d}\sigma. \tag{2.29}$$

It can be seen that the reflectivity difference between a plane wave and a finite beam is contained in the phase mismatch δ' and weighted by the spatial distribution of the incident beam.

Equations (2.27) and (2.28) are valid within the grating itself. Of great importance is additionally the far-field behaviour. For this, we use the Rayleigh-Sommerfeld diffraction formula (see e.g. [57]) in the Fraunhofer approximation, with the fields at the grating boundaries as the source terms, separately for the M and N fields. For convenience, we use the coordinates of the incident beam itself, (u, v) and (χ, ψ) as shown in Fig. (2.1). For this, we need to convert to Fourier transforms in the new coordinate system, which we denote by $\hat{M}_0(\rho, \sigma) \equiv \mathfrak{F}_{uv}^{-1}[M_0(u, v, \tilde{w})](\rho, \sigma)$, where $\tilde{w}$ is the position of the beam waist. The far-field solutions are then given by (for normalization constants C, C')

$$M_{\text{ff}}(\chi, \psi) = C\hat{M}_0(\beta\chi, \beta\psi)\, t(\delta'(\beta\chi\cos\theta, \beta\psi), d), \tag{2.30}$$

$$N_{\text{ff}}(\chi', \psi') = C'\hat{M}_0(-\beta\chi', \beta\psi')\, r(\delta'(-\beta\chi'\cos\theta, \beta\psi'), 0). \tag{2.31}$$

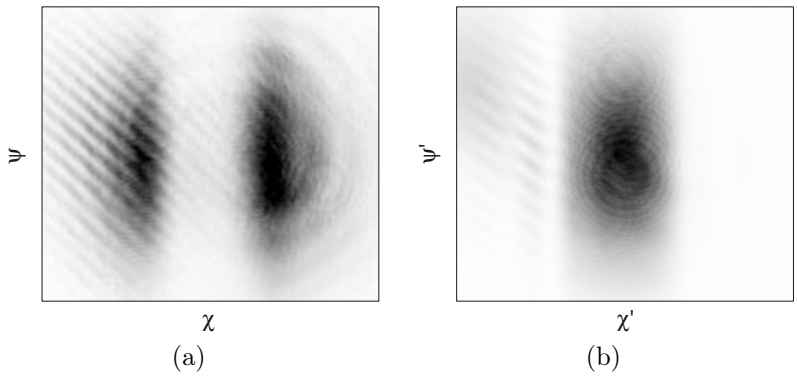

(a) (b)

Figure 2.4: Example of the far field intensity after oblique incidence of a Gaussian beam on a Bragg grating of (a) transmitted field M and (b) reflected field N. Experiments with the grating in paper VII.

The interpretation of this result is straightforward: for a finite beam, the far-field solutions are a multiplication of the far-field of the incident beam by the plane wave filter functions using the modified generalized phase mismatch $\delta'(\beta\chi\cos\theta, \beta\psi) = \beta\chi\sin\theta + \beta(\chi^2\cos\theta + \psi^2/\cos\theta)/2 + \delta$.

An experimental example for the far field distribution of the reflected and transmitted beam is shown in Fig. 2.4. It can be seen that the centre of the beam is selected by the grating and reflected, while the rest is transmitted.

Plane wave decomposition

An alternative method to find the finite beam solutions is to decompose the incoming field into its plane wave components, each with its own angle, and then treat each component separately using the plane wave solutions. This method has also been investigated by Hsieh *et al.* [55], though the treatment we present here and in paper I goes into more details and additionally simplifies the most important results.

The decomposition of the incident wave is done by applying both an inverse and a forward Fourier transform to the incident beam in the uv-plane, whereby we get [57]

$$M_{\text{in}}(\mathbf{r}) = M_0(\mathbf{r})e^{-i\beta w} = \beta^2 \iint_{-\infty}^{\infty} \mathrm{d}\chi\mathrm{d}\psi \hat{M}_0(\beta\chi, \beta\psi)e^{-i\mathbf{k}^*\cdot\mathbf{r}}, \tag{2.32}$$

where $\mathbf{k}^* = \beta(\chi\hat{\mathbf{u}} + \psi\hat{\mathbf{v}} + \sqrt{1-\chi^2-\psi^2}\hat{\mathbf{w}})$. Thus, the incident beam can be seen as a distribution of plane waves with amplitudes $\beta^2\mathrm{d}\chi\mathrm{d}\psi\hat{M}_0(\beta\chi, \beta\psi)$, each one

travelling in the $\mathbf{k}^*$ direction. Accordingly, the incidence angle of each plane wave component, α, is given by

$$\cos\alpha = \frac{\mathbf{k}^*}{\beta}\cdot\hat{\mathbf{z}} \cong -\chi\sin\theta + \cos\theta - (\chi^2+\psi^2)\cos\theta/2, \tag{2.33}$$

why the new phase mismatch is $\delta^*(\beta\chi,\beta\psi) = \beta\chi\sin\theta + \beta(\chi^2+\psi^2)\cos\theta/2 + \delta$. In conclusion, just as for the method of coupled wave equations, the plane wave decomposition solution essentially corresponds to modifying the phase mismatch.

For a plane wave, the reflected and transmitted fields are simply given by (2.13), (2.14), why the transmitted M-beam and reflected N-beam can be found directly by multiplication of the plane wave solutions with the integrand. This is allowed since the grating is a linear filter, why the order of the two operations of filtering and plane wave decomposition is unimportant. Expressed in the coordinates of the grating, the fields inside the grating are

$$M(\mathbf{r}) = \mathfrak{F}_{\rho\sigma}\left[\check{M}_0(\rho,\sigma)t(\delta^*(\tfrac{\rho}{\cos\theta},\sigma),z)\right]e^{-i(\mathbf{k}_M+\boldsymbol{\delta})\cdot\mathbf{r}}, \tag{2.34}$$

$$N(\mathbf{r}) = \mathfrak{F}_{\rho\sigma}\left[\check{M}_0(\rho,\sigma)r(\delta^*(\tfrac{\rho}{\cos\theta},\sigma),z)\right]e^{-i(\mathbf{k}_N-\boldsymbol{\delta})\cdot\mathbf{r}}. \tag{2.35}$$

As expected, there is a good correspondence with the results from the coupled wave approch, where the slight difference between δ^* and δ' is due to applying approximations in different order, but has very limited practical impact.

Next, the far-fields are found by a Fourier transformation (in the Fraunhofer approximation) [57], yielding

$$M_{\text{ff}}(\chi,\psi) = C\hat{M}_0(\beta\chi,\beta\psi)t(\delta^*(\beta\chi,\beta\psi),d), \tag{2.36}$$

$$N_{\text{ff}}(\chi',\psi') = C'\hat{M}_0(-\beta\chi',\beta\psi')r(\delta^*(-\beta\chi',\beta\psi'),0). \tag{2.37}$$

Once more, we get almost the same result as for the coupled wave solution approach. Finally, just as for the coupled wave solutions, the total reflected power is found by an integration, yielding a similar expression, due to the similarities between the solutions.

2.5 Usage in laser cavities

Angle tuning

Wide tuning of the reflected wavelength of a volume Bragg grating can be achieved by rotation of the grating to change the angle of incidence, as can be seen from the Bragg condition (2.2). For narrow beams, there are potentially some complications, as is further explained in Sec. 2.4. Another problem that must be taken care of is the beam steering that occurs, since every wavelength will be reflected at a different angle, as shown in Fig. 2.5(a). A solution to this problem is to use a retroreflector

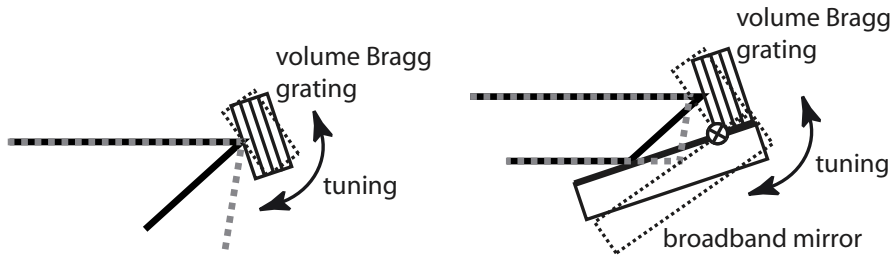

Figure 2.5: Angular tuning and the beam steering problem, illustrated for two different wavelengths (solid and dashed lines), which are reflected at two different angles. (a) No compensation, (b) Use of a retroreflector design to remedy the problem.

design, where a second broadband mirror is attached to the grating at 90°. By simultaneous rotation of the grating and the broadband mirror around an axis at the intersection of the two, the wavelength is tuned but the direction and position of the exiting beam is fixed, without beem steering, as illustrated in Fig. 2.5(b). This idea was first presented in [58], and was used intracavity for the first time for the tunable devices in paper VII, paper VIII and paper X.

Thermal tuning

By considering the Bragg condition (2.2), it can be seen that the thermal tuning of the grating peak wavelength is affected by both the thermal expansion α and the thermo-optic coefficient $\frac{\mathrm{d}n}{\mathrm{d}T}$. Since the effect is much smaller than the angle-tuning, it is of most practical interest for normal incidence, which is modelled here:

$$\frac{\mathrm{d}\lambda_B}{\mathrm{d}T} = 2\frac{\mathrm{d}n_0}{\mathrm{d}T}\Lambda + 2n_0\frac{\mathrm{d}\Lambda}{\mathrm{d}T} = \lambda_B\left(\frac{1}{n_0}\frac{\mathrm{d}n_0}{\mathrm{d}T} + \alpha\right). \tag{2.38}$$

From the material properties in Sec. 2.1, the tuning of the grating at 1066 nm is expected to be $\mathrm{d}\lambda_B/\mathrm{d}T = 9\,\mathrm{pm/K}$. Direct measurements, normalized to a wavelength of 1 μm, give values around $\mathrm{d}\lambda_B/\mathrm{d}T/\lambda_B \cong 8$ to 12 ppm/K [paper IX], [59, 60]. Thus there is a fairly good correspondance between the theory with inserted material parameters and direct measurements.

Compared to the rather wide tuning range that can be reached by angle tuning, the thermal tuning is rather limited. Consequently, its usefulness for tunable lasers is limited, though it would prove useful e.g. to fine-tune a grating to match a specific resonance wavelength. Incidentally, it can also be used as an indicator of absorption in the grating and subsequent heating, as shown in paper III and paper V.

Alignment of intra-cavity gratings

Alignment of a cavity that contains a volume Bragg grating presents a practical problem, that is more difficult than the alignment of ordinary metallic or dieletric mirrors. In contrast to ordinary mirrors, the surface of the grating cannot directly be used for alignment, since it is in general tilted with respect to the grating vector. Therefore, lasers at any wavelength, such as the commonly used HeNe-laser, cannot be used for alignment, since the grating only reflects wavelengths that are Bragg-matched. For the alignment of the cavities in this thesis, a number of alignment methods have been developed, as presented below. As usual, the alignment is most critical in low gain systems, such as the Yb lasers, which require the most sophisticated methods, while high gain devices such as the OPOs are fairly easy to align.

If possible, the best alignment method is to use a wavelength that matches the grating, either from a tunable laser such as a Ti:sapphire laser or from another laser that is locked by an identical grating.

If such a laser is not available, another method for gratings used at normal incidence is the following. First, a free running laser is set up and aligned with conventional methods, using a broadband dieletric mirror as an auxilliary output coupler. The Bragg grating is then placed in the output beam. If the free running cavity is at a shorter wavelength than the Bragg grating at normal incidence, by rotating the grating it is rather easy to find the angle for which the grating is highly reflective. This reflected spot can then be used to align one degree of freedom of the grating, with the reflected spot in the correct plane. Alignment and oscillation of the cavity at the grating wavelength is then obtained by rotating the grating back towards normal incidence, until oscillation is found. This can be done with or without the auxilliary conventional output coupler. If the free running cavity wavelength is not too far from the grating peak, it might also be the case that there is a weak residual reflection in the grating, even at normal incidence. In this case, alignment can be performed by observing this reflection with a sensitive detector, most conveniently behind the grating, after the weak Bragg-reflected beam has been reflected in the auxilliary mirror and transmitted through the grating.

A third method to align the grating is to carefully measure the deviation of the grating vector and the surfaces, by simultaneously observing the Bragg reflection and the surface reflections. A conventional HeNe laser can then be used for the cavity alignment by carefully misaligning the grating's surface reflections by the measured value. This method is most useful for realigning a grating that has once been aligned, by just repositioning the surface reflections at the correct position.

Finally, for high gain systems such as fibre lasers, which have strong, directional fluorescence emitted in the intended cavity direction, this fluorescence can be used for the alignment. The grating is then placed in the beam of fluorescence, and a spectrum analyzer is placed behind. The grating peak reflectivity is then visible as a hole in the fluorescence spectrum. Now the grating is rotated to maximize the wavelength of the hole, which then yields a grating vector that is normal to the

incident fluorescence, and thus an aligned cavity.

Bragg grating mirror in Fabry-Perot resonator

When a volume Bragg grating is used as one of the mirrors of a Fabry-Perot cavity, the longitudinal mode spacing, i.e. the free spectral range (Sec. 3.9), is an important property that needs to be considered. In fact, for a short cavity and a thick grating, the grating's physical length can be a substantial part of the total cavity length. However, the length that is needed for evaluation of the free spaectral range of the cavity should be obtained from the phase variation of the reflected light from the grating. This issue was studied in paper III, while a similar investigation for fibre Bragg gratings is presented in [61].

Light with a wave vector $k_B+\delta$ that travels a distance l aquires a phase $\varphi_0+\varphi = (k_B+\delta)l$. In comparison, the phase aquired from a reflection of a Bragg grating is given in (2.16). To be able to do a comparison, one should note that the phase variation around the Bragg peak is approximately linear, as shown in Fig. 2.2(b). A Taylor expansion of the phase yields $\varphi(\delta/\kappa) = -R_{\max}^{1/2}\delta/\kappa + O((\delta/\kappa)^3)$. From this it is possible to deduce an effective optical distance that should be used for calculations of the free spectral range. The roundtrip distance is

$$2L_{\text{cav}} = \pm\varphi/\delta = \frac{R_{\max}^{1/2}}{\operatorname{arctanh}\, R_{\max}^{1/2}} d. \tag{2.39}$$

For high reflectivities, L_{cav} goes to zero, which can also be understood intuitively, since for a strong grating, most of the reflection is taking place in the initial part of the grating. For the example grating at 1066 nm, the effective cavity length is 0.8 mm, compared to the physical length of 4 mm. An experimental demonstration of this effect is given in paper III. Finally, it should be noted that the validity of this discussion is limited by the assumption that we stay close to the Bragg peak, though this is most often the case.

For some applications, the thermal variation of the grating's effective length is of importance, e.g. the experiment described in paper IV. By differentiating the effective length with temperature, one arrives at $\mathrm{d}L_{\text{cav}}/\mathrm{d}T = \alpha d(1-R_{\max})/2$. Here it is assumed that the grating strength is not altered by temperature changes around room temperature, since they are rather far away from the grating development temperatures. For the example grating presented above, this tuning rate is $\mathrm{d}L_{\text{cav}}/\mathrm{d}T = 0.2\,\text{nm/K}$ [paper IV].

Spatial filtering

Thanks to the strong angular selectivity of reflective volume Bragg gratings, especially for oblique incidence, as shown by (2.20), these gratings can be used for spatial filtering. If the grating is used as a mirror in a laser cavity, this can be used to promote only the lowest transverse mode to oscillate, since higher order modes

have larger angular spread and thus are less efficiently reflected in the grating. In paper I, we give an example where the transmission is 3.5 times higher for TEM_{10} and 7 times higher for TEM_{20}, compared to the TEM_{00} mode. Over a number of cavity roundtrips, this gives a very strong selectivity in the selected transverse direction.

Transmission volume Bragg gratings also show a strong angular selectivity, given by $\Delta\theta = \Delta\lambda/(\lambda_B \sin\theta)$ [50]. Compared to (2.20), it can be seen that the selectivity is approximately the same as for reflection gratings at oblique incidence. With transmissive gratings, also experimental demonstrations of laser transverse mode improvement have been made [62–64].

2.6 Applications

Over the last years, there has been a large interest in using volume Bragg gratings in a number of different laser applications. Here I give an overview of the available literature to this date.

Semiconductor lasers The first laser application of a volume Bragg grating was for wavelength-locking of a high power laser diode [59], where a potential application is pumping of solid-state lasers. Similar work has also been presented by Zheng *et al.*, along with additional spatial improvement of the locked-laser [65–68] and by Glebov's group [40]. A review on volume Bragg grating locking of diode lasers can be found in [69]. The most narrow locking of a high power diode array this far is 7 GHz bandwidth in a laser used for singlet delta oxygen pumping [56]. Recently, these narrowed laser diodes have also been utilized for optical pumping of alkali vapor lasers [70–74]. It has also been shown that dual-wavelength operation is possible [75]. Other semiconductor lasers that have been locked are vertical external cavity surface emitting lasers [76, 77] and a tapered diode laser [78]. Thanks to the narrowed spectrum, efficient intra-cavity frequency doubling was possible in [77]. In the low power regime, commercial products of locked edge-emitting diodes are available with a single longitudinal mode, giving a bandwidth of 50 MHz with a side mode suppression of 30 dB at output powers of tens of milliwatts in the 600 nm to 800 nm spectral range [79].

Beam combining To boost laser intensity, coupling of a number of lasers into a single beam is an interesting solution. Volume Bragg gratings have been used in this field both for coherent coupling of two diodes [80], as well as for incoherent beam combining [42, 81–83] and spectral beam combining with a transversely chirped grating [84].

Pulsed lasers For pulsed laser amplifiers, there are two demonstrations of volume-Bragg-grating usage. For chirped pulse amplification, a longitudinally chirped grating has been used in both the stretching and compression stage [85]. In a regen-

erative pulse amplifier, a Bragg grating was used to supress amplified spontaneous emission to achieve a cleaner pulse spectrum [86].

Fibre lasers Integration of fibre Bragg gratings in high power fibre lasers can be a problem, why there are some benefits from use of a bulk component like a volume Bragg grating. This idea is further explored in [87, 88].

Solid state lasers A major part of this thesis is devoted to the locking and tuning of solid-state lasers, as explained in detail in Chapter 4. For completeness, the available literature is also listed here. The laser materials for which locking has been demonstrated are Tm:YLF [89], ErYb:glass [paper II], Nd:$GdVO_4$, [paper III, paper IV] and [90–92], Nd:YAG [64], Yb:KYW [paper V, paper VI, paper VII, paper VIII], Ti:sapphire [60, 93–96], Cr:LiSAF [60, 93] and alexandrite [93].

OPOs Locking of OPOs is treated in Chapter 6, here I just list the available publications. The first demonstration was at a signal wavelength of 975 nm with PPKTP [paper IX]. Subsequently there has been a number of publications on near-degenerate locking at 2.1 μm [97–102], using PPKTP, PPLN and MgO:PPLN. A tunable ring OPO with PPKTP at 760 nm is presented in paper X. Additionally, there has been a demonstration of locking at 709 nm for subsequent generation of 193 nm radiation [103, 104]. In a recent experiment, we have also demonstrated a tunable OPO around 1 μm using a transversely chirped Bragg grating [paper J].

2.7 Other techniques for spectral selection

Below I give a brief description of filter techniques other than volume Bragg gratings that are frequently used for spectral – and to some extent also spatial – discrimination in lasers or OPOs.

Bragg gratings in other materials

Bragg gratings of both reflective and transmissive types have a long history of being written in other materials than the photo-thermo-refractive glass that is the focus of this thesis. The most important classes of materials that have been used are photorefractive crystals, photopolymers and dichromated gelatin [57]. In comparison with the glass, the limitations for their applicablilty are lifetime-problems and a limited resistance to optical damage. Examples of applications in laser devices are spatial improvement of a laser with a transmission type photopolymer grating [62] and OPO locking and bandwidth narrowing with reflection type photorefractive gratings [105–107].

Transmission volume Bragg gratings

A transmission-type volume Bragg grating is rotated so that the grating vector is close to orthogonal to the propagation direction of the incident light, i.e. the grating fringes are orthogonal the grating surface. With this geometry, the diffracted wave is in the forward direction, at a fairly small angle to the incident light.

As discussed above, transmission volume gratings are equally useful as reflection gratings at oblique incidence for spatial filtering. This has been shown to improve the transverse properties in both solid-state laser cavities [62, 64] and a semiconductor laser external cavity [63].

A comparison can also be made to acousto-optic modulators in the Bragg regime. These are transmisson gratings, where the grating is created via the elasto-optic effect by a sound wave in a material. One difference is that since the grating is moving with the soundwave, the diffracted wave also experiences a shift in frequency, that can be understood as a Doppler-shift [108].

Multilayer coatings

Dielectric multilayer coatings is a widely used optical technology and used in almost all high power laser mirrors. In contrast to volume Bragg gratings, the multilayer coatings usually consist of only few layers, each with a rather strong refractive index modulation of about 0.1. As can be seen from (2.18), the bandwidth of such a filter is inevitably rather large. Still, this technology can be very useful (usually in combination with an etalon), e.g. to select a low gain peak in Nd:YAG to enforce lasing at 946 nm [109] or 899 nm [110], or to favour lasing at short wavelengths in Yb:YSO [111].

Fibre Bragg gratings

In a fibre Bragg grating, a periodic structure is written in the core of a single mode optical fibre, giving similar longitudinal properties as for a volume Bragg grating, although transversely they are rather different. The first demonstration of a fibre Bragg grating was in [112], and after the report in [113] of an improved transverse writing method, the field has grown substantially. These gratings are very useful for single mode fibre applications, such as low power fibre lasers, telecommunication and sensing. However, since it is difficult to couple light into a fibre without large loss, the applicability in conjuncture with bulk optical components is rather limited.

Fabry-Pérot cavities: etalons and coupled cavities

A Fabry-Pérot cavity consisting of at least two reflective surfaces provides a very simple spectral filter (see Sec 3.9). A narrow transmission band is obtained, periodically repeated every free spectral range, with filter characteristics given by the cavity length and surface refectivities. A general drawback is the free spectral range

limitation, which gives the maximum detuning of the wavelength. Typically, three different configurations are used.

In the simplest version, one very short cavity containg the gain element is used, with the idea that the free spectral range should be longer than the gain bandwidth, to only allow oscillation of one longitudinal mode. Examples where this can be used are low power end-pumped solid-state lasers with mirrors coated directly onto the gain medium faces [114, 115]. Drawbacks are limited power and that there is no freedom left in the cavity design. In paper III and paper IV we present a design that extends the usefulness of this idea.

An etalon is a thin piece of material with flat-flat surfaces, which might be coated, providing a monolithic Fabry-Perot cavity. By insertion of an etalon in a larger cavity, substantial loss is experienced for wavelengths outside of the etalon transmission peaks, and the laser [10, 11, 111, 116, 117] or OPO [118] wavelength can hence be locked. Tuning can be achieved by tilting the etalon, which slightly changes its effective length, and thus moves the transmission peaks. Drawbacks of etalon locking and tuning are the limited tuning range due to the limited free spectral range, limited spectral loss modulation as well as insertion loss [119].

Another variation on the theme is to have two coupled cavities with a common mirror in between. The only wavelengths that can sustain oscillation are then those which are resonant in both cavities, which usually gives a rather good selectivity [120, 121]. A problem with the design is typically the stability. An extension to this idea is demonstrated in paper II.

Flat surface gratings

Surface gratings were the earliest and are the most widely spread gratings. They consist of a periodic variation on the surface of a material and are used both in reflection and transmission. Different types of gratings include ruled gratings, blazed gratings, holographic gratings and lithographically produced gratings. Typically, the reflective gratings are covered by a metal film acting as a metallic mirror. For wavelength locking, they are usually used in either the Littrow [12, 13, 122] or Littman [123–125] configuration.

A limiting factor for the application of these gratings in laser cavities is the rather big loss, due to large coupling to unwanted diffraction orders of the grating. This limits the applicability to high gain systems, such as diode lasers and OPOs. The field of external cavity diode lasers [126] is nowadays large, where tuning ranges of tens of nanometers and bandwidths below 200 kHz are typically achieved [127]. For OPOs, there has been a number of demonstrations of locking using both the Littrow [128] and the Littman setup [129–132]. A limitation to the usefulness of the gratings in pulsed systems is a rather low damage threshold, although it depends on what coating is used. An estimate of what can be reached is given by grating compressors in chirped pulse amplifiers, showing a damage threshold of ~ 0.4 J/cm^2 [133]. Another limitation is that a wide beam is needed in order to interact with many grating fringes and thus get a narrow grating bandwidth.

Birefringent filters

A birefingent filter uses the spectral variation of the birefringence in a material in combination with a polarizer. The thickness of the birefringent material is chosen so that the incident polarization is rotated by 180° back to its original state for a certain wavelength. For other wavelengths the rotation will not be perfect, why they experience loss in a subsequent polarizer. A Lyot filter is a refinement of the concept that consists of a stack of multiple filters, which gives increased selectivity. Tuning of the transmission wavelength in a birefringent filter can usually be obtained by rotation of the device. Limitations of birefringent filters are that the spectral selectity might be poor and that the transmission is periodically repeated, so the filter is only useful within one free spectral range. Experimental examples include tunable Yb-lasers [134, 135].

Prisms

A prism utilizes the dispersion of the refractive index in a material to give an angular spread of different wavelengths. This is a very simple technique, and the main drawback is that the spectral selectivity is rather limited. An example of a tunable Yb-laser based on prism tuning can be found in [136].

Chapter 3

Laser theory

A *laser* is based on *l*ight *a*mplification by *s*timulated *e*mission of *r*adiation. Three things are needed to build a laser: a pump, a laser medium and a cavity, shown schematically in Fig. 3.1. The pump supplies energy to the laser medium that has appropriate energy levels, where population inversion and thereby gain via stimulated emission is obtained, and the cavity provides feedback for the amplification process. In this thesis, all lasers are pumped optically and operate in cw mode and the laser media are lanthanide ions doped in a crystal or glass host, so called solid-state lasers. The laser cavity feedback is provided by dielectric mirrors and spectrally selective volume Bragg gratings.

In this chapter, the description is focussed on the most important laser properties for the experiments in this thesis. The description is based on more comprehensive texts on laser theory that can be found elsewhere [108, 137–140].

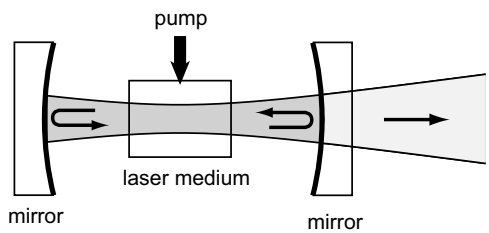

Figure 3.1: A schematic laser, containing a pump, a laser medium and a feedback cavity setup by the mirrors.

3.1 Light–matter interaction

Interaction between light and matter cause the transitions between the energy levels in the laser material. These radiative transitions are either spontaneous emission or stimulated, as in absorption and stimulated emission. In this work, the stimulated processes are modelled by the absorption and emission cross sections σ, while the spontaneous emission is modelled by the radiative lifetime of the levels τ_{rad}. The two are related at the centre of a single transition by $\sigma = \lambda^2/(4\pi^2\tau_{rad}\Delta\nu)$, where $\Delta\nu$ is the frequency FWHM bandwidth of the probability of spontaneous emission.

In addition, there are also nonradiative transitions between energy levels, that are due to interactions within the material.

3.2 Classification of laser types

An important property of a laser medium is its energy level structure. The transition scheme between the levels for pumping and lasing provides a useful classification of different laser types, which is described below. To obtain population inversion, a system with at least three participating levels is needed.

The pumping of a laser provides excitation from the ground state to a higher energy level via absorption, as shown by transition (1) in Fig. 3.2. The laser transition, based on stimulated emission, is given by (3). In addition, there are additional relaxational transitions (2), (4), which in the lasers of interest in this thesis are nonradiative transitions.

In a 4-level laser, as shown in Fig. 3.2(a), the pump absorption is followed by a relaxation (2) to the upper laser level. To accumulate states in this level, it is desired that the transistion (2) has high probability, while the lifetime in the upper laser level is long. To sustain a large population inversion over the laser transition (3), it is furthermore required that the probability of transition (4) is high, so the lower laser level is emptied quickly. Also, excitation processes from the ground level directly to the lower laser level should be avoided.

3-level lasers come in two types, type I and type II , as shown in Fig. 3.2 (b) and (c), respectively. They can be considered as 4-level lasers where the two upper or the two lower levels have merged, which introduces some difficulties, but also some potential benefits, as shown in later sections. For type I, the pumping is directly into the upper laser level, which means that only a limited fraction of the population can be pumped to the upper level before the opposite process of stimulated emission at the pump wavelength becomes a limiting factor. On the other hand, for type II, the laser transistion terminates in the the ground state, which for a cw-system is always strongly populated, meaning that at least 50% of the population must be excited before inversion is reached.

There is also an intermediate system between a 4-level laser and a 3-level laser of type II, namely a so called quasi-3-level laser. This is a 4-level laser where the lower laser level is close enough to the ground state to become substantially thermally

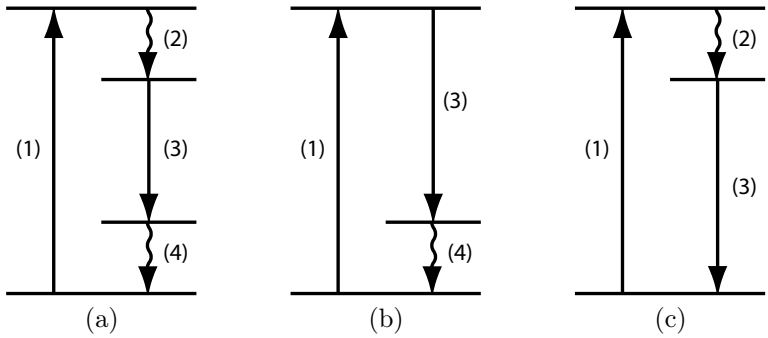

Figure 3.2: Laser types: (a) 4-level laser; (b) 3-level laser of type I pumped into the upper laser level; (c) 3-level laser of type II terminating the laser transition in the ground state. (1) is the pumping transistion, (3) the laser transition and (2), (4) are additional relaxation transitions.

populated. The energy spacing is then of the order of the thermal energy, which at room temperature is 200 cm^{-1}. With partial thermal population of the lower laser level, harder pumping is required to reach inversion, and the system becomes similar to a 3-level laser of type II. In an analogous manner, a 3-level laser of type I can have the lower laser level so close to the ground state as to be thermally populated. Such a laser can then be called a quasi-2-level laser. Although a true 2-level laser is impossible, the quasi-2-level laser is a fairly good approximation in terms of the energies of the pump and laser photons.

3.3 Solid-state laser materials

The solid-state laser materials that are used in this thesis are all composed of lanthanide trivalent ions doped into a solid-state crystal or glass host. For crystalline hosts, the lanthanide ion replaces one element of the host crystal in a number of cells, depending on the doping concentration. Preferably, the replaced element should have similar properites to the laser ion. For example, in Nd:$GdVO_4$, Nd replaces Gd, which both are lanthanides, while in Yb:$KY(WO_4)_2$, Yb replaces Y that both belong to the same column of the periodic table. In a glass host, on the other hand, there is much more flexibility to add an ion, as the glass matrix will accomodate to fit the ion.

One important reason why the trivalent lanthanides are used as laser ions, is the configuration of the highest energy electrons that belong to the 4f state, from $4f^1$ for Ce^{3+} to $4f^{14}$ for Lu^{3+}. The spatial configuration of the electrons is mostly determined by their primary quantum number. Since all the lanthanides have filled shells of 5s and 5p electrons which lie outside the 4f electrons, the latter are shielded

from the surroundings to a large degree. The resulting effect is that in many aspects, the lanthanide ions behave as though they were free ions, even though they are located in a solid-state host. In this way, the thermal and mechanical properties of the host can be combined with the long excited-state lifetime of free laser ions. Another advantage of doping the active ions into a solid, compared to having them as free atoms in a gas, is that the density can be much larger, eventually yielding smaller lasers.

Despite the shielding of the 4f electrons, the interaction between the laser ion's electronic energy states and the surrounding host still plays an important role for the determination of the laser material properties, such as the upper level lifetime, the emission and the absorption cross sections, the exact energy of the levels and the bandwidth of transitions between levels. From experiments, this is evident since the same ion in different hosts displays different properties.

To determine the total energy state of the 4f electrons in lanthanides, it is a good approximation to use Russel-Saunders or LS-coupling for the spin-orbit coupling of the electrons. This means that the total orbital momentum L and the total spin S are good quantum numbers, that are then coupled to determine the total angular momentum J. This means that the 4f energy state can be described by these three quantum numbers, usually combined as $^{2S+1}L_J$, often denoted as an energy manifold. There still remains one quantum number to determine, namely the projection of J on an axis, m_J, which is degenerate for a free ion. Parts of this degeneracy is usually lifted by the interaction with the local electric field of the surrounding host matrix through the Stark effect. This Stark splitting gives rise to additional Stark levels, whose exact location is determined by the host. This results in that the laser wavelengths for the same laser ion vary in different hosts and also for different electric field polarizations.

For a free system, the electric dipole transitions within the 4f-state that are used as the laser transitions are "forbidden" transitions with zero probability. The reason is that there is no change in parity, i.e. the matrix element for the transition is zero, since the product of the initial and final wavefunctions is even while the electric dipole operator is odd. However, the perturbation from the host admixes states of opposite parity to the wavefunctions, that gives a finite probability to the transition. Still, this resulting probability is small, which gives long lifetimes of the upper laser levels.

The bandwidth of the electric dipole transitions corresponds to the gain bandwidth in the laser. The main contribution to the bandwidth in crystalline hosts at room temperature is the interaction with the phonons of the host, giving homogeneous broadening. Two types of broadening contribute. The first is lifetime broadening, which is due to the Fourier transform limitation for the transform pair time – energy. Since the upper laser level lifetime is usually rather long, the important contribution stems from the lower level, which is depopulated via nonradiative phonon transitions. A second source for homogeneous broadening is due to dephasing of the phase of the individual oscillators that is caused by random frequency modulation induced by the lattice phonons. When viewed as a collection, the ran-

domized phase of the emission from individual ions results in broadening of the response. The strength of both mechanisms depends on both the frequency of the available phonons in the host and to what degree they couple to the laser ion. For glass hosts, there is an additional inhomogeneous broadening mechanism, that is caused by the local differences in the micro-environment of the individual ions, that perturbes the exact energy level location differently for each ion.

3.4 Effective cross sections

To determine the spectral properties of the gain, it is important to know the spectral distribution of the laser cross-sections. When determining the strength of a transition, not only the cross section, but also the population of the initial and final states must be considered. Over the different Stark levels within a manifold, the population will be thermally distributed according to Boltzmann statistics. Therefore, it is convenient to include this factor into the cross sections and use effective cross sections that are given for a certain temperature. These effective cross sections are then given for transitions between manifolds, and are directly equivalent to the values measured in the lab.

The absorption cross section is straightforward to measure, by measuring the spectral transmission through the laser material and taking into account non-absorptive losses in the surfaces. For a fractional absorption A in a sample of length l and doping concentration N, the absorption cross section is $\sigma_{abs} = -\ln(1-A)/(Nl)$.

For the emission cross section, two methods can be employed. First, it can be obtained directly from the fluorescence signal $I_F(\lambda)$, since stimulated emission is proportional to spontaneous emission. The fluorescence signal is easy to measure by pumping the laser material and measuring the spectrum of the emitted fluorescence. The relationship is given by $\sigma_{em}(\lambda) \propto \lambda^5 I_F(\lambda)$ [141]. However, this method only works for a transition where the lower level is not thermally populated.

For transitions that terminate on the lowest manifold, the thermal population for the different sublevels must be taken into account, resulting in a tendency for reabsorption of spontaneously emitted photons. If the absorption cross-section can be measured, it is therefore better to calculate the emission cross section indirectly from the absorption data by use of the reciprocity method [142]. This method relies on the fact that the probability of stimulated emission is the same as that of absorption. In addition, the effects of different population and degeneracy are also included. For transitions between an upper manifold u and a lower one l, the reciprocity relation is given by

$$\sigma_{em}(\lambda) = \sigma_{abs}(\lambda)\frac{Z_l}{Z_u}\exp[(\mathcal{E}_Z - hc/\lambda)/(k_B T)], \tag{3.1}$$

where $\mathcal{E}_k^i$ is the energy of sublevel k in the ith manifold ($i = l, u$) and $\mathcal{E}_Z = \mathcal{E}_0^u - \mathcal{E}_0^l$, Z_i is the partition function for each manifold given by $Z_i = \sum_k d_k^i \exp[-(\mathcal{E}_k^i -$

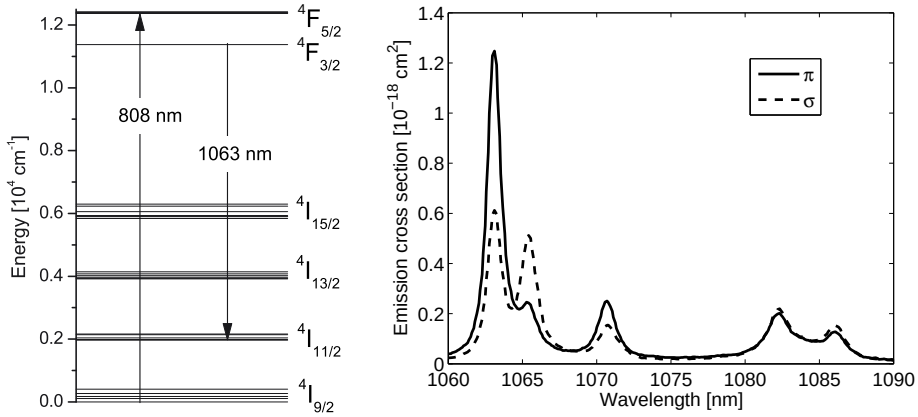

Figure 3.3: Spectroscopic properties of Nd:$GdVO_4$: (a) energy levels and important transitions in the π-polarization [143]; (b) emission cross sections for the $^4F_{3/2} \rightarrow {}^4I_{11/2}$ transition in π and σ polarization [144].

$\mathcal{E}_0^i)/(k_BT)]$ and d_k^i are the degeneracy factors for each sublevel. In reverse, for spectral regions where the absorption is much smaller than the emission, low noise data for the absorption can be calculated via the reciprocity method from the fluorescence signal.

3.5 Laser ions and host materials

Next, a short overview of the spectral properties of the laser materials that were used in this thesis is given.

Nd:$GdVO_4$

The Nd^{3+} ion is probably the most common solid-state laser ion, typically used as a four-level laser pumped at 808 nm and lasing at 1060 nm, see Fig. 3.3(a), although other configurations are also used. In this work, $GdVO_4$ was used as host crystal [143–146], mainly because of favourable spectral overlap with the available volume Bragg grating. $GdVO_4$ is birefringent, yielding slightly different laser properties for polarization parallel (π) and orthogonal (σ) to the crystal c-axis. In Nd, the coupling between the lattice phonons and the 4f electrons is not so strong, which results in fairly narrow absorption and emission lines, as can be seen in Fig. 3.3(b), with a bandwidth for each Stark line of about 0.3 THz (1 nm). The lifetime of the $^4F_{3/2}$ level in 1.2 at.% Nd:$GdVO_4$ is 90 μs [143].

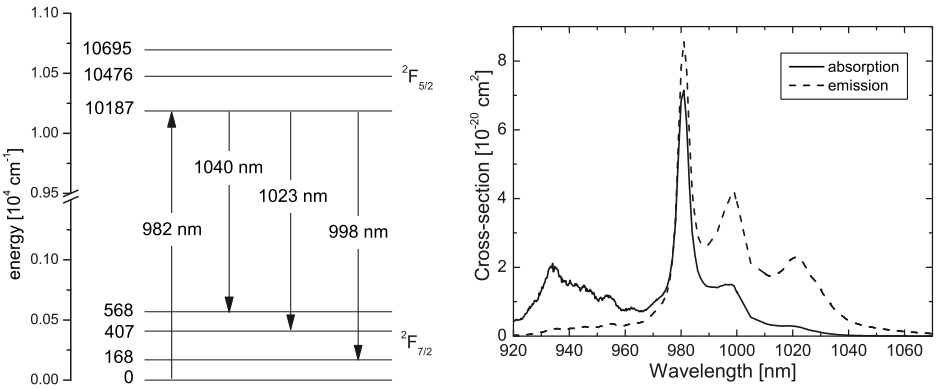

Figure 3.4: Spectroscopic properties of Yb:KYW in n_m polarization: (a) energy levels and important transitions [147]; (b) cross sections [paper VI].

Yb:KYW

In recent years, Yb^{3+} has been increasingly used as a laser ion for radiation around 1 μm, after suitable high power pump diodes have become available. The main advantages with Yb can be understood by considering the energy level structure and cross section spectral properties shown in Fig. 3.4. The close spectral spacing between pump and laser, together with the simple energy structure and thereby little parasitic transitions, both work to reduce heat problems in the laser, making high output powers possible. Also, the available gain bandwidth is broad. First, this is since for Yb, the coupling between the 4f electrons and the host phonons is rather strong, resulting in broad absorption and emission lines. As an example, the 980 nm transition in Yb:KYW has a bandwidth of 1.2 THz (4.0 nm), as shown in Fig. 3.4(b). Second, the Stark levels lie more closely spaced than the broadening of each individual line, giving a large collective bandwidth. When pumped at 980 nm, as shown in Fig. 3.4, the Yb system is a 3-level laser of type I or a quasi-2-level laser, depending on the laser wavelength. As a host crystal, the double tungstate $KY(WO_4)_2$ (KYW) was used [147–149]. In addition to having high energy phonons, that give broad bandwidths, this material also has favourable mechanical properties. KYW is biaxial, and out of the possible polarization axes, n_m shows the highest cross sections, why it has been employed in the experiments. The lifetime of the $^2F_{5/2}$ level in Yb:KYW at 5 at.% doping is 240 μs [150].

ErYb:glass

For laser radiation around 1.5 μm, the Er^{3+} ion is commonly used. To increase pump absorption, Er is often codoped with Yb, which has higher absorption cross

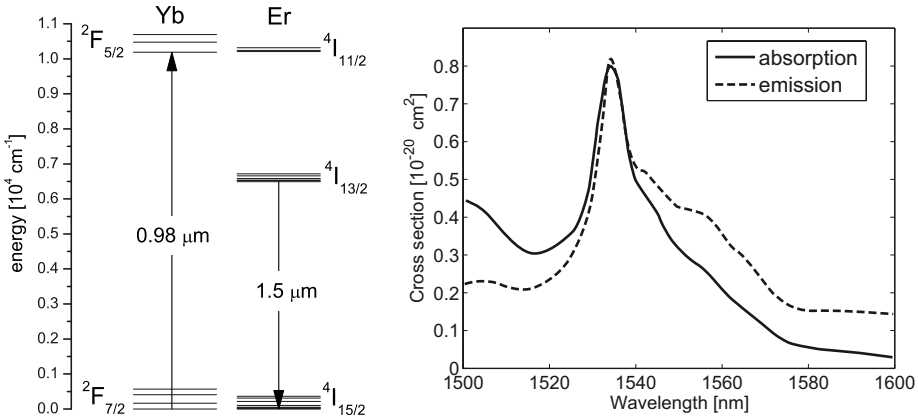

Figure 3.5: Spectroscopic properties of ErYb:glass: (a) energy levels and important transitions [153–155]; (b) Er cross sections for the $^4I_{13/2} \rightarrow {}^4I_{15/2}$ transition [156].

section. The energy level structure of the ErYb-system is shown in Fig. 3.5(a). After absorption at 980 nm in Yb, the energy is transfered from the $^2F_{5/2}$ level in Yb to the $^4I_{11/2}$ level in Er, which has almost the same energy, but with much shorter lifetime, effectively promoting the system to the upper laser level in the Er $^4I_{13/2}$ state. The lower laser level is the ground state manifold, making the ErYb system a quasi-3-level or 3-level system of type II (see Sec. 3.2). The host that was used for the ErYb system was phosphate glass [151]. Although the thermal properties of glass are not optimal compared to a crystal, a crystalline material with suitable lifetimes for the ErYb system to outperform glass is not easy to find. During the last year, one such candidate has been presented, namely ErYb:$YAl_3(BO_3)_4$ [152]. The cross sections of ErYb:glass are shown in Fig. 3.5. As can be seen, just as for Yb, broadband gain is available as a result of both strong interaction with the host phonons and many closely spaced Stark levels, as well as inhomogeneous broadening from the glass host [153]. As shown in Fig. 3.5(b), the bandwidth of the transition is about 2 THz (15 nm). In ErYb-doped phosphate glass, the lifetime of the $^4I_{13/2}$ level is about 7 ms [151].

3.6 Gain and rate equations

The amplification of the intensity I in a laser material of length L is given by $I(L) = I(0)\exp(gL)$, where g is the gain. The gain is given by the laser material properties through the cross sections σ and the pumping strength that gives the population concentrations N_i. Between an upper level u and a lower level l, the gain is

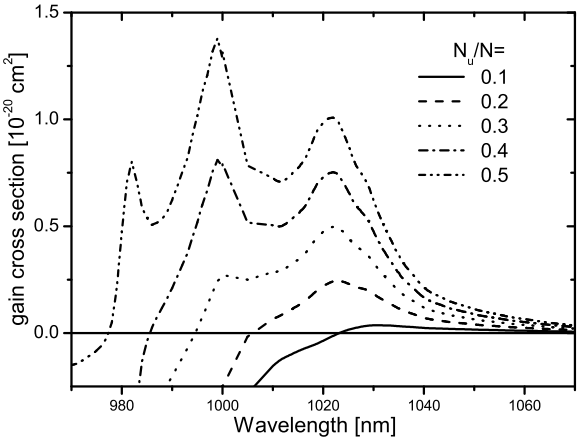

Figure 3.6: Gain cross sections g/N in Yb:KYW at various levels of inversion.

$$g = N_u\sigma_{em} - N_l\sigma_{abs}, \tag{3.2}$$

where the total concentration of laser ions is $N = N_u + N_l$. In a 4-level laser, the population in the lower level is negligable, and the gain is proportional to $N_u\sigma_{em}$. On the other hand, in a laser with a thermally populated lower level, this plays an important role for the spectral distribution of the gain. An example of this is given in Fig. 3.6, giving the gain cross section g/N in Yb:KYW for various inversions.

To determine the population of the levels for a given pump intensity, rate equations is a powerful method. By considering the possible transitions between the energy levels in the laser, it is straightforward to model the rate at which the system passes beween the different levels, and thus obtain the population of each level.

As an example, consider a two-level system with an upper level u and a lower level l. Assume that two light-fields are present in the system, pump light at λ_p with an intensity I_p and laser light at λ_l with intensity I_l. The time evolution of the concentration of laser ions N_u in the upper level is then given by a first order differential equation

$$\frac{\mathrm{d}N_u}{\mathrm{d}t} = \left(\sigma_{abs}(\lambda_l)\frac{\lambda_l}{hc}I_l + \sigma_{abs}(\lambda_p)\frac{\lambda_p}{hc}I_p\right)N_l - \left(\frac{1}{\tau} + \sigma_{em}(\lambda_l)\frac{\lambda_l}{hc}I_l + \sigma_{em}(\lambda_p)\frac{\lambda_p}{hc}I_p\right)N_u. \tag{3.3}$$

The interpretation of the right-hand-side of the equation is the following, from left to right: Level u is populated from level l by absorption of laser light and pump light. Depopulation of level u is due both to spontaneous emission (and possibly nonradiative processes) at a rate given by the upper level lifetime τ, as well as

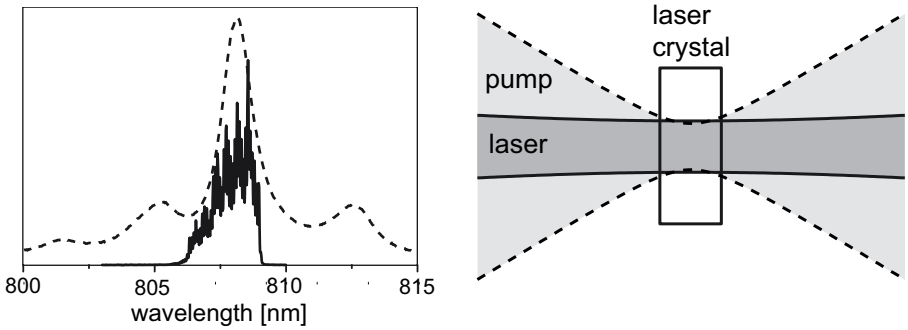

(a) (b)

Figure 3.7: Diode-pumping requirements: (a) Good spectral overlap between the pump spectrum (solid) and the laser crystal absorption (dashed). Example given for diode pumping of Nd:$GdVO_4$ in π-polarization [paper III, paper IV]. (b) Spatial overlap between pump beam (dashed) and laser cavity mode (solid) in a typical end-pumped laser.

stimulated emission at both laser and pump wavelengths. For cw lasers, the system can be simplified by assuming a steady state solution with $\mathrm{d}N_u/\mathrm{d}t = 0$. To properly model the laser, a rate equation should be solved at every space-point of the laser crystal. An example of such a modelling is given in paper VI.

3.7 Diode-pumping of solid state lasers

For optical pumping of solid-state lasers, diode-pumping is an attractive option. One reason is that diode lasers provide an efficient conversion of electrical energy to optical energy. Also, compared to lamp-pumping, the output of a laser diode is more well defined, both spatially and spectrally, which enables end-pumping into a single absorption line. Thus a good conversion efficiency from pump to laser can be achieved. Still, in a diode-pumped solid-state laser, there is a significant further improvement, from pump input to laser output, of both the spectral and spatial quality of the radiation.

For efficient pumping, a few things are required. First, the spectral overlap should be good between the pump diode and the absorption line in the laser medium, for efficient pump absorption, see Fig. 3.7(a). Second, there should be good spatial overlap between the pump diode and the Gaussian cavity mode of the laser, to efficiently excite only the fundamental transverse cavity mode. Even though the diode pump-lasers are usually far from diffraction limited, with a high M^2-value, good spatial overlap can be obtained in an end-pumped system. The approximate requirement is that the pump is focussed to the laser mode size, while

having a confocal length which is not longer than the crystal length, see Fig. 3.7(b). In contrast, for lasers with strong reabsorption, as shown in paper V and paper VI, optimal pumping is when the laser mode is substantially smaller than the pump focus. Finally, high power diode lasers have elliptical beams, so some reshaping of the pump beam to obtain a circular spot is usually required before it reaches the laser crystal.

3.8 Laser beam transverse properties

The evolution of the transverse distibution of a laser beam is governed by diffraction. Due to the diffraction, the near-field size w and the far field angle θ of a laser beam forms a Fourier transform pair. As always, the lowest product of the transform pair (w, θ) is found for Gaussian distribution of the fields, while all other distributions give a larger product.

Gaussian beams

The propagation of laser beams in free space is governed by the paraxial wave equation. A Gaussian beam is an eigensolution (of the lowest order) to this equation, which means that it will maintain the same transverse appearance as it traverses space. For this reason, the transverse field in a laser oscillator also tends to be in the form of a Gaussian.

The electric field of a Gaussian beam in cylindrical coordinates is

$$E(r,z) = \frac{1}{w(z)} \exp\left[-\frac{r^2}{w^2(z)} + i\left(-\psi - k\frac{r^2}{2R(z)} + (\omega t - kz)\right)\right], \tag{3.4}$$

where $R(z) = z + z_R^2/z$ is the radius of curvature of the phase fronts and $\psi(z) = \arctan\frac{z}{z_R}$ is the Gouy phase. $w(z)$ is the beam radius at the e^{-2} intensity point, which is related to the FWHM diameter as $d_{\mathrm{FWMH}} = 1.2w$. The axial variation of the beam radius, shown in Fig. 3.8, is given by

$$w(z) = w_0\sqrt{1 + \left(\frac{z}{z_R}\right)^2}, \tag{3.5}$$

where $z_R = \pi w_0^2 n/\lambda = k w_0^2/2$ is the Rayleigh range that is defined by $w(z_R) = \sqrt{2}w_0$. A related parameter is the confocal parameter b, given by $b = 2z_R$. In Fig. 3.8 the divergence angle of the beam θ is also shown, which can be found from (3.5) to be $\theta = \lambda/(w_0\pi n)$. As can be seen, we get the product of the Fourier transform pair $w_0\theta = (\lambda/n)/\pi$, which is the Fourier transform limit as expressed in these variables.

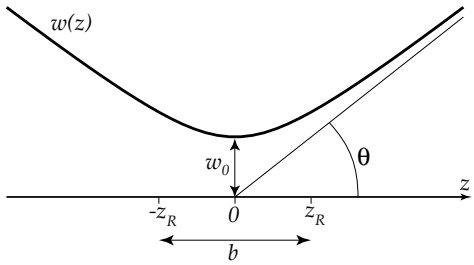

Figure 3.8: Axial evolution of the beam radius w.

Higher order transverse modes and M^2

The paraxial wave equation has a complete set of solutions, of which a Gaussian beam is only the lowest order one. Common expressions for these sets of solutions are the Hermite-Gaussian modes in rectangular symmetry, and the Laguerre-Gaussian modes in cylindrical symmetry. Since a laser cavity usually contains elements with a symmetry along a transverse axis, and also since the Laguerre-Gaussian modes have a phase singularity in the origin, lasers tend to oscillate in one or more Hermite-Gaussian modes. The Hermite-Gaussian modes are usually denoted by the order (m, n) of the solution as TEM_{mn}, where TEM_{00} corresponds to the Gaussian beam. Examples of these modes are shown in Fig. 3.9.

A real laser beam usually consists of a sum of different transverse modes, and can in principle be descibed as a superposition of Hermite-Gaussian modes, though this is difficult in practice. Instead an effective approach can be used that utilizes statistical moments, so called M^2-theory [157]. The main idea for the M^2 approach is that any beam can be assigned a generalized beam radius w_G from the standard deviation σ of its intensity distribution I. For a beam of total power $\mathcal{P}$ and a transverse coordinate x, with $x = 0$ in the centre of mass of $I(x)$, we have

$$w_G^2(z)/4 \equiv \sigma^2 = \frac{1}{\mathcal{P}} \iint x^2 I(x, y, z) \mathrm{d}x\mathrm{d}y. \tag{3.6}$$

A corresponding divergence angle is defined by $\theta_G = \lim_{z\to\infty} w_G(z)/z$ and the radius in the focus is denoted $w_{G0} = w_G(0)$. It then turns out that the beam propagation can be described in a similar way as for the Gaussian beam, if one adds a factor M^2

$$w_G(z) = w_{G0}\sqrt{1 + \left(\frac{M^2\lambda}{\pi w_{G0}^2} z\right)^2}. \tag{3.7}$$

An interpretation of what happens is to assume an underlying Gaussian beam of radius w, while the real beam $w_G(z) = Mw(z)$ is M times larger both in the focus

Figure 3.9: Intensity distributions of the first few Hermite-Gaussian modes. Two neighbouring lobes of each mode have a phase difference of π.

and in the far field. M^2 is a measure of how far the beam is from the transform-limited Gaussian beam, as can be seen from the product of the Fourier transform pair w_G and θ_G

$$M^2 = \frac{\pi}{\lambda} w_{G0} \theta_G. \tag{3.8}$$

For a Gaussian beam, $M^2 = 1$, while for a transverse mode TEM_{m0}, we have $M^2 = 2m + 1$ in the x-direction.

Measurement of transverse properties

To be able to determine the transverse properties of a laser beam, it is necessary to measure both the intensity and phase distribution at an intersecting plane. However, it is rather difficult to measure the phase of the beam. Instead, one can measure only the intensity distribution in a number of places along the beam propagation, most importantly in the near and far-fields. Then, one can make a fit to the M^2-theory described above by extracting the generalized beam radius at the different axial positions. In this way, a description of the beam in terms of the generalized radius can be obtained. Since for a Gaussian beam, the obtained beam radius gives a complete characterization of the beam, for beams with low M^2, this type of description is usually sufficient.

For the measurements in this thesis, the knife-edge method was used to determine the beam radius. This is done by translating a knife-edge (e.g. a razor blade) transversely over the beam and measuring the ratio of the transmitted power $\mathcal{P}$ to the total power $\mathcal{P}_{tot}$ as a function of knife-edge position x_0. The transmitted power is given by the integral of the beam intensity distribution $I(x, y)$. For a Gaussian beam, we get

$$\frac{\mathcal{P}(x_0)}{\mathcal{P}_{tot}} = \frac{1}{\mathcal{P}_{tot}} \int_{-\infty}^{x_0} \mathrm{d}x \int_{-\infty}^{\infty} \mathrm{d}y \, I(x, y) = \frac{1}{w}\sqrt{\frac{2}{\pi}} \int_{-\infty}^{x_0} e^{-2\frac{x^2}{w^2}} \mathrm{d}x = \frac{1}{2}(1 + \mathrm{erf}(\sqrt{2}\frac{x_0}{w})), \tag{3.9}$$

where $\mathrm{erf}(x) \equiv 2/\sqrt{\pi} \int_0^x \exp(-t^2)\mathrm{d}t$ is the so called error function. A precise measurement requires measurements of $\mathcal{P}$ at a number of positions x_0. Still, a good

estimation of the beam radius can be found from the distance between only two positions on either side of the beam centre at a certain transmitted power. A balance must then be made between low noise in the power measurement for positions close to the beam centre, and low noise in the distance measurement for positions far from the beam centre. Convenient positions are the points of 16% and 84% transmission, which are separated by a distance w. For an elliptic beam, the measurement should be made along both axes of the ellipse. Naturally, this method only gives exact results for a beam with $M^2 = 1$, but as long as M^2 is low, the error is not very large. If needed, a more exact measurement can be found by measuring the intensity distribution of the beam with some type of matrix of power meters, e.g. a CCD, and then extract the standard deviation of the measured distribution.

3.9 Laser spectral properties

The spectral properties of a laser can be divided into two distinct regimes, with either a single longitudinal mode or multiple modes oscillating. For this reason, a discussion on the spectral properties of a laser must always start by a description of its longitudinal mode structure, primarily determined by the laser cavity, that consists of a gain meadium inside a Fabry-Pérot cavity.

Fabry-Pérot cavities and longitudinal modes

A basic Fabry-Pérot cavity consists of two reflective mirrors, with reflectivities R_1 and R_2, separated by the cavity length L. For certain settings, there is a resonance of the electric field in the cavity, a so called longitudinal mode. For a linear cavity, the longitudinal modes are located at the wavelengths where a standing wave is supported, i.e. for

$$p\lambda_p = 2L \quad \text{or} \quad \nu_p = \frac{pc}{2L}, \tag{3.10}$$

for a mode (integer) number p. An alternative way to describe this is that the phase of the electric field should be the same after one cavity roundtrip, which gives a better understanding of the modes in a ring-cavity. The resonances of a Fabry-Pérot are clearly seen if the transmission of the cavity is considered, as depicted in Fig. 3.10. The spacing between the modes is called the free spectral range, which is given by $\Delta\nu_{FSR} = c/(2L)$, while the bandwidth of each peak is denoted $\delta\nu_{FP}$. The ratio between the two is a measure of the strength of the resonance called the finesse of the cavity,

$$F = \frac{\Delta\nu_{FSR}}{\delta\nu_{FP}}. \tag{3.11}$$

For perfect mirrors, perfect alignment and no losses, the finesse is given by the mirror reflectivites as $F = \pi(R_1R_2)^{1/4}/(1-(R_1R_2)^{1/2})$. However, for highly reflective mirrors, the finesse is also limited by imperfect mirror surfaces, imperfect alignment as well as loss in the cavity.

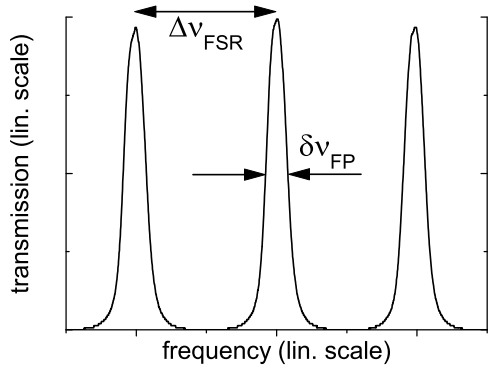

Figure 3.10: Experimental transmission through a Fabry-Pérot cavity.

For a more complete description of the longitudinal modes, coupling to the transverse modes of the cavity must be taken into account. For a Hermite-Gaussian transverse mode with a mode number (m, n), the resonant frequencies are then shifted to

$$\nu_{pmn} = \left(p + (m + n + 1) \frac{\arccos \sqrt{g_1 g_2}}{\pi} \right) \frac{c}{2L}. \tag{3.12}$$

The shift is given by the type of cavity, as determined by the radius of curvature ϱ of the cavity mirrors through the parameters $g_i = 1 - L/\varrho_i$. For a single longitudinal mode laser, this shift can be used to determine from a spectral measurement if a laser is in a single transverse mode, since otherwise an additional transverse mode will appear as a second peak in the laser spectrum. Furthermore, for measurements with Fabry-Perot interferometers, the control of this effect is important. Otherwise, accidental excitation of multiple transverse modes of the measurement interferometer might be mistakenly interpreted as multiple modes of the laser to be measured. To control this, an interferometer cavity where the frequencies of the transverse modes are degenerate should be used. One alternative is a flat-flat cavity, so that $g_1 = g_2 = 0$ and there is no shift. Another option is to shift the mode (p, m, n) for one longitudinal mode p to overlap the the next longitudinal mode $p + 1$ at the fundamental transverse mode $(p + 1, 0, 0)$, i.e. $\nu_{pmn} = \nu_{(p+1)00}$. Additional peaks then appear in the interferometer transmission spectrum at a regular spacing between the modes $(0, 0, p)$ and $(0, 0, p + 1)$, but they can be disregarded, since they are known to originate from the interferometer. An example of this is shown in Fig. 4.7(a), where the cavity is designed so that the transverse modes with $m + n = 3$ are degenerate with the next longitudinal mode.

Laser longitudinal modes

The spectrum of a laser is given by which longitudinal modes are excited, as primarily determined by the saturation properties of the gain medium. For a homogeneously broadened medium in a simple model, the first mode to lase should saturate the gain completely and no other modes would appear. However, the geometry of the laser must also be taken into account. In a linear cavity, the modes in the cavity form a standing wave, which means that there is only intensity to saturate the gain in the anti-nodes of the first mode to lase. This effect is called spatial hole-burning, and means that there is still gain available for another mode to lase, as long as its standing waves overlap sufficiently with the remaining gain. A model that predict at what pump power a second mode will start to lase is available in the literature [158], and was used to predict the performance of the laser in paper III.

Laser narrowing methods

In order to narrow the bandwidth of a laser in the presence of spatial hole-burning and limit the number of oscillating modes, additional intra-cavity filtering must be introduced. The simplest such filter is the gain spectrum itself, in combination with the longitudinal mode structure of the cavity, as illustrated in Fig. 3.11(a). Here it can be seen that below a certain pump power, only the mode that is located within the gain peak will lase, since that is the only mode for which sufficient gain is available. An approximate requirement is then that the mode spacing is larger than the gain bandwidth. This puts strict requirements on the cavity length, and although such lasers have been demonstrated [114, 115], they only give low output power.

By introduction of an additional filter into the laser cavity, better selectivity of one mode is obtained, giving higher output power and allowing denser mode spacing. In this thesis, volume Bragg gratings were employed for this filtering, while there are a number of other filters available, see Sec. 2.7. An example of the effect of such an intra-cavity filter is shown in Fig. 3.11(b). Here, a volume Bragg grating is used as one of the laser cavity mirrors to select only one longitudinal mode, as demonstrated in paper III and paper IV. An additional benefit is that the laser wavelength can be selected anywhere in the laser gain, here illustrated by the off-centre placement.

In lasers with broadband gain, e.g. Yb, the effect of the gain filtering described above is not very strong, and in a free-running laser, the wavelength fluctuates a lot. Introduction of a spectrally selective element into these lasers significantly improves the spectral quality of the laser, even if more than one mode is lasing, as shown in paper V, paper VI, paper VII and paper VIII, .

In addition to the introduction of a spectrally selective element into the laser cavity, other methods are available to narrow the laser bandwidth. First, one can use a seed laser to promote a certain wavelength of a second laser or (better) a laser amplifier. Still, this just moves the problem to that of spectral narrowing

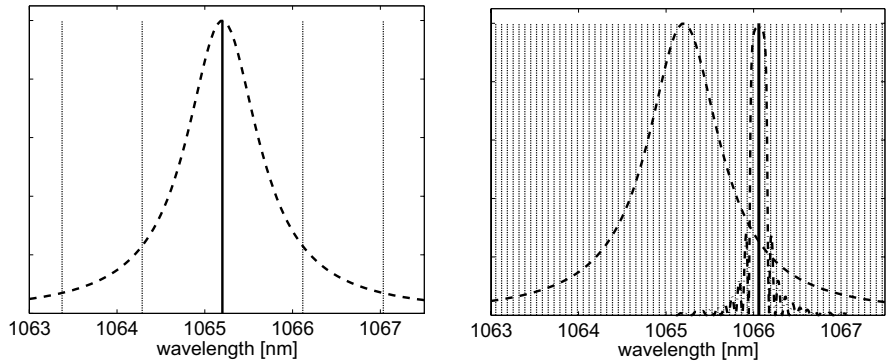

Figure 3.11: Requirements imposed on mode-spacing for single-longitudinal-mode lasing in a hypothetic Nd gain medium at 30 times above threshold, showing emission cross section (dashed), volume Bragg grating reflectivity (dash-dotted) and longitudinal modes, both the selected mode (solid) and all other modes (dotted). The simulation is based on the model described in paper III. (a) No additional filtering yielding 0.6 mm optical cavity length. (b) Filtering with a volume Bragg grating (see Fig. 2.2), yielding a 8.5 mm long cavity.

of the seed laser itself, and therefore provides no real solution. Nevertheless, it is a useful technique especially for pulsed Q-switched lasers. Second, spatial hole-burning can be avoided all together by the use of a unidirectional ring oscillator, without standing waves, so that the first mode to lase can completely saturate the gain. This method is quite useful, but additionally complicates the laser cavity design, since a unidirectional element, i.e. an optical diode, is needed to promote unidirectional lasing only.

Single-longitudinal-mode bandwidth

If only one mode oscillates, the laser is called a single-longitudinal-mode laser. Sometimes these lasers are also denoted single-frequency lasers, although it is somewhat unphysical, since the laser certainly has a non-zero frequency bandwidth. In a laser with a single longitudinal mode, the laser bandwidth is given by the instantaneous variations of the laser frequency. For a diode-pumped solid-state laser, the main limitation of the bandwidth is technical noise in the laser, caused by e.g. mechanical vibrations, fluctuations in pump power and ambient temperature, and pressure variations. This technical noise cause fluctuations of the cavity length, that immediately translates into fluctuations of the laser frequency, and thus increased laser bandwidth. A primary remedy to this problem is to use stable cavity

designs, such as the cavity used in paper II and the monolithic cavity in paper IV. In addition, active feedback loops can be employed to further reduce the linewidth. Then, the instantaneous laser frequency is compared to a reference, such as a very stable high finesse cavity or an atomic or molecular absorption line, and the position of a cavity mirror is adjusted to compensate for any cavity length variations. In this way, bandwidths down to sub-Hz levels can be obtained. Ultimately, the laser bandwidth is limited by quantum noise due to the presence of spontaneous emission in the laser mode. The laser bandwidth limitation is given by the Schawlow-Townes limit

$$\frac{\Delta\nu}{\nu} = \frac{N_u}{N_u - N_l}\frac{2\pi h(\delta\nu_{FP})^2}{\mathcal{P}}, \tag{3.13}$$

where N_u and N_l are the upper and lower level populations and $\mathcal{P}$ is the laser power.

3.10 Bandwidth measurement techniques

For the measurement of the spectrum of a laser, a number of techniques can be used, see e.g. [159]. Here the three main methods that were used in this thesis are presented in order of increasing resolution. It should be noteded that many of the methods that can be used intracavity to narrow the laser spectrum (Sec. 2.7) can also be used extra-cavity for spectral measurements.

Grating spectrometers

By the use of diffraction gratings, absolute measurements of the laser spectrum can be made. Essentially, the resolution is given by how many periods of the grating structure are used in the measurement, and it is usually limited to 10s of GHz.

A typical grating spectrometer [159] is depicted in Fig. 3.12. The light source to be measured enters through the entrance slit. Two mirrors of focal length f then image the entrance slit onto the exit slit, with a collimated beam in between. The spectral selection is done by a surface grating that provides angular dispersion of different spectral components in the collimated beam. The second mirror transforms the angular distribution into a spatial one, and the exit slit selects a narrow part of the spectrum to be measured by the detector. To avoid formation of an image of the grating on the exit slit, the distance between the grating and the second mirror is chosen as the focal length. Scanning of the selected wavelength is done by rotation of the grating. The spectral resolution of a properly adjusted grating-based spectrometer is given by the number of grating grooves that are used. Hence, a wide beam at the grating is to be preferred.

Fabry-Pérot interferometer

For a Fabry-Pérot interferometer, a Fabry-Pérot cavity is used to perform the measurement. The resolution, given by the finesse of the interferometer, is typically

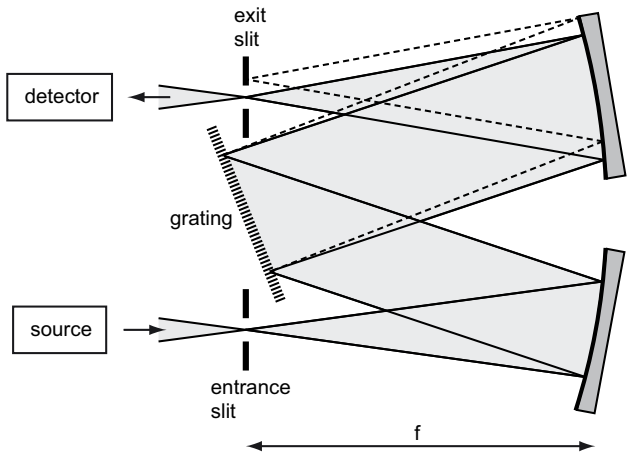

Figure 3.12: Typical setup of grating-spectrometer, showing the selected wavelength (solid) and a rejected wavelength (dashed).

much better than for a grating measurement. In this thesis, a resolution down to 10s of MHz was obtained. However, the measurement only gives relative spectra, not absolute, and the practical measurement range is limited to some 100 GHz by the free spectral range.

In a scanning Fabry-Pérot interferometer, the measurement is performed by scanning the cavity length, so that the transmission peaks of the interferometer scan over the laser spectrum. The measurement is then given by the transmitted laser power, as a function of interferometer length. Usually, piezo-electric actuators are used to scan the length over a few free spectral ranges, corresponding to a few μm distance. For a good measurement, it is important that the actuator position is linear with the driving voltage, and that the cavity alignment is preserved during the scan. The calibration of the interferometer is done by determining the free spectral range. This can be done either by measuring the cavity length, or by performing a simultaneous measurements with e.g. a grating-based spectrometer.

As described above, it is vital that the transverse modes of the interferometer do not interfer with the measurement, as guaranteed by using a flat-flat cavity or one with curved mirrors and degenerate transverse modes. A flat-flat cavity is easier to use, since then the cavity length can be changed freely. But on the other hand, a flat-flat cavity is on the verge of being geometrically unstable, so perfect alignment is difficult, meaning the obtained finesse is usually not so high. With curved mirrors, a stable cavity is easy to obtain, so that the alignment is not so critical. However, to have degenerate transverse modes, the length of the cavity must be precisely controlled to a limited number of points. This complicates alignment and reduces the flexibility of the device.

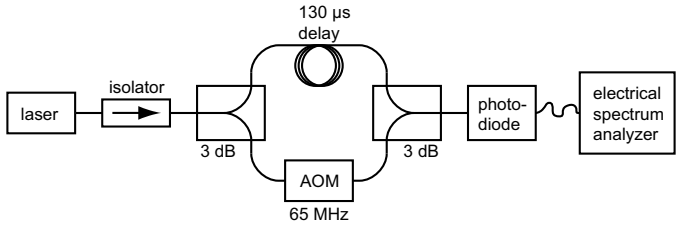

Figure 3.13: Fibre-based setup for self-heterodyne bandwidth measurements.

Heterodyne and homodyne techniques

With heterodyne and homodyne measurements techniques, beating of the laser against a second laser is used for the spectral measurements. To perform a useful measurement, a single-longitudinal-mode laser is required. The measurement range is essentially limited by the bandwidth of the detector of the beat signal, both for the photodetector and the electronics, while the resolution is given by the integration time. In this work, bandwidths down to 100s of kHz were measured.

For the measurements in this thesis, a delayed self-heterodyne measurement technique was used [160, 161]. Here, the laser is beating against a time-delayed and frequenecy-shifted replica of itself in a Mach-Zender type interferometer. The fibre-based setup that was used is depicted in Fig. 3.13. After passing an optical isolator to prevent parasitic feedback into the laser, the light is split into two in a 3 dB (50-50) beam splitter. One portion is then delayed in a long piece of fibre, by a time that should be longer than the coherence length of the laser, i.e. longer than the inverse frequency bandwidth. The reason for this is to avoid coherent effects at the detection of the beating, where interference fringes make the measurement more difficult. The other portion of the light is frequency-shifted in an acousto-optic modulator (AOM). This causes the beat signal to shift too, away from the region around 0 Hz where the detection noise is large, and gives a better measurement. The two split up portions of the laser light are then merged in another 3 dB beam splitter, and finally placed at a photo-detector. The electrical signal from the photo-detector is then fed into an electrical spectrum analyzer. The recorded electrical spectrum then corresponds to a convolution of the laser spectrum with itself, and from the electrical spectrum, the optical bandwidth can be deduced. An example of such a spectrum is given in Fig. 4.3.

Chapter 4

Laser experiments

In this chapter, I describe a number of experiments [paper II-paper VIII], where solid-state lasers are locked with volume Bragg gratings. These were the first ever experimental demonstrations of such lasers, in addition to a brief conference paper on Tm:YLF from 2004 [89] and a demonstration of multi-mode locking of Ti:sapphire and Cr:LiSAF from 2006 [60].

4.1 ErYb:glass laser

In this experiment, an ErYb:glass laser is locked by a volume Bragg grating and lases in a single longitudinal mode [paper II]. This was the first demonstration of a single-longitudinal-mode laser using a volume Bragg grating. The laser setup is depicted in Fig. 4.1, and consisted of a double cavity, with the ErYb:glass gain medium in an internal cavity and the Bragg grating in an external one. The internal cavity provides the low loss cavity needed to sustain laser action in the low gain ErYb-system at 1.5 μm, while the external feedback is used to select only one of the internal cavity's longitudinal modes, thereby enabling single longitudinal mode

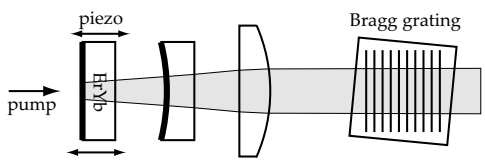

Figure 4.1: ErYb:glass laser double-cavity setup. The length of the inner cavity could be tuned by a piezo actuator, and the outer cavity was locked by a volume Bragg grating at 1552.6 nm with a FWHM bandwidth of 0.44 nm.

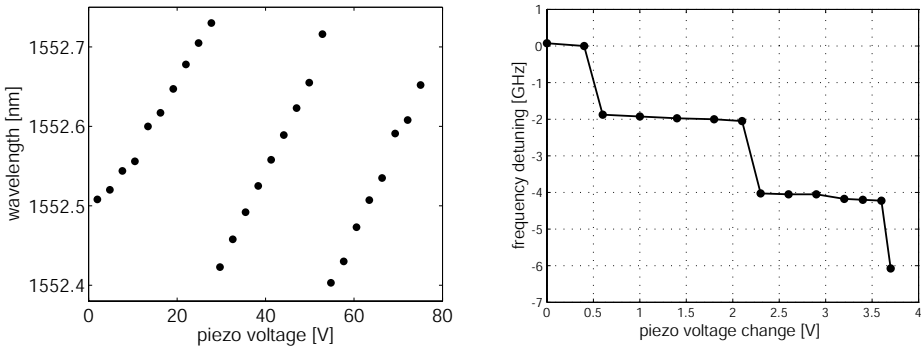

Figure 4.2: Tuning of the ErYb:glass laser by translation of the piezo actuator. (a) Coarse tuning over three modes of the inner cavity. (b) Fine-tuning around 1552.55 nm, showing the outer cavity modes.

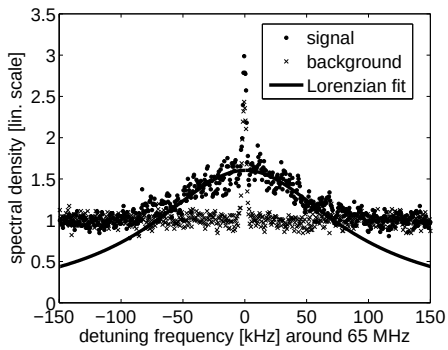

Figure 4.3: Spectrum of the self-heterodyne measurement of the ErYb:glass, with a fit yielding a laser bandwidth of 90 kHz. The delta-spike in the centre of both the signal and the background is due to pick-up noise from the driver of the acousto-optic modulator.

operation. With this setup, lasing anywhere in the gain bandwidth can be obtained by use of a proper Bragg grating. Furthermore, this setup shows a way to lock a low gain system, even if the volume Bragg grating has too high output coupling to be used inside a single cavity.

By changing the length of the internal cavity with a piezoelectric stack, the internal longitudinal mode and thus the laser wavelength can be tuned over the whole bandwidth of the Bragg grating feedback, as shown in Fig. 4.2(a). The laser

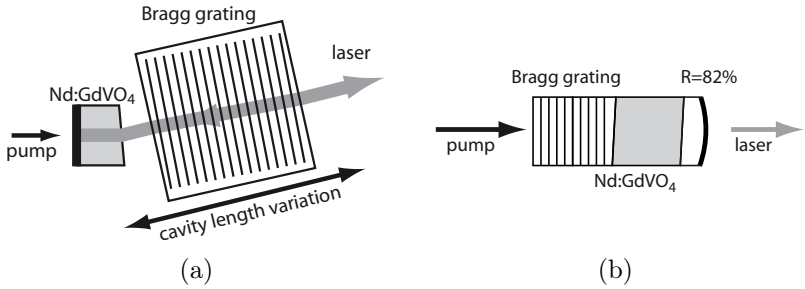

Figure 4.4: Nd:GdVO$_4$ laser setups. (a) Two free-standing components. (b) Monolithic setup.

was locked at a wavelength around 1552.6 nm, with a single-mode tuning range of 0.25 nm (31 GHz). This should be compared to a free running laser, that lases at about 1535 nm with multiple longitudinal modes. The details of the tuning is shown in Fig. 4.2(b), where it can be seen how the laser tunes in steps corresponding to the mode-spacing of the external cavity.

The laser was pumped by a fibre-coupled laser diode at 975 nm, and the total output power was about 13 mW for single-mode operation. The surfaces of the volume Bragg grating were left uncoated and thereby worked as an output coupler, in addition to the transmission of the grating itself, giving a total of three output beams.

To measure the linewidth of the laser, a fibre-based self-heterodyne technique was used, as described in Sec. 3.10. The result of the measurement is shown in Fig. 4.3, giving a laser linewidth of about 90 kHz.

4.2 Nd:GdVO$_4$ laser

In this section, I present a Nd:GdVO$_4$ laser locked with a volume Bragg grating in a single cavity [paper III, paper IV]. Thanks to the grating, single-longitudinal-mode operation was obtained and furthermore, the laser could be locked at 1066 nm off the main gain peak, as described in Sec. 3.9. With the grating as one of the cavity mirrors, one obtains a combination of the narrow linewidth of a Fabry-Pérot cavity and the single spectral peak selection of the Bragg grating. Below, two different experimental setups of the laser are described.

In the first experiments, reported in paper III, the laser consisted of two components, the gain medium with a deposited dielectric mirror on one surface, and the volume Bragg grating used as output coupler, see Fig. 4.4(a). The grating at 1066 nm is further described in Fig. 2.2. This laser was the first demonstration of a volume-Bragg-grating laser that was continuously tunable in a single longitudinal mode.

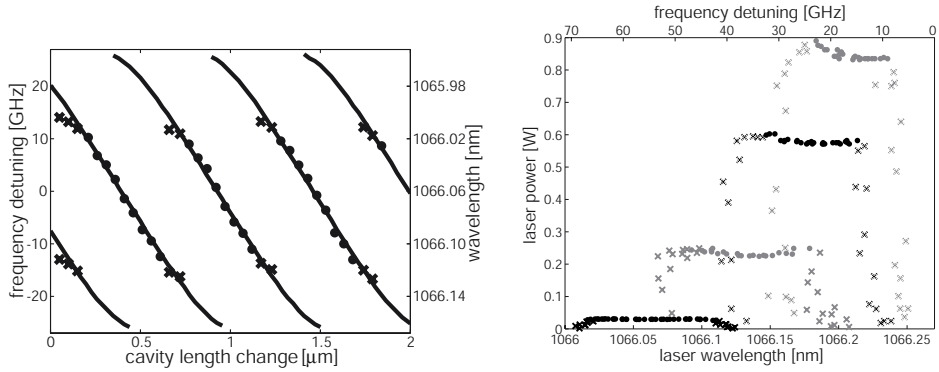

Figure 4.5: Tuning of Nd:$GdVO_4$ laser wavelength, dots for single longitudinal mode and crosses for multi-mode operation. (a) Detuning of laser wavelength with cavity length variation, experimental data (points) and theoretical prediction (lines). (b) Laser power and wavelength range at various absorbed pump powers, 0.14 W, 0.69 W, 1.5 W and 2.1 W.

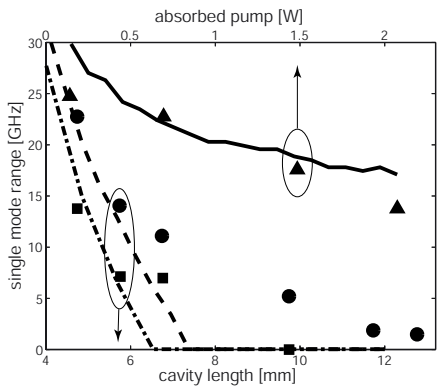

Figure 4.6: Range of operation in a single longitudinal mode for the Nd:$GdVO_4$ laser, experiments and theory, versus absorbed power (solid, triangles) for a 4.7 mm long cavity, and versus cavity length for a pump power of 0.69 W (dashed, circles) and 2.1 W (dash-dotted, squares).

By translation of the grating, the whole cavity length could be tuned, and thus the laser wavelength, as shown in Fig. 4.5(a). This is an experimental demonstration of the phase properties of the grating and the effective grating length, as described

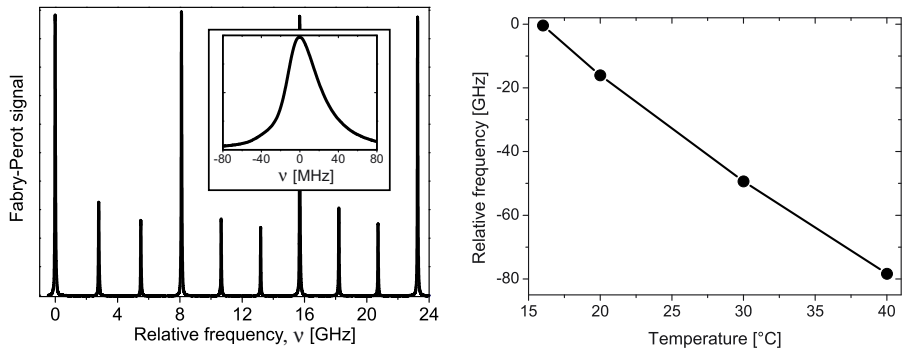

Figure 4.7: Spectral properties of the monolithic Nd:GdVO$_4$ laser. (a) Fabry-Pérot scan giving a linewidth upper limit of 40 MHz. The trace subpeaks are due to an interferometer transverse mode degeneracy of order 3 (cf. Sec. 3.9). (b) Temperature tuning of the laser frequency.

in Sec. 2.3. In Fig. 4.5(b), the laser power and wavelength at various pump powers is shown. At every pump power, the laser is tuned by grating translation, displaying the tuning interval. For increasing powers, the single-mode interval decreases, since more gain becomes available for the competing modes. Also, the grating peak and thus the laser wavelength are red-shifted, due to some minor absorption and subsequent heating of the grating.

To better understand for what conditions, both in terms of pump power and cavity length, that the laser can operate in a single longitudinal mode, a theoretical model was developed. The spatial hole-burning in the laser was modelled based on [158], with the filtering properties of the volume Bragg grating added. The predictions of the model, compared to the experimental findings, is shown in Fig. 4.6. As shown, the model gives fairly accurate predictions, although the interval of single-mode operation is somewhat underestimated.

Monolithic version

To maximize the stability and provide narrow linewidth, the Nd:GdVO$_4$ laser was also constructed in a monolithic version, described in detail in paper IV. In a monolithic setup, the technical noise that is the most important contribution to the broadening of a single laser line can be minimized. The setup was built from three different components glued together to form a single unit, shown in Fig. 4.4(b). The pump was coupled in through the volume Bragg grating and into the gain medium. Finally, the cavity was completed by a curved output coupler. With a curved output coupler, this mirror could be aligned by transverse translation of the

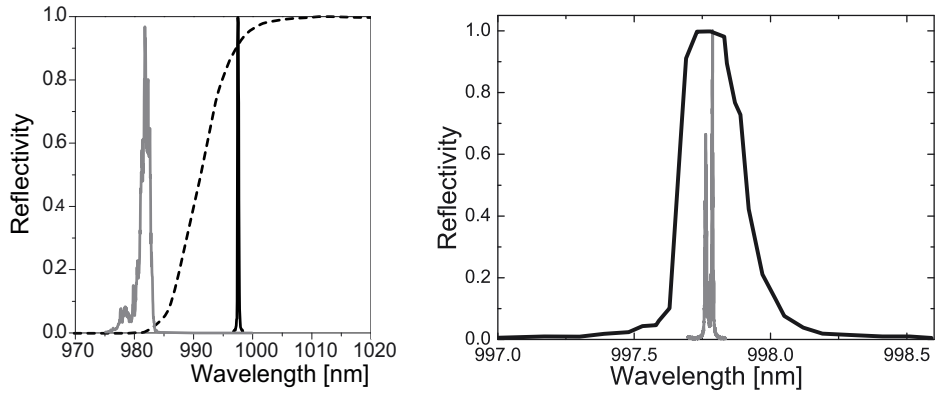

Figure 4.8: Spectral properties of the low quantum defect Yb:KYW laser. (a) Comparison between input couplers, a conventional dielectric one (dashed) and a volume Bragg grating (solid), next to the pump spectrum (grey). (b) Zoom in on the volume Bragg grating reflectivity (black) and the laser spectrum (grey) at maximum pump power.

whole monolithic piece, that was decoupled from the alignment of the flat grating mirror, which was done by rotation of the piece.

The laser bandwidth was measured with a scanning Fabry-Pérot interferometer, resulting in an instrument-limited bandwidth of 40 MHz, as shown in Fig. 4.7(a). Tuning of the wavelength of this laser was obtained by temperature tuning of the whole monolithic piece. Continuous tuning in a single mode could be performed over 80 GHz, see Fig 4.7(b). This is much longer than the cavity mode-spacing of 23 GHz, since simultaneously, both the cavity modes and the grating peak are tuned with temperature at approximately the same rate.

4.3 Yb:KYW laser with low quantum defect

Thanks to the strong spectral selectivity of a volume Bragg grating, combined with a peak reflectivity of almost 100%, it is especially suitable as an input coupler in an end-pumped laser with low quatum defect, i.e. small difference in energy between the pump and laser photons. Lowering the quantum defect of a laser can be desireable for two main reasons, to reduce the heating in the laser material, and to tune the laser to short wavelengths. These experiments [paper V, paper VI], with the volume Bragg grating as input coupler to reach low quantum defects, were the first demonstrations of this idea.

In this thesis, lasing with low quantum defect in Yb:KYW was studied. The

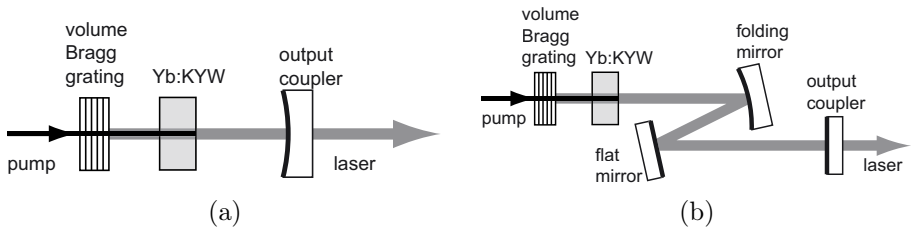

Figure 4.9: Low quantum defect diode-pumped Yb:KYW laser setups.

material Yb:KYW is interesting in this application both since it has high cross sections for closely spaced pump and laser wavelengths, and since the nonradiative losses are low.

At room temperature, the thermal population in the lower laser level is high in a laser with a low quantum defect. This can be understood by comparing the difference between the pump and laser energies in our experiments of 100 - 160 cm^{-1}, with the room temperature thermal energy of 200 cm^{-1}. To reach population inversion in a laser with a thermally populated lower level, intense pumping is needed, as demonstrated in Fig. 3.6. This is most easily achieved by end-pumping, but this poses a problem for the input coupler, that has to accommodate for the small spectral difference between pump and laser. A volume Bragg grating is a solution to this, since it provides much better spectral selectivity than a conventional mirror with dielectric coating. An example of this is shown in Fig 4.8(a). In addition, the volume Bragg grating will also lock the laser wavelength.

One application for these lasers with low quantum defect is to reach high powers. Thanks to the low quantum defect, little heat is deposited in the laser crystal, which enables high powers before the thermal limit is reached, either with too strong thermal lensing or by cracking the crystal due to too high temperature gradients. Ultimately, such lasers can be seen as brightness converters from the pump diodes into the Yb laser output. Both lasers are at approximately the same wavelength, but the transverse and spectral properties of the radiation are improved. If needed, pulsing or frequency conversion of the emitted laser light can also be added.

Diode-pumped laser

One additional advantage with Yb lasers is that they can be diode-pumped by high power semiconductor lasers at $\sim$ 980 nm. In paper V, a diode-pumped Yb:KYW laser with a volume Bragg grating as input coupler is described. The laser was pumped at 982 nm and locked by the grating to lase at 998 nm, see Fig. 4.8, with a quantum defect of 1.6%.

The setup of the laser is shown in Fig. 4.9. Initially, we used the setup in Fig. 4.9(a), but in order to control the laser mode size and the output coupler

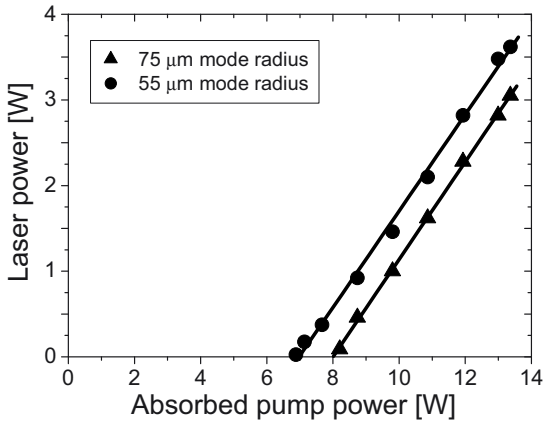

Figure 4.10: Output power of the diode-pumped Yb:KYW laser at 998 nm, for two different laser mode sizes. The pump mode size was ~ 90 μm.

reflectivity independently, and since no appropriate mirrors were available in our lab, the setup of Fig. 4.9(b) was used in subsequent experiments. Due to the thermal population of the lower laser level, the mode of the laser should preferably be smaller than the size of the pumped region, to reduce reabsorption loss. This mode size was controlled by the radius of curvature of the folding mirror, while the output coupling was determined by the flat output coupler. The laser output power is shown in Fig. 4.10 for two different mode sizes and the optimal output coupler reflectivity of 77%. The details of the laser spectrum, shown in Fig. 4.8(b), was measured with a scanning Fabry-Pérot interferometer, yielding a laser bandwidth of 10 GHz.

Ti:sapphire-pumped laser

In order to further investigate the limits of a low-quantum-defect laser with a volume-Bragg-grating input coupler, a Ti:sapphire-pumped setup was constructed [paper VI]. The Ti:sapphire pump laser has high brightness, so that very high pump intensity can be obtained, to counteract the strong reabsorption loss at low quantum defects. The level of inversion needed at various wavelengths is shown in Fig. 3.6. The laser setup is depicted in Fig. 4.11, providing a tight focus of both the pump and laser in the Yb:KYW laser crystal.

With the same setup, different input couplers were investigated, highly reflective volume Bragg gratings at 990 nm, 997 nm and 1066 nm, as well as an ordinary dielectric input coupler mirror (described in Fig. 4.8(a)). The corresponding laser wavelengths are shown in Fig. 4.12(a), together with the Ti:sapphire pump wavelength at 980 nm. For the lasing at 990 nm, at quantum defect of only 1.0% could

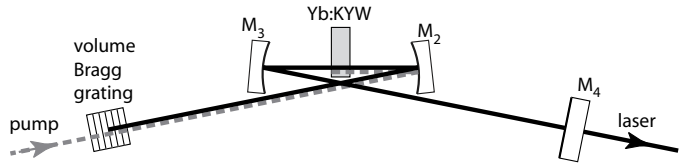

Figure 4.11: Setup of the Ti:sapphire-pumped Yb:KYW laser.

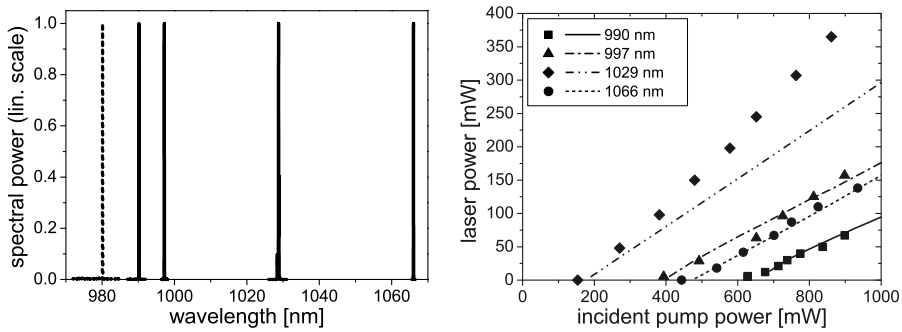

(a) (b)

Figure 4.12: Experimental results for the Ti:sapphire-pumped Yb:KYW laser. (a) pump and laser spectra. (b) Laser power at the various wavelengths, experiments (points) and theoretical predictions (lines).

thus be obtained. The output powers at the various wavelengths are shown in Fig. 4.12(b).

In addition, a theoretical model was developed to describe the laser system, based on numerically solving the rate equations locally at every point in the laser crystal. This model is described in more detail in paper VI. The predictions of the laser power is also shown in Fig. 4.12(b), displaying a fairly good agreement between experiments and theory.

4.4 Widely tunable Yb:KYW laser

Yb lasers provide a wide gain in the 1 μm region (see Figs. 3.4, 3.6), and can be diode-pumped to achieve an efficient laser system. Thus, a large tuning range is available, when combined with a spectrally selective element. Volume Bragg gratings can provide this strong spectral selectivity, and are therefore ideal for use as the wavelength selective element in an Yb laser. By use of the grating at oblique incidence, a widely tunable laser can be made possible by rotating the grating. Such

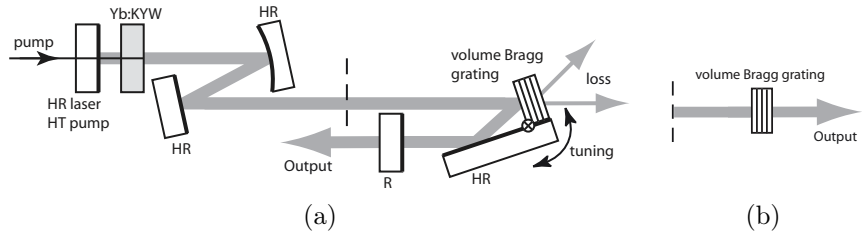

Figure 4.13: (a) Setup of the widely tunable Yb:KYW laser. (b) Setup with the grating at normal incidence.

lasers are presented in paper VII and paper VIII, and were the first experimental demonstrations of laser tuning by rotation of a volume Bragg grating.

Special attention has to be paid to some features of the laser design. First, to avoid beam steering of the grating-tuned laser, we used a retroreflector setup for the Bragg grating, as described in Sec. 2.5. Second, due to the increased angular selectivity of the grating, when used at oblique incidence, there is a risk of a severely reduced grating reflectivity, as described in Sec. 2.4. To minimize this loss, we designed the laser, so that the laser mode in the grating part of the laser was large. Also, the polarization of the light on the grating affects this loss. In the first experiments [paper VII], p-polarization was used. Subsequently, we found experimentally [paper I] that s-polarization leads to lower loss. Thus, a laser running at s-polarization was constructed [paper VIII], showing better efficiency.

In Fig. 4.13(a), the setup for realizing the widely tunable Yb:KYW laser is shown. The laser was diode-pumped at 982 nm through a dielectric input coupler (see Fig. 4.8(a)). The volume Bragg grating that was used for the tuning had a reflectivity for normal incidence of 97% at 1063 nm and 0.55 nm FWHM bandwidth.

The performance of the laser is displayed in Fig. 4.14, showing the output power at various conditions. Tuning from 996 nm to 1048 nm is obtained, with output powers up to 3 W in a single beam. As can be seen, the reduced losses with s-polarization indeed leads to higher output power. The limitations of the tuning range are determined at short wavelengths by the input coupler loss (Fig. 4.8(a)), and at longer wavelengths by the reduced gain (Fig. 3.6). A detailed measurement of the laser spectrum was performed with a scanning Fabry-Pérot interferometer, revealing a bandwidth of 10 GHz.

The laser was also investigated with the grating at normal incidence, as shown in Fig. 4.13(b). Then, the outcoupling loss was reduced and an efficient laser at 1063 nm could be demonstrated, with 3 W of output power (Fig. 4.14).

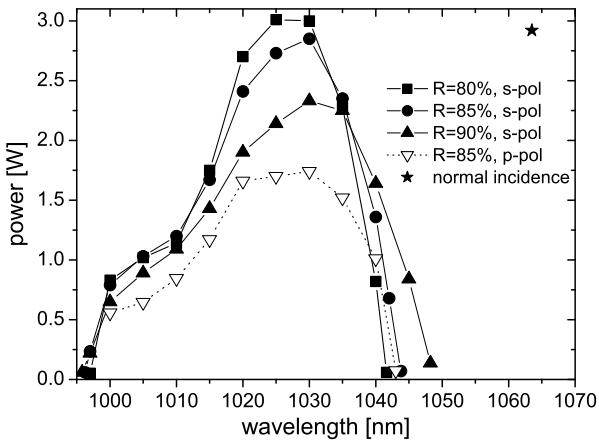

Figure 4.14: Maximum output power at various wavelengths of the tunable Yb:KYW laser.

Chapter 5

OPO theory

5.1 Nonlinear optics

Light at new wavelengths can be generated with nonlinear optics, via conversion of the photon energy through interaction with a nonlinear material polarization in a medium. Nonlinear effects appear if the driving electric field in a material is strong enough so that the material polarization response is nonlinear. In a laser beam, very high fields can be obtained, why nonlinear optical processes are usually pumped by lasers. Like most physical processes, the efficiency of the nonlinear interaction is regulated by conservation of energy and momentum, the latter most often referred to as phase-matching in the field of optics. The discussion given in this chapter is based on references [108, 162, 163].

To understand how new wavelengths are generated in nonlinear optical interactions, consider Fig. 5.1. Here it is assumed that an electric field E at two frequencies ω_1 and ω_2 interacts with a material that has a response shown in Fig. 5.1(a). The generated material polarization P then contains new frequencies (Fig. 5.1(b)), due to the nonlinear material response. Finally, P acts as a source for generating light and the material radiates waves at the generated frequencies.

If the nonlinear process is not too close to an absorption resonance, the material polarization P and thus the generated electric field can be described by a series expansion of the incident field E

$$P = \epsilon_0 \sum_{n=1}^{\infty} \chi^{(n)} E^n. \tag{5.1}$$

In this work, the second order term is of special interest, as governed by the second order susceptibility $\chi^{(2)}$. The first order term is responsible for ordinary linear optics as described by the refractive index $n = (\mathrm{Re}\left[\chi^{(1)}\right]+1)^{1/2}$ and linear absorption $\alpha = \mathrm{Im}\left[\chi^{(1)}\right]\omega/(nc)$. The third order term is also of practical importance, being

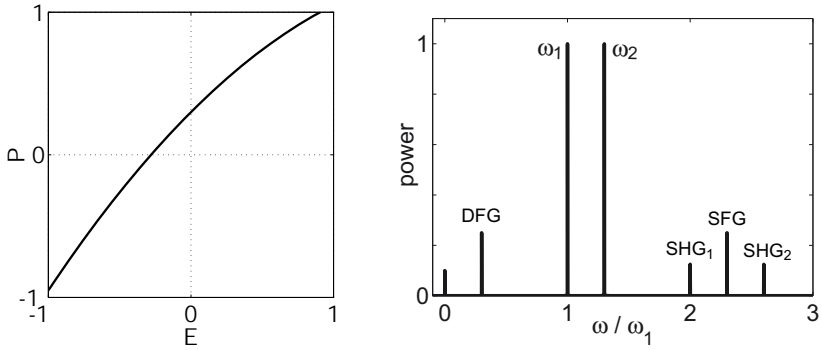

Figure 5.1: Example of a second order nonlinear process with an incident electric field E at two frequencies ω_1 and $\omega_2 = 1.3\omega_1$ generating a material polarization P. (a) Nonlinear material polarization response. (b) Power spectrum of the material polarization P, with different processes identified.

the first nonlinear term in isotropic materials, where $\chi^{(2)} = 0$ (see below). The 4th and higher order terms, however, are usually too weak to be of interest.

The nonlinear interaction of interest is then

$$P_i^{(2)} = \sum_{jk} \chi_{ijk}^{(2)} E_j E_k, \tag{5.2}$$

for the different polarization directions of the fields $(i, j, k) = 1, 2, 3$. For narrow-band optical signals, it is convenient to consider the Fourier components of the fields, given by $E_i(t, z) = 1/2 \sum_m E_i(\omega_m, z) \exp(i(\omega_m t - k_m z)) + c.c.$ etc, for a plane wave travelling in the z-direction. The nonlinear interaction is then given by

$$P_i^{(2)}(\omega_\alpha) = \sum_{jk} \sum_{\beta\gamma} \chi_{ijk}^{(2)}(-\omega_\alpha; \omega_\beta, \omega_\gamma) E_j(\omega_\beta) E_k(\omega_\gamma), \tag{5.3}$$

The labelling of the arguments of $\chi^{(2)}$ is chosen to reflect energy conservation, $-\omega_\alpha + \omega_\beta + \omega_\gamma = 0$.

Symmetry relations

The description of nonlinear optics can be simplified by considering a number of symmetry relations, given below.

First, the nonlinear susceptibility reflects the structural symmetry of the nonlinear material. This reduces the number of non-zero components of $\chi_{ijk}^{(2)}$. Another consequence is that second order processes can only exist in a material without

inversion symmetry. Thus, anisotropic crystals are used as the nonlinear medium for second order interactions.

Furthermore, $\chi^{(2)}_{ijk}$ has a permutation symmetry, since multiplication of electric fields is commutative, thus $\chi^{(2)}_{ijk} = \chi^{(2)}_{ikj}$. To reflect this symmetry, it is common to re-express the nonlinear tensor as $\chi^{(2)}_{ijk} = 2d_{il}$. Here the index l is given by the transformation $\begin{smallmatrix} jk = & 11 & 22 & 33 & 23 & 32 & 13 & 31 & 12 & 21 \\ l = & 1 & 2 & 3 & 4 & 4 & 5 & 5 & 6 & 6 \end{smallmatrix}$.

Finally, Kleinman symmetry is valid if all interacting waves are far from absorption and with no absorption in between the waves' frequencies. Then, the nonlinear tensor is independent of the frequency of the interacting fields, so that $\chi^{(2)}_{ijk}(-\omega_1;\omega_2,\omega_3) = \chi^{(2)}_{ijk}(\omega_2;-\omega_1,\omega_3) = \chi^{(2)}_{ijk}(\omega_3;\omega_2,-\omega_1)$ etc. This means, e.g., that the nonlinear coefficient has the same value for both SHG and OPG.

As an example, consider the second order nonlinear susceptibility of the nonlinear crystal used in this thesis, $KTiOPO_4$ (KTP). KTP belongs to the symmetry class $mm2$. Furthermore, if the interacting waves are in the transparency region between 0.4 - 3 μm [164], Kleinman symmetry holds. The tensor structure is then

$$d = \begin{pmatrix} 0 & 0 & 0 & 0 & d_{31} & 0 \\ 0 & 0 & 0 & d_{32} & 0 & 0 \\ d_{31} & d_{32} & d_{33} & 0 & 0 & 0 \end{pmatrix}, \tag{5.4}$$

with the numerical values of d_{31}=2 pm/V, d_{32}=4 pm/V, d_{33}=15 pm/V, measured for frequency doubling of 1064 nm light [165].

5.2 Energy conservation

The Fourier components of the generated material polarization, and thus the generated optical wave, is determined by the frequencies of the incident fields, shown in (5.3). This can be expressed as conservation of photon energy from the incident frequencies ω_1 and ω_2 to the generated frequency ω_3

$$\omega_3 = \omega_1 + \omega_2. \tag{5.5}$$

The different possible second order processes can be characterized by the energy relations between the interacting fields:

second harmonic generation	SHG	$2\omega = \omega + \omega$
sum frequency generation	SFG	$\omega_3 = \omega_1 + \omega_2$
difference frequency generation	DFG	$\omega_3 = \omega_1 - \omega_2$
optical parametric amplification	OPA	$\omega_i = \omega_p - \omega_s$
optical parametric generation	OPG	$\omega_i = \omega_p - \omega_s$
optical parametric oscillation	OPO	$\omega_i = \omega_p - \omega_s$

As can be seen, DFG, OPA, OPG and OPO are all based on the same energy conversion processes, depicted in Fig 5.2(a). For the parametric processes, the

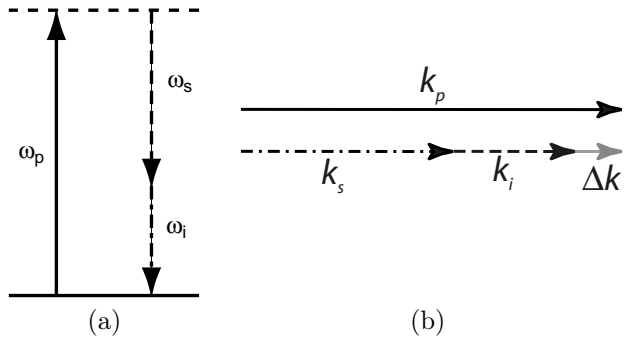

Figure 5.2: Physical restrictions of a parametric process: (a) Conservation of energy. (b) Phase-matching.

interacting waves are called pump p, signal s and idler i, with $\omega_p > \omega_s > \omega_i$. The distinction between the processes is given by the relative distribution of energy in the incident beams. For DFG, the incident pump and signal energies are of the same order, while for OPA the signal is much weaker than the pump, and subsequently amplified in the process. In OPG, the only incident beam is the pump, but the required signal (or idler) incident energy is taken from the very small vacuum fluctuations of the radiation field. In an OPO, the OPG process is enhanced by providing cavity feedback for the signal (and/or idler).

Since there are vacuum fluctuations at all possible frequencies, with OPG or OPO processes, any signal and idler frequencies that are lower than the pump frequency can be generated from the photon energy conservation point of view. Instead, the limiting and governing process is the phase-matching described below. In an OPO, the cavity feedback provides another means to control the generated frequencies, as described in Sec. 5.7.

5.3 Phase-matching

In order for a nonlinear process to be efficient over a distance, the phase velocities of the interacting waves must be the same, something called phase-matching. This corresponds to momentum conservation for the interacting photons. For a second order process with the Fourier description, the phase mismatch is

$$\Delta\mathbf{k} = \mathbf{k}_3 - \mathbf{k}_1 - \mathbf{k}_2, \tag{5.6}$$

shown in Fig 5.2(b) for a parametric process. Phase-matching is achieved when $\Delta k = 0$. Because of dispersion of the refractive index, with $k_i = \omega_i n(\omega_i)/c$, phase-matching is usually not the case for waves of different frequencies.

Birefringent phase-matching, first suggested in [15, 16, 166, 167], is a method for phase-matching where a birefringent crystal with different refractive indices for

orthogonal polarizations is used. By having different polarizations of the interacting waves and by an appropriate rotation of the crystal, most interactions where the phase mismatch is not too large can be birefringently phase-matched. A drawback is that in some directions of a birefringent crystal, there is walk-off between beams of orthogonal polarization, limiting the interaction length and generating a distorted output beam. Also, not all components of the nonlinear tensor can be used, since the interacting waves must be of orthogonal polarizations.

In this thesis, I use another method for phase matching, called quasi phase-matching (QPM), first suggested in 1962 [168]. The idea is to reset the phase of the generated wave periodically, so that the phase of the generated wave is never more than 180° out of phase with the generating wave, thereby preventing back-conversion. This is done by a periodic modulation of the nonlinear susceptibility, with a period $\Lambda = 2l_c$ given by the coherence length of the interaction $l_c = \pi/\Delta k$. Typically, l_c has a size of 10s of μm. In the Fourier picture, quasi phase-matching can be described by a QPM wave vector $k_Q = 2\pi/\Lambda$ in the direction of the modulation, given by a Fourier transform of the susceptibility modulation. The phase mismatch is then modified to

$$\Delta\mathbf{k}' = \mathbf{k}_3 - \mathbf{k}_1 - \mathbf{k}_2 - \mathbf{k}_Q. \tag{5.7}$$

By tailoring the period Λ appropriately, phase-matching $\Delta k' = 0$ can thus be obtained. Since the phase is only reset at discrete positions, the efficiency of the interaction with QPM is reduced. For a first order interaction and 50% duty cycle, as used in this work, the d-coefficient is then reduced to $d_{QPM} = 2d/\pi$.

For the experiments in this thesis, electric field poling, first demonstrated in [169], was used to obtain the QPM structure. The idea is to invert the material polarization of a ferroelectric material periodically, and thus obtain the desired susceptibility modulation. This is done by applying an electric field over the crystal via a periodic electrode. If the field is larger than the coercive field, the crystal can be periodically poled (PP). In reality, this process is not so easy, as shown by the more detailed description given in [170], with details of electric field poling in KTP.

The main benefit with QPM compared to birefringent phase-matching is that the material is engineered to suit the desired application. In addition, the largest nonlinear coefficient can be used, d_{33} in KTP, with all the interacting waves in the same polarization.

5.4 Optical parametric oscillators

As described in the preceding sections, with parametric processes in QPM crystals, it is possible to generate any desired wavelength longer than the pump wavelength, with the restriction that the generated waves should be within the transparency range of the nonlinear crystal.

The experiments in this work were based on optical parametric oscillators (OPOs), where the nonlinear crystal is placed in a cavity, shown in Fig. 5.3. The cavity mir-

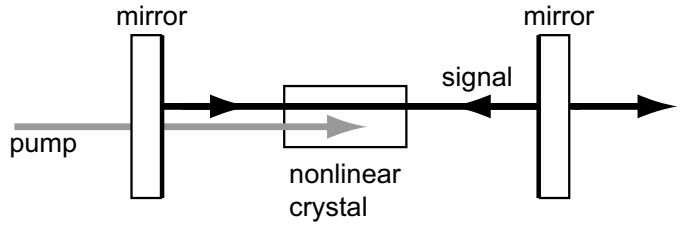

Figure 5.3: A schematic OPO, containing a pump, a nonlinear medium and a feedback cavity for the OPO signal.

rors around the parametric gain provide feedback for the generated signal (and/or idler) which increases the efficiency of the process. The cavity also provides a means to control the generated waves.

Obviously, there are some similarities between an OPO and a laser, since both are oscillators composed of a gain element inside a Fabry-Pérot feedback cavity. Because of the similarities, they both have a threshold of operation and can display a longitudinal mode structure. On the other hand, an OPO differs from a laser in that there is no energy storage from the pump to the output, since the nonlinear response is much faster (some fs) than the cavity roundtrip time. Also, in an OPO, the phase of the interacting beams is very important, while in a laser, most of the properties of the absorbed pump beam, such as phase, are forgotten before the stimulated laser emission takes place.

In this thesis, singly resonant OPOs (SROs) were used, where only the signal wave is resonated in the cavity. A doubly resonant OPO (DRO), in contrast, resonates both signal and idler. In a DRO, the requirements on the cavity are very strict, since two waves must be resonant at the same time, usually requiring active cavity stabilization. In an SRO, the signal is free to be adjusted to the cavity, and the setup can be made simple and passive.

To reach oscillation in an OPO, a high pump intensity is needed, as shown below. With the high pump intensity, the damage threshold of the involved components is also an important issue. The nonlinear crystal used in this work, KTP, has a damage threshold of about 5 J/cm^2 for nanosecond pulses at 500 nm, while special attention must also be paid to have durable coatings on the cavity mirrors.

5.5 Parametric gain

Some understanding of the evolution of the fields in a nonlinear interaction can be found by considering the governing differential equations in the plane wave approximation. These are derived from the wave-equation with the nonlinear polarization $P^{(2)}$ as the driving term. By assuming that the envelope of the fields varies slowly

spatially, a set of first order coupled equations for the Fourier amplitudes of the fields is obtained

$$\frac{\mathrm{d}E(\omega_s)}{\mathrm{d}z} = -i\frac{\omega_s d_{\text{eff}}}{cn_s}E^*(\omega_i)E(\omega_p)e^{-i\Delta kz} \tag{5.8}$$

$$\frac{\mathrm{d}E(\omega_i)}{\mathrm{d}z} = -i\frac{\omega_i d_{\text{eff}}}{cn_i}E^*(\omega_s)E(\omega_p)e^{-i\Delta kz} \tag{5.9}$$

$$\frac{\mathrm{d}E(\omega_p)}{\mathrm{d}z} = -i\frac{\omega_p d_{\text{eff}}}{cn_p}E(\omega_s)E(\omega_i)e^{i\Delta kz}. \tag{5.10}$$

The frequencies of the fields are determined by conservation of energy (5.5). In addition, it can be seen that the phase mismatch Δk (see (5.6) and (5.7)) plays a crucial role in the interaction. In these equations, the polarization direction of the fields, the type of phase-matching and the material properties are all incorporated in the effective nonlinear coefficient d_{eff}. As an example, for QPM in PPKTP with all fields in the c-direction, $d_{\text{eff}} = 2d_{33}^{\text{KTP}}/\pi$.

From the coupled wave equations, a condition for the energy flow between the fields can be determined, called the Manley-Rowe relation. It states that for the intensities of the beams,

$$-\frac{1}{\omega_p}\frac{\mathrm{d}I_p}{\mathrm{d}z} = \frac{1}{\omega_s}\frac{\mathrm{d}I_s}{\mathrm{d}z} = \frac{1}{\omega_i}\frac{\mathrm{d}I_i}{\mathrm{d}z}. \tag{5.11}$$

This can be interpreted by considering the individual photons, for each pump photon, one signal photon and one idler photon is created.

Next we consider the single-pass signal amplification in a parametric device of length L, pumped by a plane wave. If the incident signal is small, we can initially assume a constant pump without depletion. The amplification is given by integration of the coupled wave equation, yielding

$$\frac{I_s(L)}{I_s(0)} = 1 + \Gamma^2\frac{\sinh^2\left(L\sqrt{\Gamma^2 - (\Delta k/2)^2}\right)}{\Gamma^2 - (\Delta k/2)^2}, \tag{5.12}$$

where we define the parameters

$$\Gamma^2 = \kappa I_p, \quad \kappa = \frac{8\pi^2 d_{\text{eff}}^2}{\epsilon_0 c n_p n_s n_i \lambda_s \lambda_i}. \tag{5.13}$$

To simplify the equation, we assume that $\Gamma L \gg 1$, giving the approximation

$$\frac{I_s(L)}{I_s(0)} = \frac{1}{4}\exp\left(2L\sqrt{\Gamma^2 - (\Delta k/2)^2}\right) \tag{5.14}$$

This shows that the amplification is exponential, which is the reason for talking about a parametric gain. For phase-matching $\Delta k = 0$, the gain coefficient is Γ. In

a typical PPKTP crystal under OPO pumping conditions, the single-pass small-signal gain is about $\Gamma L \sim 10$, giving an amplification of ~ 80 dB.

The above equations assume that we have plane waves. However, it can be seen that the interactions are more efficient for higher intensity, so the properties for strongly focussed beams might be of interest. Still, for the experiments in this thesis, with PP materials and nanosecond pump lasers with flashlamp pumping, the limiting factor for the beam intensity is usually optical damage to the components. Thus, to obtain as high energies as possible, the focussing is then adjusted to fill the aperture of the PP crystal. For typical situations, the confocal length of the beams is then larger than the crystal length, which justifies the use of plane-wave theory.

5.6 OPO energy properties

An OPO reaches threshold when the gain exceeds losses. For a nanosecond OPO, the pump energy threshold is [171]

$$\mathcal{E}_{th} = \frac{0.6\tau(w_p^2 + w_s^2)}{\kappa L^2}\left[\frac{25l}{\tau c} + \frac{1}{2}\ln\frac{2}{R(1-A)}\right]^2. \tag{5.15}$$

Here R is the output coupler reflectivity, A the roundtrip losses, τ the FWHM pulse length, l the cavity optical length, L the crystal physical length and w_p, w_s the mode radius of the pump and signal, respectively.

Above threshold, the generated signal and idler depletes the pump, so that the gain still equals the losses. For a nanosecond OPO, the dynamics of these processes is rather complex, and no simple theoretical model exists to describe it. An experimental investigation of the temporal and spectral dynamics of a nanosecond OPO can be found in [172].

As a measure of how well the OPO is working, both the pump depletion η_{depl} and the efficiency η_{eff} are used. The pump depletion shows the nonlinear loss for the pump in the OPO. This can be measured by a comparison with the pump transmission below OPO threshold, where there is only linear loss. If we let $\mathcal{E}_p^*$ be the pump energy at some point below OPO threshold, the pump depletion is given by

$$\eta_{\text{depl}} = 1 - \frac{\mathcal{E}_p^{\text{out}}}{\mathcal{E}_p^{\text{in}}}\frac{\mathcal{E}_p^{*\text{in}}}{\mathcal{E}_p^{*\text{out}}}. \tag{5.16}$$

The efficiency of the OPO measures how much of the pump energy is converted into signal and idler

$$\eta_{\text{eff}} = \frac{\mathcal{E}_s^{\text{out}} + \mathcal{E}_i^{\text{out}}}{\mathcal{E}_p^{\text{in}}}. \tag{5.17}$$

If the idler energy is not measured, it can be deduced from the Manley-Rowe relation (5.11) as $\mathcal{E}_i^{\text{out}} = \mathcal{E}_s^{\text{out}}\lambda_s/\lambda_i$. For a perfect OPO, all the depleted pump should go into signal and idler, and the depletion and efficiency should be equal. In a real

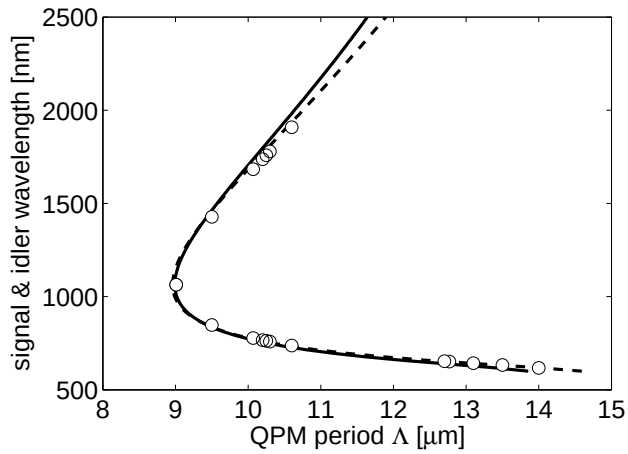

Figure 5.4: QPM phase-matching conditions for a parametric interaction in PPKTP at 532 nm pump wavelength and room temperature, with all waves polarized in the c-direction. Theoretical simulations with refractive indices taken from Fan *et al.* (solid) [173] and Fradkin *et al.* (dashed) [174], as well as our experimental results (circles).

system, there is usually some loss in the OPO process, and a comparison of the depletion and efficiency is a good measure of this.

5.7 OPO spectral properties

In an OPO, the spectrum of the generated signal and idler are determined both by the gain spectrum and the cavity conditions.

Gain tuning

The spectral location of the parametric gain is given by the phase-matching conditions, for a QPM interaction (5.7) given by explicitly as

$$\omega_p n_p \hat{\mathbf{k}}_p - \omega_s n_s \hat{\mathbf{k}}_s - \omega_i n_i \hat{\mathbf{k}}_i - \frac{2\pi c}{\Lambda}\hat{\mathbf{k}}_Q = 0. \tag{5.18}$$

Tuning of the gain and thus the signal wavelength can be done by working on the phase-matching condition, by acting on different parameters of the above equation. For QPM, the methods for tuning of the signal wavelength include changing the QPM period, tuning of the pump wavelength, changing the temperature of the

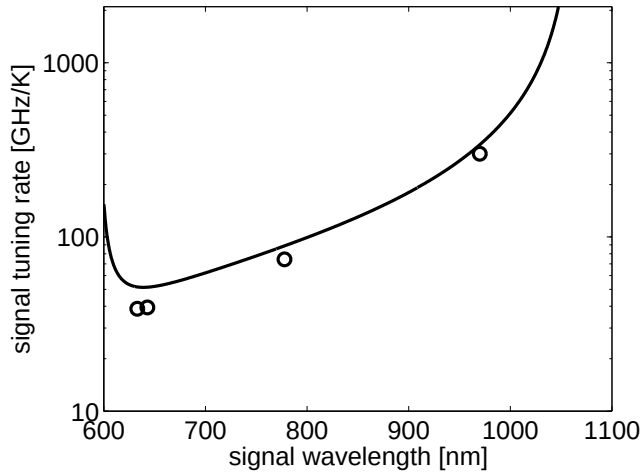

Figure 5.5: Temperature tuning rate of the parametric signal in PPKTP pumped at 532 nm with all waves polarized in the c-direction. Theoretical simulations (line) with n taken from [174], $\mathrm{d}n/\mathrm{d}T$ from [175] and α in the a-direction from [176], as well as our experimental results (circles).

nonlinear crystal and changing the angles between the interacting beams and the crystal.

Fabricating the desired QPM period is the main method to determine the signal wavelength. From the QPM condition (5.18), the period in a collinear interaction is given by

$$\Lambda = \frac{c}{\nu_p n_p - \nu_s n_s - \nu_i n_i} = \frac{1}{\frac{n_p}{\lambda_p} - \frac{n_s}{\lambda_s} - \frac{n_i}{\lambda_i}}. \tag{5.19}$$

An example is given in Fig. 5.4 for the type of OPOs used in this thesis. The accuracy of the prediction is shown by the comparison to the experimentally measured data, and depends on the accuracy in the used refractive indices.

Once the QPM crystal has been fabricated, it is often desirable to slightly move the gain spectrally. In this work, this was done by temperature tuning of the crystal. The tuning rate of the frequency is given by differentiating (5.18) with respect to temperature, yielding for a collinear interaction

$$\frac{\mathrm{d}\nu_s}{\mathrm{d}T} = \frac{1}{c\left(\frac{1}{v_{gs}} - \frac{1}{v_{gi}}\right)} \left[\nu_p \frac{\mathrm{d}n_p}{\mathrm{d}T} - \nu_s \frac{\mathrm{d}n_s}{\mathrm{d}T} - \nu_i \frac{\mathrm{d}n_i}{\mathrm{d}T} + \frac{c}{\Lambda}\alpha\right], \tag{5.20}$$

with the coefficient of thermal expansion α and the group velocity $v_g = 1/(\partial k/\partial\omega)$. At degeneracy, the temperature tuning rate is singular, but this is of little practical

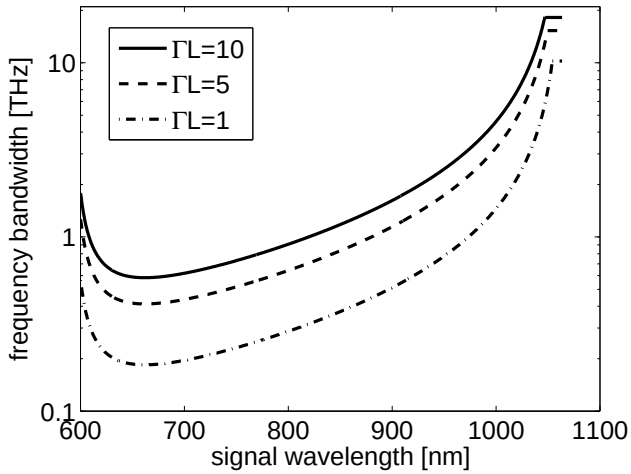

Figure 5.6: Simulation of collinear OPG signal bandwidth (5.23) and (5.24) at various gain levels for 532 nm pump and all beams polarized in the c-direction of a 10 mm long PPKTP (refractive index from [173]).

interest, since the large bandwidth of the gain is the dominant effect there (see below). An example of the theoretical temperature tuning rate is given in Fig. 5.5, together with some experimental data.

Fine adjustments of the signal wavelength can also be done with angular tuning, by changing the angles of the wave vectors of (5.18). A more detailed description can be found in [177–179], where also some experimental examples are given.

Gain bandwidth

The bandwidth of the OPG gain can be obtained from (5.14). First, the value of Δk for which the amplification is reduced to half is determined, which is given by

$$\Delta k_{1/2} = 2(\ln 2)^{1/2}(\Gamma/L)^{1/2}. \tag{5.21}$$

Next, this mismatch is related to a detuning of the signal frequency $\Delta\omega_s$ around the point $\Delta k = 0$. For a collinear interaction, a series expansion of Δk yields

$$\Delta k = (1/v_{gs} - 1/v_{gi})\Delta\omega_s + (1/2)(\beta_{2s} + \beta_{2i})(\Delta\omega_s)^2. \tag{5.22}$$

Here, the group velocity is $v_g = 1/(\partial k/\partial\omega)$ and the group velocity dispersion is $\beta_2 = \partial^2 k/(\partial\omega^2)$. Finally, the FWHM gain bandwidth off degeneracy is

$$\Delta\nu = \frac{2(\ln 2)^{1/2}}{\pi}\left(\frac{\Gamma}{L}\right)^{1/2}\frac{1}{\left|\dfrac{1}{v_{gs}} - \dfrac{1}{v_{gi}}\right|}. \tag{5.23}$$

At degeneracy, where $v_{gs} = v_{gi}$ for signal and idler in the same polarization, the bandwidth is instead given by

$$\Delta\nu = \frac{2(\ln 2)^{1/4}}{\pi}\left(\frac{\Gamma}{L}\right)^{1/4}\frac{1}{|\beta_{2s} + \beta_{2i}|^{1/2}}. \tag{5.24}$$

An example of the bandwidth is given in Fig. 5.6.

Since the signal wavelength is sensitive to angular tuning, the angle of the fields also have impact on the gain bandwidth. First the incident beam is usually not a perfect plane wave. Thus, parts of the beam with slightly different directions will experience different phase-matching conditions, leading to a broader bandwidth overall for the beam. Second, the gain bandwidth is sensitive to the angles of the incident beams, and can be increased by using a non-collinear interaction [179].

Cavity effects

The cavity of an OPO acts on the spectrum of the signal in two main ways. First, the repeated passes around the cavity will narrow the bandwidth compared to the parametric gain, effectively by multiplying the gain by itself. Second, the longitudinal modes of the cavity might be imposed on the gain spectrum. However, in a pulsed OPO with a pump with larger bandwidth than the longitudinal mode spacing, such as the OPOs in this thesis, the mode buildup is limited. The reason is that the buildup of modes requires the signal to have a constant phase over a number of cavity roundtrips. This is limited both by a short pump pulse and if the pump phase varies due to the pump spectral bandwidth, since the signal phase is sensitive to this.

To control and narrow the OPO signal spectrum further, additional filters can be introduced into the OPO cavity. An overview of such filters is given in Sec. 2.7. In addition to provide narrow bandwidth and low losses, such a filter must also be able to handle the high intensities that are present in an OPO cavity. Another option is to use a seed source to spectrally control the signal wavelength, in a combination of an OPO and an OPA. Still, if there is a good seed source available, an OPA is usually a less complicated solution, while OPOs serve best where there are no good seed sources.

In this thesis, volume Bragg gratings were used as intracavity filters in the OPO cavity, by simply replacing one of the cavity mirrors by a grating. The gratings show narrow bandwidth and low loss, in addition to high damage threshold, as described in Sec. 2.1.

5.8 OPO pumping

To reach oscillation in an OPO, a high pump intensity is needed, as shown above. In this work, the pumping was done by a pulsed, Q-switched Nd:YAG laser with flashlamp pumping giving nanosecond long pulses. Such lasers are based on a mature technology and provide reliable pump sources around 1 μm or at higher harmonics, such as the 532 nm wavelength used in this work.

Due to the phase dependence of the signal on the pump, the transverse and spectral properties of the pump laser has impact on the signal. For this reason, the behaviour of an OPO might be rather different, depending on the pump laser. In this work, I used a multimode pulsed (5 ns) laser with a spectral bandwidth of ~ 50 GHz and an M^2 value of > 5. Consequently, it can be expected that the signal beam at best inherits similar values. Furthermore, perfect mode-matching of the signal cavity-mode and the pump laser was not of primary concern, since the inherited pump properties were more important. Thus, flat-flat OPO cavities were used, for increased simplicity.

Chapter 6

OPO experiments

Optical parametric oscillators are useful as sources of coherent light at wavelengths where there are no efficient lasers available. With nanosecond pumping of singly resonant OPOs based on periodically poled materials, efficient conversion can be obtained to any selected wavelength longer than that of the pump. However, a drawback is that the generated radiation has a rather broad spectral bandwidth, unless appropriate measures are taken. To narrow this bandwidth, a spectrally selective element should be incorporated in the OPOs.

In this thesis, I demonstrate how reflective volume Bragg gratings can be used in OPOs to narrow the bandwidth, as presented in paper IX, paper X and paper J. Volume Bragg gratings in photo-thermo-refractive glass are especially suited for nanosecond OPOs for two main reasons, they can provide narrow bandwidth and they can endure the high optical fluency needed to run the OPO.

6.1 Narrowband OPO at 975 nm

In this experiment, a linear OPO cavity was used, where the output coupler was a volume Bragg grating. This was the first ever demonstration of locking and narrowing of an OPO with a volume Bragg grating [paper IX].

The experimental setup is depicted in Fig. 6.1(a), consisting of an input coupler, a nonlinear crystal and the volume Bragg grating output coupler. The OPO was pumped by 5 ns pulses at 532 nm from a frequency doubled Nd:YAG laser. The nonlinear crystal was a PPKTP with a period of 9.01 μm heated to 66 °C to provide parametric gain at the signal wavelength of 975 nm. This wavelength was matched to the Bragg grating, with a peak reflectivity of 27% at 975.3 nm with 0.73 nm FWHM bandwidth. For comparison, a conventional dielectric mirror of 50% reflectivity was also used as output coupler.

The spectrum of the OPO signal is shown in Fig. 6.2(a). The bandwidth of the Bragg grating OPO signal was 50 GHz (0.16 nm), 20 times reduction compared to

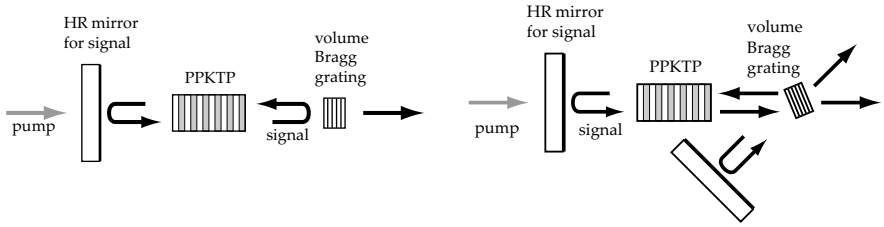

(a) (b)

Figure 6.1: Setup of the OPO at 975 nm. (a) Linear cavity. (b) Folded cavity for angular tuning.

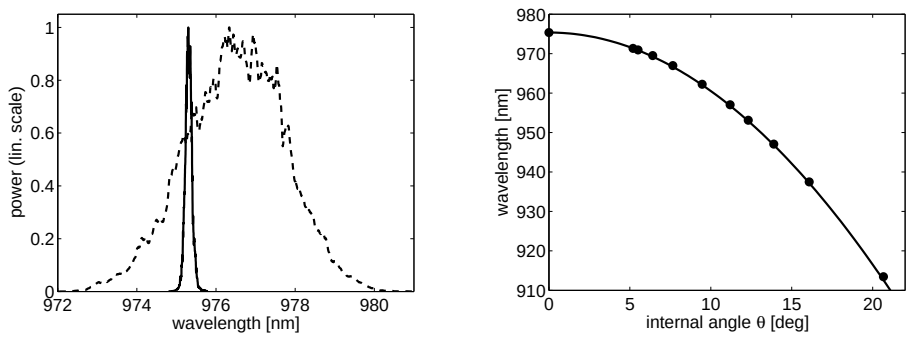

(a) (b)

Figure 6.2: Spectral properties of the OPO at 975 nm. (a) Spectrum at normal incidence, with a volume Bragg grating (solid) or a conventional mirror (dashed) as output coupler. (b) Tuning for oblique incidence, experiments (circles) and theory (line).

that of the conventional mirror. The output energy of the Bragg-locked OPO was at the same time comparable to that of the conventional OPO. In Fig. 6.3, the signal power as well as the pump depletion and the OPO efficiency are shown. Fairly efficient conversion from pump to signal was obtained, with pump depletion up to 55%. As can be seen by the difference between the depletion and efficiency, there is some loss in the OPO process. This loss was also seen with the conventional ouput coupler, and is thus not due to the volume Bragg grating. A possible explanation of the loss is diffraction loss of the signal in the OPO cavity.

In order to tune the OPO wavelength, the Bragg grating was also used at oblique incidence and rotated, as shown in Fig. 6.1(b). By rotation of the grating, the signal wavelength could be tuned, shown in Fig. 6.2(b), with the expected cosinusoidal

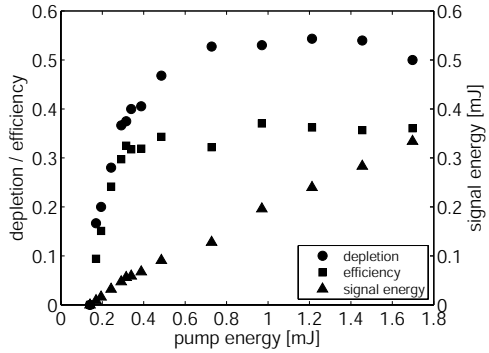

Figure 6.3: Energy properties of the 975 nm Bragg-locked OPO.

dependence on the incidence angle (2.2). Simultaneously, the parametric gain was tuned by changing the temperature of the PPKTP crystal.

6.2 Angle-tuned ring OPO at 760 nm

In this experiment, it is shown how angular tuning of the Bragg wavelength in a ring OPO can be done in a more convenient way than in the previous section. These experiments were published in paper X.

The OPO setup is given in Fig. 6.4. With the grating at oblique incidence used as output coupler, a ring oscillator is useful to only get one output beam, compared to two beams in a standing wave oscillator (Fig. 6.1(b)). Also, the tuning could be done very conveniently by rotation of a single unit, the volume Bragg grating and a broadband mirror in a retroreflector setup, as explained in Sec. 2.5. To accommodate for the ring oscillation in a compact way, the nonlinear PPKTP

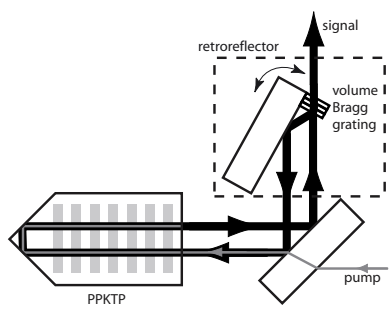

Figure 6.4: Setup of the 760 nm ring OPO.

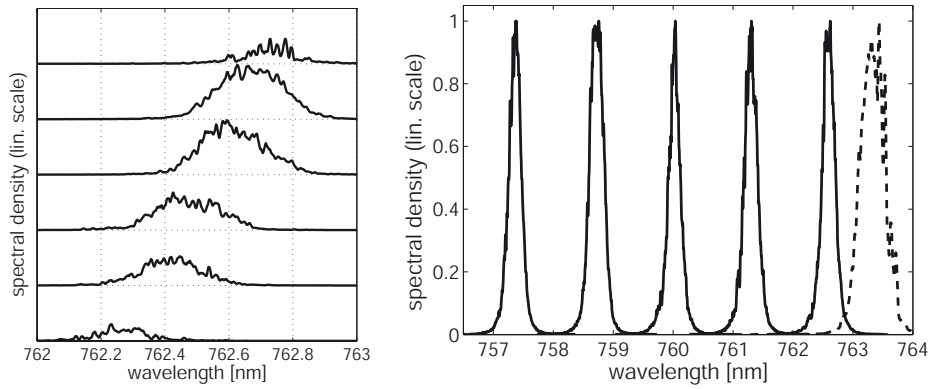

Figure 6.5: Spectra of the 760 nm ring OPO. (a) Fine-tuning by only angle-tuning of the grating. (b) Coarse tuning by simultaneous angle-tuning of the grating and temperature-tuning of the PPKTP (solid). The spectrum of an OPO with a conventional output coupler is also shown (dashed).

crystal was fabricated with one end having two bevelled surfaces to retroreflect the beams back into the crystal.

The OPO was pumped at 532 nm and the signal wavelength was at 760 nm, determined by a PPKTP period of 10.25 μm and the volume Bragg grating. At normal incidence, the grating had 28% reflectivity at 808 nm with 0.37 nm FWHM bandwidth, and was rotated to reflect light at 760 nm at an internal angle of 20°.

In Fig. 6.5, the tuning properties of the OPO are shown. First, tuning of the grating for a fixed PPKTP temperature is shown in Fig. 6.5(a). Since the parametric gain bandwidth is not so wide at 760 nm, as can be seen in Fig. 5.6, the tuning range is rather limited. To achieve larger tuning, shown in Fig. 6.5(b), the PPKTP temperature was changed simultaneously with rotation of the grating. The spectrum of the Bragg-locked OPO had a bandwidth of 130 GHz (0.25 nm), which was half compared to a conventional output coupler, also shown in Fig. 6.5(b).

The input-output curves for the OPO energy is shown in Fig. 6.6. The pump depletion reached values of 85%, indicating an efficient parametric process. Still, as shown by the significantly lower efficiency, there is some loss in the OPO, similar to the 975 nm OPO, possibly attributed to diffraction loss in the OPO cavity. It can also be seen that the OPO loss is the same for a cavity with a volume Bragg grating or a conventional output coupler, indicating that there is no inherent loss in the grating.

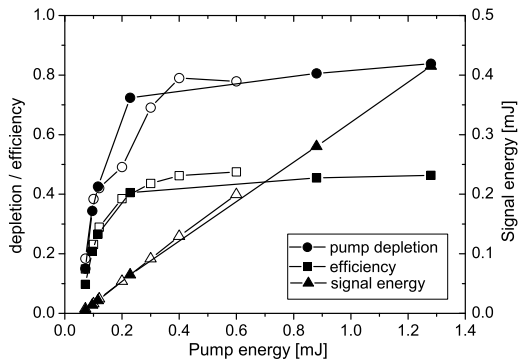

Figure 6.6: Energy properties of the ring OPO at 760 nm, both for the grating-locked OPO (filled symbols) and a conventional output coupler (open symbols).

6.3 Tunable OPO at 1 μm with a transversely chirped grating

In a recent experiment, we have also investigated how a tunable and narrowband OPO can be constructed with a volume Bragg grating that has a transversely varying period [paper J]. Tuning of the signal wavelength is then very easily done by translation of the grating, with preserved cavity alignment.

The setup of this experiment is shown in Fig. 6.7. The experiment was conducted with an OPO signal near degeneracy, to make use of the broadband parametric gain there. The nonlinear crystal was a PPKTP with a 9.01 μm period, tuned by temperature to 40 °C to provide gain around 1007 nm. The exact OPO wavelength was determined by the volume Bragg grating, that was transversely chirped by having a fan-shaped grating structure. Over the 18 mm wide grating, the chirp rate was 1.1 nm/mm, providing tuning from 997 nm to 1016 nm.

The signal and idler spectra of the OPO at various grating positions is shown

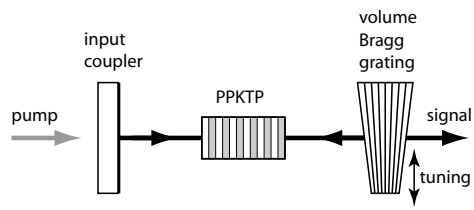

Figure 6.7: Setup of the OPO with a transversely chirped volume Bragg grating.

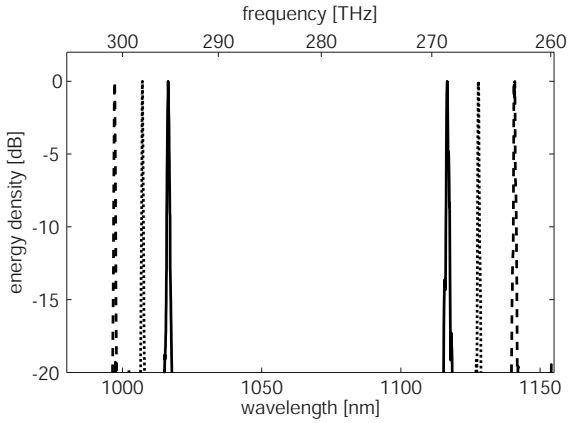

Figure 6.8: Signal and idler spectra of the OPO with a transversely chirped Bragg grating

in Fig. 6.8. The FWHM bandwidth of the signal was found to be 90 GHz (0.3 nm). As can be seen, the difference between the signal and idler frequency is some 10s of THz. This indicates a potential application of this OPO as a pump source for a subsequent nonlinear difference frequency generation to obtain tunable THz waves.

6.4 Multi-step nonlinear conversion

One interesting application of the volume-Bragg-grating OPOs is as a first step in a multiple nonlinear conversion. With the narrowed signal, it can be used as an efficient pump source for a second stage of the conversion, that usually has a limited acceptance bandwidth.

To generate coherent radiation with high pulse energy in the mid IR, an OPO is a good source. Usually, the pump wavelength of mid IR OPOs must be above 2 μm, to avoid absorption in the nonlinear crystal. Not so many efficient and reliable lasers above 2 μm are available, so an interesting pump source is another near-degenerate OPO, pumped at 1 μm by existing efficient lasers. To obtain an efficient first stage OPO, locking of the OPO with a volume Bragg grating is viable solution, and has been demonstrated in a number of publications [97–102], as a direct application of the OPO presented in paper IX.

In the opposite spectral direction, red OPOs can be used as an intermediate step in conversion from 1 μm into the UV, to provide for radiation at any desired UV wavelength [180]. Also for this application, narrowing of the signal radiation of the OPO would make the conversion process more efficient, and experimental work to demonstrate this is presently being pursued.

Chapter 7

Conclusions

In this thesis, I have described how volume Bragg gratings can be used for spectral control of solid-state lasers and optical parametric oscillators.

Lasers

For the solid-state lasers, it is demonstrated in a number of experiments, how volume Bragg gratings can be used as a cavity mirror to lock the wavelength of cw lasers. Thanks to the grating's strong spectral selectivity, the lasers could be locked anywhere in the laser gain spectrum. Furthermore, the laser bandwidth was substantially narrowed.

In an ErYb-laser [paper II], it is shown how a grating can be used in an external cavity to lock the laser in a single longitudinal mode. With this technique, it is possible to lock any low-gain laser even if the total output coupling and loss of the grating are too high for intra-cavity usage. Furthermore, tuning can be accomplished over the whole grating bandwidth by tuning of the longitudinal mode of the inner laser cavity.

In another experiment, a grating is used directly as one of the cavity mirrors in a Nd:$GdVO_4$ laser [paper III], thus yielding single-longitudinal-mode lasing by counteracting the effects of spatial hole-burning. Also, the wavelength of the laser can be chosen freely by the grating anywhere in the gain spectrum of the laser. This method provides an efficient way to select operation at any of the Stark components of the gain in a lanthanide laser medium. Furthermore, the laser can be tuned continuously over the whole grating bandwidth. In a monolithic setup [paper IV], it is furthermore shown how very stable laser operation can be obtained.

The grating can also be used to enforce laser operation at a very low quantum defect, thus minimizing the heating of the laser crystal. By use of the grating as input coupler to the laser, efficient end-pumping can be used even for closely spaced pump and laser wavelengths. This method was demonstrated in an Yb:KYW laser

[paper V, paper VI], but is widely applicable for many other lanthanide solid-state lasers, such as Nd, Er, Ho and Tm.

Using the grating at oblique incidence, wide tuning can be obtained by rotation of the grating. This was shown in an Yb:KYW laser [paper VII, paper VIII], while the demonstrated tuning technique would be useful in other broadband gain lasers as well, e.g. Ti:sapphire and Er lasers. The grating was used intracavity in a retroreflector setup for re-alignment-free tuning. Special attention has to be paid to the design of the laser cavity, to ensure that the angular spectrum of the laser beam is not wider than the narrow angular acceptance of the grating at oblique incidence. This issue was further investigated in a separate study [paper I].

Optical parametric oscillators

With nanosecond OPOs based on periodically poled materials such as PPKTP, coherent radiation at any selected wavelength can be obtained. However, unless taken care of, the bandwidth of the generated light is fairly broad. In this thesis, it is demonstrated how the bandwidth can be narrowed in a very simple way, by merely replacing one of the OPO cavity mirrors with a volume Bragg grating [paper IX].

Tuning of the locked OPO signal is also shown by rotation of the grating, while maintaining a narrow bandwidth. To achieve practical tuning, it is demonstrated how the grating can be used in a retroreflector setup, preferably in combination with a ring OPO cavity [paper X]. Another method of locking is demonstrated by use of a volume Bragg grating with a transverse chirp, whereby tuning is performed by simple translation of the grating [paper J].

7.1 Outlook

In this thesis, a new field of research is explored. Therefore, many interesting experiments still await to be performed.

The laser experiments in this thesis demonstrate a number of methods in different laser materials, but there are still more laser media left to be investigated for each method. For example, it would be interesting to obtain single-longitudinal-mode operation in Yb-lasers, similar to the experiments performed in Nd-lasers. Also, it might be attractive to use the method for wide tuning, demonstrated in Yb, with other broadband laser materials such as Ti:sapphire and Er.

Furthermore, the developed lasers could prove useful for intracavity second harmonic generation, an application that has not yet been pursued. Also, pulsed lasers, both Q-switched and mode-locked, is an area that awaits exploring.

In this thesis it is also demonstrated that the strong angular selectivity of reflective volume Bragg gratings at oblique incidence could be used for spatial improvement of a laser. However, experimental demonstration of this effect in a laser cavity has still not been done.

For the OPO locking with volume Bragg gratings, there are still many aspects left to investigate. In this thesis, relatively incoherent pumping from a flashlamp-pumped laser was used for the experiments. Since the OPO process is sensitive to the phase of the pump, the properties of the pump are carried over to the generated signal to a certain extent. Also, for an OPO, there is a coupling between the transverse spatial properties and the spectral properties. Therefore, it would be interesting to study volume-Bragg-grating-locking of OPOs for different pump-laser properties, such as coherence length/bandwidth and M^2. In addition, the transverse OPO cavity properties would be of importance for some types of pumps. For a pump with better coherence, the longitudinal modes of the OPO cavity might play a bigger role, something that should be examined, by detailed studies of the signal spectrum. Also it would be interesting to study in more detail the signal bandwidth as a function of the bandwidth of the volume Bragg grating, as well as the parametric gain bandwidth.

In addition, there is no conclusive explanation of the loss that is typical in the demonstrated OPOs, seen as a difference between the depletion and efficiency. In this thesis, it is shown that the loss is not due to the volume Bragg gratings. One potential reason is diffraction loss in the OPO cavity, but this deserves further investigation.

References

[1] T. H. Maiman, *Stimulated optical radiation in ruby*, Nature **187**, 493 (1960).

[2] L. F. Johnson and K. Nassau, *Infrared fluorescence and stimulated emission of Nd^{3+} in $CaWO_4$*, Proc. IRE **49**, 1704 (1961).

[3] H. W. Etzel, H. W. Gandy and R. J. Ginther, *Stimulated emission of infrared radiation from ytterbium activated silicate glass*, Appl. Opt. **1**, 534 (1962), [in *Letters to the Editor*, Appl. Opt. **1**, 533 (1962)].

[4] E. Snitzer and R. Woodcock, *Yb^{3+}-Er^{3+} glass laser*, Appl. Phys. Lett. **6**, 45 (1965).

[5] A. Javan, W. R. Bennett and D. R. Herriott, *Population inversion and continuous optical maser oscillation in a gas discharge containing a He-Ne mixture*, Phys. Rev. Lett. **6**, 106 (1961).

[6] R. N. Hall, G. E. Fenner, J. D. Kingsley, T. J. Soltys and R. O. Carlson, *Coherent light emission from GaAs junctions*, Phys. Rev. Lett. **9**, 366 (1962).

[7] R. J. Keyes and T. M. Quist, *Injection luminescent pumping of CaF_2:U^{3+} with GaAs diode lasers*, Appl. Phys. Lett. **4**, 50 (1964).

[8] F. J. McClung and R. W. Hellwarth, *Giant optical pulsations from ruby*, J. Appl. Phys. **33**, 828 (1962).

[9] L. E. Hargrove, R. L. Fork and M. A. Pollack, *Locking of He-Ne laser modes induced by synchronous intracavity modulation*, Appl. Phys. Lett. **5**, 4 (1964).

[10] S. A. Collins and R. G. White, *Interferometer laser mode selector*, Appl. Opt. **2**, 448 (1963).

[11] D. Roess, *Ruby laser with mode-selective etalon reflector*, Proc. IEEE **52**, 196 (1964).

[12] G. Moeller and J. D. Rigden, *Observation of laser action in the r-branch of CO_2 and N_2O vibrational spectra*, Appl. Phys. Lett. **8**, 69 (1966).

[13] B. H. Soffer and B. B. McFarland, *Continuously tunable, narrow-band organic dye lasers*, Appl. Phys. Lett. **10**, 266 (1967).

[14] P. A. Franken, A. E. Hill, C. W. Peters and G. Weinreich, *Generation of optical harmonics*, Phys. Rev. Lett. **7**, 118 (1961).

[15] P. D. Maker, R. W. Terhune, M. Nisenoff and C. M. Savage, *Effects of dispersion and focusing on the production of optical harmonics*, Phys. Rev. Lett. **8**, 21 (1962).

[16] J. A. Giordmaine, *Mixing of light beams in crystals*, Phys. Rev. Lett. **8**, 19 (1962).

[17] M. Bass, P. A. Franken, A. E. Hill, C. W. Peters and G. Weinreich, *Optical mixing*, Phys. Rev. Lett. **8**, 18 (1962).

[18] J. M. DiDomenico, R. H. Pantell, O. Svelto and J. N. Weaver, *Optical frequency mixing in bulk semiconductors*, Appl. Phys. Lett. **1**, 77 (1962).

[19] C. C. Wang and G. W. Racette, *Measurement of parametric gain accompanying optical difference frequency generation*, Appl. Phys. Lett. **6**, 169 (1965).

[20] S. A. Akhmanov, A. I. Kovrigin, A. S. Piskarskas, V. V. Fadeev and R. V. Khokhlov, *Observation of parametric amplification in the optical range*, JETP Lett. **2**, 191 (1965), [Russian original: Pis'ma Zh. Tekh. Fiz. **2**, 300 (1965)].

[21] J. A. Giordmaine and R. C. Miller, *Tunable coherent parametric oscillation in $LiNbO_3$ at optical frequencies*, Phys. Rev. Lett. **14**, 973 (1965).

[22] K. Kincade and S. G. Anderson, *Laser marketplace 2008: Innovation opens the door for next wave of success*, Laser Focus World **44**, (Jan.) 74 (2008).

[23] R. V. Steele, *Laser marketplace 2008: Diode lasers track longterm trend*, Laser Focus World **44**, (Feb.) 59 (2008).

[24] W. H. Bragg and W. L. Bragg, *The Reflection of X-rays by Crystals*, Proc. R. Soc. London A **88**, 428 (1913).

[25] S. D. Stookey, *Photosensitive Glass*, Ind. Eng. Chem. **41**, 856 (1949).

[26] V. A. Borgman, L. B. Glebov, N. V. Nikonorov, G. T. Petrovskii, V. V. Savvin and A. D. Tsvetkov, *Photothermal refractive effect in silicate glasses*, Sov. Phys. Dokl. **34**, 1011 (1989), [Russian original: Dokl. Akad. Nauk SSSR **309**, 336 (1989)].

[27] L. B. Glebov, N. V. Nikonorov, E. I. Panysheva, G. T. Petrovskiĭ, V. V. Savvin, I. V. Tunimanova and V. A. Tsekhomskiĭ, *Polychromic glasses–a new material for recording volume phase holograms*, Sov. Phys. Dokl. **35**, 878 (1990), [Russian original: Dokl. Akad. Nauk SSSR **314**, 849 (1990)].

[28] L. B. Glebov, N. V. Nikonorov, E. I. Panysheva, G. T. Petrovskiĭ, V. V. Savvin, I. V. Tunimanova and V. A. Tsekhomskiĭ, *New ways to use photosensitive glasses for recording volume phase holograms*, Opt. Spectrosc. **73**, 237 (1992), [Russian original: Opt. Spektrosk. **72**, 404 (1992)].

[29] O. Efimov, L. Glebov, L. Glebova, K. Richardson and V. Smirnov, *High-efficiency Bragg gratings in photothermorefractive glass*, Appl. Opt. **38**, 619 (1999).

[30] L. B. Glebov, *Kinetics modeling in photosensitive glass*, Opt. Mater. **25**, 413 (2004).

[31] O. M. Efimov, L. B. Glebov and H. P. Andre, *Measurement of the induced refractive index in a photothermorefractive glass by a liquid-cell shearing interferometer*, Appl. Opt. **41**, 1864 (2002).

[32] O. M. Efimov, L. B. Glebov and V. I. Smirnov, *High-frequency Bragg gratings in a photothermorefractive glass*, Opt. Lett. **25**, 1693 (2000).

[33] T. Cardinal, O. M. Efimov, H. G. Francois-Saint-Cyr, L. B. Glebov, L. N. Glebova and V. I. Smirnov, *Comparative study of photo-induced variations of X-ray diffraction and refractive index in photo-thermo-refractive glass*, J. Non-Cryst. Solids **325**, 275 (2003).

[34] L. B. Glebov, *Volume Bragg gratings in PTR glass – new optical elements for laser design*, Advanced solid-state photonics (Optical Society of America, 2008), MD1.

[35] L. Glebova, J. Lumeau, M. Klimov, E. D. Zanotto and L. B. Glebov, *Role of bromine on the thermal and optical properties of photo-thermo-refractive glass*, J. Non-Cryst. Solids **354**, 456 (2007).

[36] P. G. Johannsen, *Refractive index of the alkali halides. I. Constant joint density of states model*, Phys. Rev. B **55**, 6856 (1997).

[37] L. B. Glebov, *High-brightness laser design based on volume Bragg gratings*, Proc. SPIE **6216**, 621601 (2006).

[38] J. Lumeau, L. Glebova and L. Glebov, *Influence of UV-exposure on the crystallization and optical properties of photo-thermo-refractive glass*, J. Non-Cryst. Solids **354**, 425 (2007).

[39] J. W. Zwanziger, U. Werner-Zwanziger, E. D. Zanotto, E. Rotari, L. N. Glebova, L. B. Glebov and J. F. Schneider, *Residual internal stress in partially crystallized photothermorefractive glass: Evaluation by nuclear magnetic resonance spectroscopy and first principles calculations*, J. Appl. Phys. **99**, 083511 (2006).

[40] G. B. Venus, A. Sevian, V. I. Smirnov and L. B. Glebov, *High-brightness narrow-line laser diode source with volume Bragg-grating feedback*, Proc. SPIE **5711**, 166 (2005).

[41] S. Santran, M. Martinez-Rosas, L. Canioni, L. Sarger, L. N. Glebova, A. Tirpak and L. B. Glebov, *Nonlinear refractive index of photo-thermo-refractive glass*, Opt. Mater. **28**, 401 (2006).

[42] A. Sevian, O. Andrusyak, I. Ciapurin, V. Smirnov, G. Venus and L. Glebov, *Efficient power scaling of laser radiation by spectral beam combining*, Opt. Lett. **33**, 384 (2008).

[43] O. M. Efimov, L. B. Glebov, S. Papernov and A. W. Schmid, *Laser-induced damage of photo-thermo-refractive glasses for optical holographic element writing*, Proc. SPIE **3578**, 564 (1999).

[44] L. B. Glebov, L. N. Glebova, V. I. Smirnov, M. Dubinskii, L. D. Merkle, S. Papernov and A. W. Schmid, *Laser damage resistance of photo-thermo-refractive glass bragg gratings*, Solid-state and diode laser technology review (Albuquerque, USA, June 8-10, 2004).

[45] J.-Y. Natoli, L. Gallais, H. Akhouayri and C. Amra, *Laser-induced damage of materials in bulk, thin-film, and liquid forms*, Appl. Opt. **41**, 3156 (2002).

[46] H. Kogelnik, *Coupled wave theory for thick hologram gratings*, Bell. Sys. Tech. J. **48**, 2909 (1969).

[47] T. K. Gaylord and M. G. Moharam, *Analysis and applications of optical diffraction by gratings*, Proc. IEEE **73**, 894 (1985).

[48] R. S. Chu, J. A. Kong and T. Tamir, *Diffraction of Gaussian beams by a periodically modulated layer*, J. Opt. Soc. Am **67**, 1555 (1977).

[49] B. Benlarbi, P. S. J. Russel and L. Solymar, *Bragg diffraction of Gaussian beams by thick gratings: two rival theories*, Appl. Phys. B **28**, 63 (1982).

[50] I. V. Ciapurin, L. B. Glebov and V. I. Smirnov, *Modeling of phase volume diffractive gratings, part 1: transmitting sinusoidal uniform gratings*, Opt. Eng. **45**, 015802 (2006).

[51] M. G. Moharam, T. K. Gaylord and R. Magnusson, *Bragg diffraction of finite beams by thick gratings*, J. Opt. Soc. Am. **70**, 300 (1980).

[52] P. S. J. Russel and L. Solymar, *Borrmann-like anomalous effects in volume holography*, Appl. Phys. **22**, 335 (1980).

[53] M. G. Moharam, E. B. Grann, D. A. Pommet and T. K. Gaylord, *Formulation for stable and efficient implementation of the rigorous coupled-wave analysis of binary gratings*, J. Opt. Soc. Am. A **12**, 1068 (1995).

[54] M. R. B. Forshaw, *Diffraction of a narrow laser beam by a thick hologram: experimental results*, Opt. Comm. **12**, 279 (1974).

[55] H.-T. Hsieh, W. Liu, F. Havermeyer, C. Moser and D. Psaltis, *Beam-width-dependent filtering properties of strong volume holographic gratings*, Appl. Opt. **45**, 3774 (2006).

[56] L. S. Meng, B. Nizamov, P. Madasamy, J. K. Brasseur, T. Henshaw and D. K. Neumann, *High power 7-GHz bandwidth external-cavity diode laser array and its use in optically pumping singlet delta oxygen*, Optics Express **14**, 10469 (2006).

[57] J. W. Goodman, *Introduction to Fourier optics* (McGraw-Hill, New York, 1996).

[58] F. Havermeyer, W. Liu, C. Moser, D. Psaltis and G. Steckman, *Volume holographic grating-based continuously tunable optical filter*, Opt.l Eng. **43**, 2017 (2004).

[59] B. Volodin, S. Dolgy, E. Melnik, E. D. J. Shaw and V. Ban, *Wavelength stabilization and spectral narrowing of high power multimode laser diodes and arrays by use of volume Bragg gratings*, Opt. Lett. **29**, 1891 (2004).

[60] T. Chung, A. Rapaport, V. Smirnov, L. B. Glebov, M. C. Richardson and M. Bass, *Solid-state laser spectral narrowing using a volumetric photothermal refractive Bragg grating cavity mirror*, Opt. Lett. **31**, 229 (2006).

[61] Y. Barmenkov, D. Zalvidea, S. Torres-Peiró, J. L. Cruz and M. Andés, *Effective length of short Fabry-Perot cavity formed by uniform fiber Bragg gratings*, Opt. Express **14**, 6394 (2006).

[62] S. Yiou, F. Balembois, P. Georges and J.-P. Huignard, *Improvement of the spatial beam quality of laser sources with an intracavity Bragg grating*, Opt. Lett. **28**, 242 (2003).

[63] G. Venus, L. Glebov, V. Rotar, V. Smirnov, P. Crump and J. Farmer, *Volume Bragg semiconductor lasers with near diffraction limited divergence*, Proc. SPIE **6216**, 621602 (2006).

[64] N. Vorobiev, V. I. Smirnov and L. Glebov, *Single-frequency-mode Q-switched Nd:YAG laser controlled by volume Bragg gratings*, Advanced Solid-State Photonics (Optical Society of America, 2008), MC11.

[65] Y. Zheng, X. Gao, H. Miyajima and H. Kan, *High-brightness narrow-bandwidth high-power laser-diode array based on an external-cavity technique*, Jpn. J. Appl. Phys. **43**, L1299 (2004).

[66] Y. Zheng and H. Kan, *Effective bandwidth reduction for a high-power laser-diode array by an external-cavity technique*, Opt. Lett. **30**, 2424 (2005).

[67] Y. Zheng, A. Watanabe, T. Morita and H. Kan, *High-brightness narrow-bandwidth operation of a broad-area laser diode with a rear external cavity*, Jpn. J. Appl. Phys. **45**, L1025 (2006).

[68] Y. Zheng and H. Kan, *Narrow-bandwidth high-brightness external-cavity laser diode bar*, Jpn. J. Appl. Phys. **46**, L218 (2007).

[69] G. Steckman, W. Liu, R. Platz, D. Schroeder, C. Moser and F. Havermeyer, *Volume holographic grating wavelength stabilized laser diodes*, IEEE J. Sel. Topics Quantum Electron. **13**, 672 (2007).

[70] Y. Wang, T. Kasamatsu, Y. Zheng, H. Miyajima, H. Fukuoka, S. Matsuoka, M. Niigaki, H. Kubomura, T. Hiruma and H. Kan, *Cesium vapor laser pumped by a volume-Bragg-grating coupled quasi-continuous-wave laser-diode array*, Appl. Phys. Lett. **88**, 141112 (2006).

[71] Y. Wang, M. Niigaki, H. Fukuoka, Y. Zheng, H. Miyajima, S. Matsuoka, H. Kubomura, T. Hiruma and H. Kan, *Approaches of output improvement for a cesium vapor laser pumped by a volume-Bragg-grating coupled laser-diode-array*, Phys. Lett. A **360**, 659 (2007).

[72] R. H. Page, R. J. Beach, V. K. Kanz and W. F. Krupke, *Multimode-diode-pumped gas (alkali-vapor) laser*, Opt. Lett. **31**, 353 (2006).

[73] A. B. Petersen and J. Gloyd, *Tunable, high power, narrow band emission from a volume grating-controlled diode bar*, Advanced solid-state photonics (Optical Society of America, 2008), MD2.

[74] A. Gourevitch, G. Venus, V. Smirnov and L. Glebov, *High power volume Bragg laser bar for efficient pumping of alkali (Rb) lasers*, Advanced Solid-State Photonics (Optical Society of America, 2008), MC12.

[75] S. A. Zolotovskaya, N. Daghestani, G. B. Venus, L. B. Glebov, V. I. Smirnov and E. U. Rafailov, *Stable dual-wavelength operation of InGaAs diode lasers with volume Bragg gratings*, Appl. Phys. Lett. **91**, 171113 (2007).

[76] S. Giet, H. Sun, S. Calvez, M. Dawson, S. Suomalainen, A. Harkonen, M. Guina, O. Okhotnikov and M. Pessa, *Spectral narrowing and locking of a vertical-external-cavity surface-emitting laser using an intracavity volume Bragg grating*, IEEE Photon. Technol. Lett. **18**, 1786 (2006).

[77] S. Hallstein, G. P. Carey, R. Carico, R. Dato, J. J. Dudley, A. M. Earman, M. J. Finander, G. Giaretta, J. Green, H. J. Hofler, F. Hu, M. Jansen, C. P. Kocot, S. Lim, J. Krueger, A. Mooradian, G. Niven, Y. Okuno, F. G. Patterson, A. Tandon and A. Umbrasas, *RGB laser light sources for projection displays*, Lasers and Electro-Optics Society conference (2007), TuL3.

[78] D. Paboeuf, G. Lucas-Leclin, P. Georges, B. Sumpf, G. Erbert, C. Varona, P. Loiseau, G. Aka and B. Ferrand, *900 nm Emission of a Nd:ASL Laser Pumped by an Extended-Cavity Tapered Laser Diode*, Advanced solid-state photonics (2007), WB20.

[79] Ondax Inc., http://www.ondaxinc.com/ (accessed March 16 2008).

[80] G. B. Venus, A. Sevian, V. I. Smirnov and L. B. Glebov, *Stable coherent coupling of laser diodes by a volume Bragg grating in photothermorefractive glass*, Opt. Lett. **31**, 1453 (2006).

[81] Y. Kaneda, L. Fan, T. C. Hsu, N. Peyghambarian, M. Fallahi, A. R. Zakharian, J. Hader, J. V. Moloney, W. Stoltz, S. Koch, R. Bedford, A. Sevian and L. Glebov, *High brightness spectral beam combination of high-power vertical-external-cavity surface-emitting lasers*, IEEE Photon. Technol. Lett. **18**, 1795 (2006).

[82] O. Andrusyak, I. Ciapurin, V. Smirnov, G. Venus and L. Glebov, *Spectral beam combining of fiber lasers with increased channel density*, Proceedings of SPIE **6453**, 64531L (2007).

[83] O. Andrusyak, I. Ciapurin, A. Sevian, V. Smirnov, G. Venus and L. Glebov, *Power scaling of laser systems using spectral beam combining with volume Bragg gratings in PTR glass*, Conference on lasers and electro-optics (2007), JTuA85.

[84] B. Chann, A. K. Goyal, T. Y. Fan, A. Sanchez-Rubio, B. L. Volodin and V. S. Ban, *Efficient, high-brightness wavelength-beam-combined commercial off-the-shelf diode stacks achieved by use of a wavelength-chirped volume Bragg grating*, Opt. Lett. **31**, 1253 (2006).

[85] K.-H. Liao, M.-Y. Cheng, E. Fletcher, V. S. Smirnov, L. B. Glebov and A. Galvanauskas, *Large aperture chirped volume Bragg grating based CPA system*, Opt. Express **15**, 4876 (2007).

[86] A. V. Okishev, C. Dorrer, V. I. Smirnov, L. B. Glebov and J. D. Zuegel, *Spectral filtering in a diode-pumped Nd:YLF regenerative amplifier using a volume Bragg grating*, Opt. Express **15**, 8197 (2007).

[87] P. Jelger and F. Laurell, *Efficient narrow-linewidth volume-Bragg grating-locked Nd:fiber laser*, Opt. Express **15**, 11336 (2007).

[88] P. Jelger and F. Laurell, *Efficient skew-angle cladding-pumped tunable narrow-linewidth Yb-doped fiber laser*, Opt. Lett. **32**, 3501 (2007).

[89] A. Dergachev, P. F. Moulton, V. Smirnov and L. Glebov, *High power CW Tm:YLF laser with a holographic output coupler*, Conference on lasers and electro-optics (2004), CThZ3.

[90] T.-Y. Chung, S. S. Yang, C.-W. Chen, H.-C. Yang, C.-R. Liao, Y.-H. Lien and J.-T. Shy, *Wavelength tunable single mode Nd:$GdVO_4$ laser using a volume Bragg grating fold mirror*, Conference on lasers and electro-optics (2007), CThE4.

[91] S. S. Yang, T.-Y. Chung, C. W. Chen and H. C. Yang, *Noise elimination of intracavity doubled lasers by single-mode operation with volumetric Bragg grating*, Conference on lasers and electro-optics (2007), CTuU7.

[92] C.-J. Liao, Y.-H. Lien, T.-Y. Chung, S. S. Yang and J.-T. Shy, *Lasing action of Nd:$GdVO_4$ at 1070 nm by volumetric Bragg grating*, Conference on lasers and electro-optics (2007), CThE3.

[93] T. Chung, A. Rapaport, Y. Chen, V. Smirnov, M. Hemmer, L. B. Glebov, M. C. Richardson and M. Bass, *Spectral narrowing of solid state lasers by narrow-band PTR Bragg mirrors*, Proc. SPIE **6216**, 621603 (2006).

[94] T. Chung, V. Smirnov, M. Hemmer, L. Glebov, M. Richardson and M. Bass, *Unexpected properties of a laser resonator with volumetric Bragg grating end mirrors*, Conference on lasers and electro-optics (2006), CFB5.

[95] M. Hemmer, T. Chung, Y. Chen, V. Smirnov, L. Glebov, M. Richardson and M. Bass, *Spectral narrowing in a dual volume Bragg grating Ti:Sapphire oscillator*, Conference on lasers and electro-optics (2007), CThE5.

[96] M. Hemmer, Y. Joly, L. Glebov, M. Bass and M. Richardson, *Broad tunability in a volume Bragg grating narrow line Ti:sapphire oscillator*, Annual Meeting of the IEEE Lasers and Electro-Optics Society (2007), WC4.

[97] M. Henriksson, M. Tiihonen, V. Pasiskevicius and F. Laurell, *$ZnGeP_2$ parametric oscillator pumped by a linewidth narrowed 2 μm source*, Opt. Lett. **31**, 1878 (2006).

[98] M. Henriksson, L. Sjöqvist, V. Pasiskevicius and F. Laurell, *Narrow linewidth 2 μm optical parametric oscillation in periodically poled $LiNbO_3$ with volume Bragg grating outcoupler*, Appl. Phys. B **86**, 497 (2007).

[99] M. Henriksson, M. Tiihonen, V. Pasiskevicius and F. Laurell, *Mid-infrared ZGP OPO pumped by near-degenerate narrowband type-I PPKTP parametric oscillator*, Appl. Phys. B **88**, 37 (2007).

[100] J. Saikawa, M. Fujii, H. Ishizuki and T. Taira, *High-energy, narrow-bandwidth periodically poled Mg-doped $LiNbO_3$ optical parametric oscillator with a volume Bragg grating*, Opt. Lett. **32**, 2996 (2007).

[101] M. Henriksson, L. Sjöqvist, M. Tiihonen, V. Pasiskevicius and F. Laurell, *Tandem OPO system for mid-infrared generation using quasi phase-matching and volume Bragg gratings*, Proc. SPIE **6738**, 673805 (2007).

[102] M. Henriksson, L. Sjöqvist, V. Pasiskevicius and F. Laurell, *Longitudinal mode structure of degenerate OPO with volume Bragg grating output coupler*, Conference on lasers and electro-optics (2008), CTuY4.

[103] A. J. Merriam, J. J. Jacob, D. S. Bethune and J. A. Hoffnagle, *Efficient nonlinear frequency conversion to 193-nm using cooled BBO*, Advanced solid-state photonics (2007), MB11.

[104] A. Merriam, D. Bethune, J. Hoffnagle, W. Hinsberg, C. Jefferson, J. Jacob and T. Litvin, *A solid-state 193-nm laser with high spatial coherence for sub-40-nm interferometric immersion lithography*, Proc. SPIE **6520**, 65202Z (2007).

[105] T. Lépine, S. Victori, P. Georges and A. Brun, *Spectral narrowing of a pulsed optical parametric oscillator using an intracavity photorefractive crystal*, Advanced solid-state lasers (2002), MB9.

[106] A. C. Chiang, Y. Y. Lin, T. D. Wang, Y. C. Huang and J. T. Shy, *Distributed-feedback optical parametric oscillation by use of a photorefractive grating in periodically poled lithium niobate*, Opt. Lett. **27**, 1815 (2002).

[107] Y. He and B. J. Orr, *Narrowband tuning of an injection-seeded pulsed optical-parametric oscillator based on a self-adaptive, phase-conjugatecavity mirror*, Opt. Lett. **29**, 2169 (2004).

[108] A. Yariv, *Quantum Electronics* (Wiley, 1989).

[109] S. Bjurshagen, D. Evekull and R. Koch, *Efficient generation of blue light by frequency doubling of a Nd:YAG laser operating on* $^4F_{3/2} \rightarrow {}^4I_{9/2}$ *transitions*, Appl. Phys. B **76**, 135 (2003).

[110] M. Castaing, E. Hérault, F. Balembois, P. Georges, C. Varona, P. Loiseau and G. Aka, *Diode-pumped Nd:YAG laser emitting at 899 nm and below*, Opt. Lett. **32**, 799 (2007).

[111] M. Jacquemet, F. Balembois, S. Chénais, F. Druon, P. Georges, R. Gaumé and B. Ferrand, *First diode-pumped Yb-doped solid-state laser continuously tunable between 1000 and 1010 nm*, Appl. Phys. B **78**, 13 (2004).

[112] K. O. Hill, Y. Fujii, D. C. Johnson and B. S. Kawasaki, *Photosensitivity in optical fiber waveguides: Application to reflection filter fabrication*, Appl. Phys. Lett. **32**, 647 (1978).

[113] G. Meltz, W. W. Morey and W. H. Glenn, *Formation of Bragg gratings in optical fibers by a transverse holographic method*, Opt. Lett. **14**, 823 (1989).

[114] J. J. Zayhowski and A. Mooradian, *Single-frequency microchip Nd lasers*, Opt. Lett **14**, 24 (1989).

[115] P. Laporta, S. Taccheo, S. Longhi, O. Svelto and G. Sacchi, *Diode-pumped microchip Er-Yb:glass laser*, Opt. Lett. **18**, 1232 (1993).

[116] H. G. Danielmeyer, *Stabilized efficient single-frequency Nd:YAG laser*, IEEE J. Quantum Electron. **6**, 101 (1970).

[117] J. E. Hellström, S. Bjurshagen, V. Pasiskevicius, J. Liu, V. Petrov and U. Griebner, *Efficient Yb:KGW lasers end-pumped by high-power diode bars*, Appl. Phys. B **83**, 235 (2006).

[118] L. B. Kreuzer, *Single mode oscillation of a pulsed singly resonant optical parametric oscillator*, Appl. Phys. Lett. **15**, 263 (1969).

[119] M. Hercher, *Tunable single mode operation of gas lasers using intracavity tilted etalons*, Appl. Opt. **8**, 1103 (1969).

[120] F. F. Heine and G. Huber, *Tunable single frequency thulium:YAG microchip with external feedback*, Appl. Opt **37**, 3268 (1998).

[121] P. Lichtenberg Hansen, C. Pedersen, P. Buchhave and T. Skettrup, *Frequency tuning and stability of Nd: YVO4 in a dual coupled cavity*, Opt. Commun. **127**, 353 (1996).

[122] M. Merimaa, H. Talvitie, P. Laakkonen, M. Kuittinen, I. Tittonen and E. Ikonen, *Compact external-cavity diode laser with a novel transmission geometry*, Opt. Commun. **174**, 175 (2000).

[123] I. Shoshan, N. N. Danon and U. P. Oppenheim, *Narrowband operation of a pulsed dye laser without intracavity beam expansion*, J. Appl. Phys. **48**, 4495 (1977).

[124] M. G. Littman and H. J. Metcalf, *Spectrally narrow pulsed dye laser without beam expander*, Appl. Opt. **17**, 2224 (1978).

[125] K. Liu and M. G. Littman, *Novel geometry for single-mode scanning of tunable lasers*, Opt. Lett. **6**, 117 (1981).

[126] M. Fleming and A. Mooradian, *Spectral characteristics of external-cavity controlled semiconductor lasers*, IEEE J. Quantum Electron. **17**, 44 (1981).

[127] D. Wandt, M. Laschek, K. Przyklenk, A. Tunnermann and H. Welling, *External cavity laser diode with 40 nm continuous tuning range around 825 nm*, Opt. Commun. **130**, 81 (1996).

[128] S. Brosnan and R. Byer, *Optical parametric oscillator threshold and linewidth studies*, IEEE J. Quantum Electron. **15**, 415 (1979).

[129] W. R. Bosenberg and D. R. Guyer, *Broadly tunable, single-frequency optical parametric frequency-conversion system*, J. Opt. Soc. Am. B **10**, 1716 (1993).

[130] L. A. W. Gloster, I. T. McKinnie, Z. X. Jiang, T. A. King, J. M. Boon-Engering, W. E. van der Veer and W. Hogervorst, *Narrow-band β-BaB_2O_4 optical parametric oscillator in a grazing-incidence configuration*, J. Opt. Soc. Am. B **12**, 2117 (1995).

[131] J. M. Boon-Engering, W. E. van der Veer, E. Bente and W. Hogervorst, *Scanning and locking of a single longitudinal mode β-BaB_2O_4 OPO in a grazing incidence configuration*, Opt. Commun. **136**, 261 (1997).

[132] G. W. Baxter, P. Schlup, I. T. McKinnie, J. Hellström and F. Laurell, *Single-mode near-infrared optical parametric oscillator amplifier based on periodically poled $KTiOPO_4$*, Appl. Opt. **40**, 6659 (2001).

[133] M. D. Perry, D. Pennington, B. C. Stuart, G. Tietbohl, J. A. Britten, C. Brown, S. Herman, B. Golick, M. Kartz, J. Miller, H. T. Powell, M. Vergino and V. Yanovsky, *Petawatt laser pulses*, Opt. Lett **24**, 160 (1999).

[134] A. Baum, D. Grebner, W. Paa, W. Triebel, M. Larionov and A. Giesen, *Axial mode tuning of a single frequency Yb:YAG thin disk laser*, Appl. Phys. B **81**, 1091 (2005).

[135] R. Peters, C. Kränkel, K. Petermann and G. Huber, *Broadly tunable high-power $Yb:Lu_2O_3$ thin disk laser with 80% slope efficiency*, Opt. Express **15**, 7075 (2007).

[136] W. Li, Q. Hao, H. Zhai, H. Zeng, W. Lu, G. Zhao, C. Yan, L. Su and J. Xu, *Low-threshold and continuously tunable $Yb:Gd_2SiO_5$ laser*, Appl. Phys. Lett. **89**, 101125 (2006).

[137] A. E. Siegman, *Lasers* (University science books, 1986).

[138] W. T. Silfvast, *Laser fundamentals* (Cambrigde university press, 2004).

[139] O. Svelto, *Principles of lasers* (Plenum press, 1998).

[140] W. Koechner, *Solid-state laser engineering* (Springer, 2006).

[141] B. Aull and H. Jenssen, *Vibronic interactions in Nd:YAG resulting in nonreciprocity of absorption and stimulated emission cross sections*, IEEE J. Quantum Electron. **18**, 925 (1982).

[142] S. A. Payne, L. L. Chase, L. K. Smith, W. L. Kway and W. F. Krupke, *Infrared cross-section measurements for crystals doped with Er^{3+}, Tm^{3+}, and Ho^{3+}*, IEEE J. Quantum Electron. **28**, 2619 (1992).

[143] T. Jensen, V. G. Ostroumov, J. P. Meyn, G. Huber, A. I. Zagumennyi and I. A. Shcherbakov, *Spectroscopic characterization and laser performance of diode-laser-pumped Nd:$GdVO_4$*, Appl. Phys. B **58**, 373 (1994).

[144] C. Czeranowsky, M. Schmidt, E. Heumann, G. Huber, S. Kutovoi and Y. Zavartsev, *Continuous wave diode pumped intracavity doubled Nd:$GdVO_4$ laser with 840 mW output power at 456 nm*, Opt. Commun. **205**, 361 (2002).

[145] H. Zhang, J. Liu, J. Wang, C. Wang, L. Zhu, Z. Shao, X. Meng, X. Hu, M. Jiang and Y. T. Chow, *Characterization of the laser crystal Nd:$GdVO_4$*, J. Opt. Soc. Am. B **19**, 18 (2002).

[146] Y. Sato and T. Taira, *The studies of thermal conductivity in $GdVO_4$, YVO_4, and $Y_3Al_5O_{12}$ measured by quasi-one-dimensional flash method*, Opt. Express **14**, 10528 (2006).

[147] N. V. Kuleshov, A. A. Lagatsky, A. V. Podlipensky, V. P. Mikhailov and G. Huber, *Pulsed laser operation of Yb-doped $KY(WO_4)_2$ and $KGd(WO_4)_2$*, Opt. Lett. **22**, 1317 (1997).

[148] M. C. Pujol, M. Rico, C. Zaldo, R. Solé, V. Nikolov, X. Solans, M. Aguiló and F. Díaz, *Crystalline structure and optical spectroscopy of Er^{3+}-doped $KGd(WO_4)_2$ single crystals*, Appl. Phys. B **68**, 187 (1999).

[149] S. Biswal, S. P. O'Connor and S. R. Bowman, *Thermo-optical parameters measured in ytterbium-doped potassium gadolinium tungstate*, Appl. Opt. **44**, 3093 (2005).

[150] K. Petermann, D. Fagundes-Peters, J. Johannsen, M. Mond, V. Peters, J. J. Romero, S. Kutovoi, J. Speiser and A. Giesen, *Highly Yb-doped oxides for thin-disc lasers*, J. Crystal Growth **275**, 135 (2005).

[151] G. Karlsson, *Diode-pumped Er-Yb lasers for eye-safe applications*, Ph.D. thesis, KTH – Royal Institute of Technology, Stockholm, Sweden, 2003.

[152] N. A. Tolstik, S. V. Kurilchik, V. E. Kisel, N. V. Kuleshov, V. V. Maltsev, O. V. Pilipenko, E. V. Koporulina and N. I. Leonyuk, *Efficient 1 W continuous-wave diode-pumped Er,Yb:$YAl_3(BO_3)_4$ laser*, Opt. Lett. **32**, 3233 (2007).

[153] R. Francini, U. M. Grassano and G. G. Tarasov, *Broadening of Er electronic states in phosphate glasses*, J. Chem. Phys. **115**, 7975 (2001).

[154] J. B. Gruber, D. K. Sardar, B. Zandi, J. A. Hutchinson and C. W. Trussell, *Modeling the absorption spectra of Er^{3+} and Yb^{3+} in a phosphate glass*, Journal of Applied Physics **94**, 4835 (2003).

[155] S. Dai, A. Sugiyama, L. Hu, Z. Liu, G. Huang and Z. Jiang, *The spectrum and laser properties of ytterbium doped phosphate glass at low temperature*, J. Non-Cryst. Solids **311**, 138 (2002).

[156] P. Laporta, S. Taccheo, S. Longhi, O. Svelto and C. Svelto, *Erbium–ytterbium microlasers: optical properties and lasing characteristics*, Opt. Mater. **11**, 269 (1999).

[157] A. E. Siegman, G. Nemes and J. Serna, in *How to (maybe) measure laser beam quality*, DPSS (Diode Pumped Solid State) Lasers: Applications and Issues (Optical Society of America, 1998), MQ1.

[158] J. J. Zayhowski, *Limits imposed by spatial hole burning on the single-mode operation of standing-wave laser cavities*, Opt. Lett. **15**, 431 (1990).

[159] W. Demtröder, *Laser spectroscopy* (Springer, 1996).

[160] P. Gallion and G. Debarge, *Quantum phase noise and field correlation in single frequency semiconductor laser systems*, IEEE J. Quantum Electron. **20**, 343 (1984).

[161] H. Ludvigsen, M. Tossavainen and M. Kaivola, *Laser linewidth measurements using self-homodyne detection with short delay*, Opt. Commun. **155**, 180 (1998).

[162] R. L. Sutherland, *Handbook of nonlinear optics* (Marcel Dekker, 1996).

[163] R. W. Boyd, *Nonlinear optics* (Academic Press, 2003).

[164] G. Hansson, H. Karlsson, S. Wang and F. Laurell, *Transmission Measurements in KTP and Isomorphic Compounds*, Appl. Opt. **39**, 5058 (2000).

[165] M. V. Pack, D. J. Armstrong and A. V. Smith, *Measurement of the $\chi(2)$ tensors of $KTiOPO_4$, $KTiOAsO_4$, $RbTiOPO_4$, and $RbTiOAsO_4$ crystals*, Appl. Opt. **43**, 3319 (2004).

[166] D. A. Kleinman, *Nonlinear dielectric polarization in optical media*, Phys. Rev. **126**, 1977 (1962).

[167] S. A. Akhmanov, A. I. Kovrigin, R. V. Khokhlov and O. N. Chunaev, *Coherent interaction length of light waves in a nonlinear medium*, Sov. Phys. JETP **18**, 919 (1964), [Russian original: Zh. Eksp. Theor. Fiz. **45**, 1336 (1963)].

[168] J. A. Armstrong, N. Bloembergen, J. Ducuing and P. S. Pershan, *Interactions between light waves in a nonlinear dielectric*, Phys. Rev. **127**, 1918 (1962).

[169] M. Yamada, N. Nada, M. Saitoh and K. Watanabe, *First-order quasi-phase matched $LiNbO_3$ waveguide periodically poled by applying an external field for efficient blue second-harmonic generation*, Appl. Phys. Lett. **62**, 435 (1993).

[170] C. Canalias, *Domain engineering in $KTiOPO_4$*, Ph.D. thesis, KTH – Royal Institute of Technology, 2005.

[171] S. Brosnan and R. Byer, *Optical parametric oscillator threshold and linewidth studies*, IEEE J. Quantum Electron. **15**, 415 (1979).

[172] G. Anstett and R. Wallenstein, *Experimental investigation of the spectro-temporal dynamics of the light pulses of Q-switched Nd:YAG lasers and nanosecond optical parametric oscillators*, Appl. Phys. B **79**, 827 (2004).

[173] T. Y. Fan, C. E. Huang, B. Q. Hu, R. C. Eckardt, Y. X. Fan, R. L. Byer and R. S. Feigelson, *Second harmonic generation and accurate index of refraction measurements in flux-grown $KTiOPO_4$*, Appl. Opt. **26**, 2390 (1987).

[174] K. Fradkin, A. Arie, A. Skliar and G. Rosenman, *Tunable midinfrared source by difference frequency generation in bulk periodically poled $KTiOPO_4$*, Appl. Phys. Lett. **74**, 914 (1999).

[175] W. Wiechmann, S. Kubota, T. Fukui and H. Masuda, *Refractive-index temperature derivatives of potassium titanyl phosphate*, Opt. Lett. **18**, 1208 (1993).

[176] J. D. Bierlein and H. Vanherzeele, *Potassium titanyl phosphate: properties and new applications*, J. Opt. Soc. Am. B **6**, 622 (1989).

[177] V. Smilgevičius, A. Stabinis, A. Piskarskas, V. Pasiškevičius, J. Hellström, S. Wang and F. Laurell, *Noncollinear optical parametric oscillator with periodically poled KTP*, Optics Communications **173**, 365 (2000).

[178] J.-P. Fève, O. Pacaud, B. Boulanger, B. Ménaert, J. Hellström, V. Pasiskevicius and F. Laurell, *Widely and continuously tunable optical parametric oscillator based on a cylindrical periodically poled $KTiOPO_4$ crystal*, Opt. Lett. **26**, 1882 (2001).

[179] A. Fragemann, V. Pasiskevicius and F. Laurell, *Broadband nondegenerate optical parametric amplification in the mid infrared with periodically poled $KTiOPO_4$*, Opt. Lett. **30**, 2296 (2005).

[180] M. Tiihonen, V. Pasiskevicius and F. Laurell, *Tailored UV-laser source for fluorescence spectroscopy of biomolecules*, Opt. Lasers Eng. **45**, 444 (2007).